WL-TR-96-3030

UNIFIED PILOT-INDUCED OSCILLATION THEORY
VOLUME III: PIO ANALYSIS USING MULTIVARIABLE METHODS

DR. MARK R. ANDERSON
ANTHONY B. PAGE
Department of Aerospace and Ocean Engineering
Virginia Polytechnic Institute and State University
Blacksburg VA 24061

DECEMBER 1995
FINAL REPORT FOR PERIOD OCTOBER 1994 - SEPTEMBER 1995

FLIGHT DYNAMICS DIRECTORATE
WRIGHT LABORATORY
AIR FORCE MATERIEL COMMAND
WRIGHT-PATTERSON AIR FORCE BASE, OHIO 45433-7562

NOTICE

When Government drawings, specifications, or other data are used for any purpose other than in connection with a definitely Government-related procurement, the United States Government incurs no responsibility or any obligation whatsoever. The fact that the government may have formulated or in any way supplied the said drawings, specifications, or other data, is not to be regarded by implication, or otherwise in any manner construed, as licensing the holder, or any other person or corporation; or as conveying any rights or permission to manufacture, use, or sell any patented invention that may in any way be related thereto.

This report is releasable to the National Technical Information Service (NTIS). At NTIS, it will be available to the general public, including foreign nations.

This technical report has been reviewed and is approved for publication.

DAVID B. LEGGETT
Project Engineer
Control Dynamics Branch
Flight Control Division

SIVA S. BANDA, Chief
Control Dynamics Branch
Flight Control Division

DAVID P. LEMASTER
Chief, Flight Control Division
Flight Dynamics Directorate

If your address has changed, if you wish to be removed from our mailing list, or if the addressee is no longer employed by your organization please notify WL/FIGC-2, WPAFB, OH 45433-7531 to help us maintain a current mailing list.

Copies of this report should not be returned unless return is required by security considerations, contractual obligations, or notice on a specific document.

REPORT DOCUMENTATION PAGE

Form Approved
OMB No. 0704-0188

1. AGENCY USE ONLY (Leave blank)	2. REPORT DATE	3. REPORT TYPE AND DATES COVERED
	December 1995	Final Report: Sep 94 thru Sep 95

4. TITLE AND SUBTITLE
Unified Pilot-Induced Oscillation Theory, Volume III
PIO Analysis Using Multivariable Methods

5. FUNDING NUMBERS
CONTRACTS:
F33615-94-C-3611
PE 62201F
PR 2403
TA 05
WU 9A

6. AUTHOR(S)
Dr. Mark R. Anderson
Anthony B. Page

7. PERFORMING ORGANIZATION NAME(S) AND ADDRESS(ES)
Depart of Aerospace and Ocean Engineering
Virginia Polytechnic Institute and State University
Blacksburg VA 24061-0203

8. PERFORMING ORGANIZATION REPORT NUMBER

9. SPONSORING/MONITORING AGENCY NAME(S) AND ADDRESS(ES)
Flight Dynamics Directorate
Wright Laboratory
Air Force Materiel Command
Wright-Patterson AFB OH 45433-7562

10. SPONSORING/MONITORING AGENCY REPORT NUMBER
WL-TR-96-3030

11. SUPPLEMENTARY NOTES

12a. DISTRIBUTION/AVAILABILITY STATEMENT
Approved for Public Release
Distributio Unlimited

12b. DISTRIBUTION CODE

13. ABSTRACT *(Maximum 200 words)*

This work was conducted as part of a USAF initiative to develop a comprehensive theory to predict pilot-induced oscillation (PIO) tendencies due to the combined effect of all influencing elements. A PIO is a very complicated phenomenon stemming from a dynamic interaction between the pilot and the aircraft. When tight control is required of the pilot, an undesired oscillation can result. However, the adaptive nature of the human pilot makes such oscillations difficult to predict. This report describes an analysis method capable of predicting PIO tendencies due to several simultaneous dynamic factors. A unified approach involving pilot modeling, stability robustness analysis, and multivariable describing function analysis is applied to the problem of identifying aircraft with PIO tendencies. The approach is shown to have ties to existing PIO criteria and is successfully applied to the prediction of PIO tendencies of the M2-F2 lifting body.

14. SUBJECT TERMS	15. NUMBER OF PAGES
Flying Qualities, Pilot-Induced Oscillation, Pilot Modeling, Stability Robustness, Describing Function	109
	16. PRICE CODE

17. SECURITY CLASSIFICATION OF REPORT	18. SECURITY CLASSIFICATION OF THIS PAGE	19. SECURITY CLASSIFICATION OF ABSTRACT	20. LIMITATION OF ABSTRACT
Unclassified	Unclassified	Unclassified	UL

FOREWORD

A pilot-induced oscillation (PIO) results from the interaction of the pilot and the dynamics of the vehicle being controlled. It may be caused or affected by several elements of the aircraft design or the mission task. PIO affects the pilot's ability to perform a given task, ranging from an annoying aircraft motion to inability to complete the task to, in the most extreme cases, jeopardizing the safety of the aircraft and crew. Because it occurs sporadically, PIO can be one of the most insidious flying qualities problems.

Criteria currently exist for some of the elements of aircraft design which influence PIO tendencies; however, the criteria in the flying qualities standard (MIL-STD-1797) address the effect of these elements individually rather than cumulatively. These elements include sluggish response modes, low damping, excessive phase lag or time delay, overly sensitive stick gradients, unstable response modes, coupled response modes, etc. Furthermore, there are some elements that are known to influence PIO tendencies which are not addressed in MIL-STD-1797. Some examples of these elements are aerodynamic nonlinearities, control system nonlinearities, actuator rate limits, nonlinear stick gradients, etc.

This report is the first step of an Air Force initiative to develop a comprehensive and unifying theory to explain the nature of the interaction of pilot and vehicle which results in PIO and to develop the capability to predict an aircraft's PIO tendencies due to the combined effect of all influencing elements. This theory must be consistent with several PIOs which have been documented in research, development, and operational aircraft. This effort should also produce design criteria which can be used in the development process to assess the risk of PIO prior to manned simulation.

The four volumes of this report represent a broad-band approach to developing this comprehensive theory. There were five contractors involved: Calspan Corporation; Hoh Aeronautics, Inc.; McDonnell Douglas Aerospace; Systems Technology, Inc.; and Virginia Polytechnic Institute and State University. The objectives of the contractors were to develop their theories and partially validate them against existing data.

Volume I is the work of Systems Technology, Inc. This research included: compilation of available PIO time histories and references as an initial step toward a comprehensive PIO database; refinement of the proposed PIO categories defined in NASA CR-4683; development of PIO theories based on these categories; development of methods to handle the higher frequency and nonlinear aspects of PIO analysis with an emphasis on rate limiting; and a review of existing and proposed linear PIO criteria.

Volume II is the combined work of McDonnell Douglas Aerospace, Advanced Transport Aircraft at Long Beach, CA, McDonnell Douglas Aerospace, Advanced Programs, at St. Louis, MO, and Hoh Aeronautics, Inc. at Lomita, CA. There are primarily two components associated with this study. One element is an examination of PIO events that have occurred in the course of initial flight development on several aircraft produced by

the McDonnell Douglas Corporation. The other element is an exploration of several theories associated with PIOs, particularly those with rate limiting involved.

Volume III was produced by the Virginia Tech Department of Aerospace and Ocean Engineering. This report describes an analysis method capable of predicting PIO tendencies due to several simultaneous factors. A unified approach involving pilot modeling, stability robustness analysis, and multivariable describing function analysis is applied to the problem of identifying aircraft with PIO tendencies. The approach is shown to have ties to existing PIO criteria and is successfully applied to the prediction of PIO tendencies of the M2-F2 lifting body.

Volume IV is the result of Calspan's efforts. This report presents the theory, fundamental principles, and analytical procedures of a quantitative criterion for the prediction of PIO tendencies based on a "time-domain Neal-Smith" approach. The criterion is validated against three very reliable flying qualities data bases. At present the criterion is intentionally limited to the evaluation of pitch control only. No fundamental limitations were discovered which preclude the evolution of this methodology and analytical procedures to PIO analysis of roll control or "outer-loop" longitudinal control, such as control of aircraft flight path.

After further evaluation and deliberation of these reports, the Air Force will pursue the most promising ideas, or combination of ideas, and validate them with further simulation and flight testing.

TABLE OF CONTENTS

TABLE OF CONTENTS (continued)

TABLE OF CONTENTS (continued)

List of Figures

List of Tables

PREFACE

A pilot-induced or pilot-in-the-loop oscillation (PIO) is a very complicated phenomenon stemming from a dynamic interaction between the pilot and the aircraft. This interaction means that the aircraft can be otherwise well behaved and the pilot can be very well trained; however, when tight interaction between the pilot and the aircraft is required, an undesired oscillation can result. Furthermore, the adaptive nature of the human pilot makes such oscillations very difficult to predict. This report describes an analysis method capable of predicting PIO tendencies due to several simultaneous dynamic factors. A unified approach involving pilot modeling, stability robustness analysis, and multivariable describing function analysis is applied to the problem of identifying aircraft with PIO tendencies. The approach is shown to have ties to existing PIO criteria and is successfully applied to the prediction of PIO tendencies of the M2-F2 lifting body..

ACKNOWLEDGMENTS

Effort sponsored by Wright Laboratory (WL/FIGC-2), Wright-Patterson AFB OH, under contract F33615-94-C-3611. Mr. Wayne Thor is the Technical Monitor. The U.S. Government is authorized to reproduce and distribute reprints for Government purposes notwithstanding any copyright notation therein. The views and conclusions contained herein are those of the authors and should not be interpreted as necessarily representing the official policies or endorsements, either expressed or implied, of Wright Laboratory or any other agency of the U.S. Government.

The authors wish to thank Dave Leggett for his coordination of the Unified Pilot-Induced Oscillation Theory program under which this research was completed

1 Introduction

A pilot-induced or pilot-in-the-loop oscillation (PIO) is a very complicated phenomenon stemming from a dynamic interaction between the pilot and the aircraft. This interaction means that the aircraft can be otherwise well behaved and the pilot can be very well trained; however, when tight interaction between the pilot and aircraft is required, an undesired oscillation can result. Furthermore, the adaptive nature of the human pilot makes such oscillations very difficult to predict.

One of the most recent aircraft loses due to a PIO was the Lockheed/Boeing YF-22A advanced tactical fighter prototype.[1] Figure 1-1 shows a re-creation of the PIO that occurred in the YF-22A. This figure was created electronically scanning the last seven seconds of the time history of Reference [1]. While the figure is not drawn completely to scale (the altitude excursions have been accentuated), the figure does illustrate the rather dramatic changes in flight attitude that can occur during a fully developed PIO.

The YF-22A prototype crash is an example of a very complicated dynamic situation that led to a PIO. Several significant changes occurred simultaneously in the aircraft dynamics. According to Reference [1], the landing gear of the aircraft were retracted at nearly the same time

Figure 1-1. YF-22A Pilot-Induced Oscillation.

as the afterburner was ignited to initiate a planned go-around. These configuration changes caused significant mode switching in the aircraft control laws. The control law changes are usually governed by "transient-free" switches that slow the transition of control system gains from landing to up-and-away configuration. The pilot, on the other hand, must adapt his control strategy continuously and at the same rate as the aircraft dynamics are changing. Therefore, the PIO of the YF-22A is an example of several different dynamic elements contributing to the oscillation.

The increased complexity of modern aircraft appears to increase the likelihood of PIO due to several interacting dynamic factors. Since the YF-22A prototype was highly instrumented and the PIO event was captured on film, it was possible to deduce the various dynamic phenomenon that ultimately lead to the crash.

Could any of the existing PIO analysis methods have predicted the YF-22A PIO *before* it occurred? Most existing PIO analysis methods and criteria were developed to address individual dynamic effects. For example, it is usually assumed that the pilot is only controlling a single axis or moving only one manipulator. Other criteria cannot handle nonlinearities and few, if any, can address the combined effect of several dynamic factors as in the YF-22A crash. Consequently, it is unlikely that an existing analysis method could have predicted the YF-22A PIO incident.

1.1 Scope

This report deals primarily with computational analysis techniques designed to predict PIO susceptibility of modern aircraft. These techniques are intended for use during aircraft development or modification prior to flight. Methods to study PIO behavior during flight test and

manned simulations will not be discussed. Aircraft and pilot modeling will only be addressed to the extent required to utilize the PIO analysis methods.

1.2 Objective

A comprehensive and unified PIO analysis method is sought. This unified method must be able to handle the combined effect of all influencing dynamic elements. The theory must also explain the nature of interaction of the pilot and vehicle that causes the PIO. And finally, it must be consistent with several PIOs which have been documented over the last few years.

The basic premise of this research is that a PIO-resistant aircraft is resistant to closed-loop pilot dynamic variations in the face of nonlinear aircraft behavior. It could be argued that nonlinear aircraft behavior causes the pilot to change his/her equalization instead of vice versa. From an analysis point-of-view, the simultaneous action of the aircraft and pilot dynamics are addressed from either viewpoint.

The possible variations in pilot dynamics that might lead to or "trigger" a PIO include primarily an increase in pilot gain due to an excited or overly aggressive pilot. In addition, aggressiveness may also alter the pilot's inherent time delay or phase lead generating capability. Human operators are also known to exhibit nonlinear behavior, such as "bang-bang" control.[2] Any unified PIO analysis method should be able to address any or all of these variations.

The principal nonlinear aircraft dynamic effect that is known to contribute to PIO is control surface actuator rate and deflection limiting. Other effects such as control system mode switching and nonlinear stick gradients are known to contribute to PIO susceptibility. Some PIO events have lead to such large amplitude oscillations that nonlinear aerodynamics have played a

significant role. A unified PIO analysis method should be able to handle each of these dynamic elements as well as combinations of them.

1.3 Plan

Since the basic premise of this research involves the study of pilot/aircraft stability robustness and nonlinear system oscillations, the unified analysis method proposed is a combination of multivariable stability robustness analysis and multivariable describing function analysis. These methods were developed specifically to handle multiple dynamic effects simultaneously. In addition to this final report, the following work plan was devised.

The first task consists of the development of the necessary stability analysis software. Existing computational analysis algorithms have been collected and refined. The MATLAB™ computer-aided engineering software package is used as the computational environment in which all analysis is conducted. Since, other competing packages have similar programming (or macro) features, it is expected that translation to other packages can be easily completed.

The four basic computational tasks that must be carried out are: 1) compute the pilot model, 2) construct the block diagram, 3) perform a structured singular value analysis, and 4) search for limit cycles. Algorithms already exist (in MATLAB™ form) to compute optimal control models of the human pilot [3], and no modification is necessary for use in the current PIO analysis. SIMULINK™, an optional program linked to MATLAB™, is used to perform the necessary block diagram manipulations and simulations. SIMULINK™ is an excellent environment for study of systems with simple isolated nonlinearities of the type generally used in PIO investigations. The algorithms to perform the real structured singular value analysis and the limit cycle search were

also coded within the computational framework of MATLAB™. The algorithms are based on those currently available in the open literature.

The second task was to perform verification case studies. Once all of the analysis codes have been implemented and tested, case studies are conducted using existing aircraft data. The HAVE PIO database is used to study existing criteria using multivariable stability robustness methods. This activity is intended to show that the new unified PIO analysis methods can be readily tied to existing methods using an existing database.

The multivariable limit cycle software is separately validated using a previous study of back-up control system designs for the F-4 aircraft. The original study was intended to show the PIO susceptibility of the back-up control systems. This application is particularly appealing because both control surface rate and deflection limiting were shown to occur simultaneously.

The third task was to develop new design criteria from the new PIO theory. The HAVE PIO database is used again to develop a new single-loop PIO criteria from multivariable stability robustness theories. The M2-F2 aircraft is used to study the effect of combinations of nonlinear dynamic elements. The M2-F2 application illustrates how the unified PIO analysis method can be used to isolate combinations of dynamic elements which lead to oscillatory behavior.

2 Background

Aircraft characteristics that are known to contribute to pilot-in-the-loop oscillation tendencies include: sluggish response modes, low damped modes, excessive phase lag or time delay, sensitive stick gradients, unstable response modes (that cannot be stabilized by the pilot), and unusual coupling responses. These characteristics have been studied by researchers since the early 1960's. The existing research literature and the current military flying qualities specification present analysis methods that have been successful in predicting pilot-in-the-loop oscillation behavior for each of these characteristics. However, with the exception of Reference [4], very little research has been devoted to the study of several of these dynamic effects occurring simultaneously.

Early research concerning PIO behavior is typified by the paper by Hirsch and McCormick.[5] Hirsch and McCormick used fixed- and motion-based simulations to study generalized longitudinal aircraft configurations. However, their inclusion of simple pilot compensation strategies was recognized early. Their analysis consisted of experimental observations and simple root-locus charts. In addition, Hirsch and McCormick revealed the criticality of including both visual and motion cues in their analysis.

The PIO theory developed by R. Smith is perhaps the most widely recognized analysis and prediction method.[6] Smith's method is described in the military flying qualities specification and has been evaluated by other researchers.[7,8,9] In the authors' view, the success of Smith's method is due to the fact the interaction of the pilot and aircraft is properly modeled using elements of McRuer's crossover pilot model.[10] Thus, the criterion is based not just on the dynamics of the aircraft, but also on the human pilot capabilities.

One of the most prolific researchers in the area of PIO investigation has been R.A. Hess.[11-13] Dr. Hess has used much more complex and intricate models of the human operator in an effort to more completely represent the interaction between the pilot and the aircraft. Hess's 1991 paper, Reference [11], develops a PIO prediction method that limits the bandwidth and slope of the pilot/vehicle open-loop transfer function. The success of Hess's method therefore relies heavily on an accurate model of the human pilot.

In his PIO studies, Hess has been using the optimal control model (OCM) of the human operator. This model was developed by Kleinman, Baron, and Levison in 1970.[14] It has also been used by other researchers to develop PIO criteria for different aircraft types and flight tasks.[15-17] Like Hess's criteria, these researchers have developed criteria using frequency-domain representations of either the open- or closed-loop pilot vehicle transfer functions. Closed-loop resonant peaking behavior (References [15] and [16]) and open-loop crossover properties (References [13] and [17]) have been effective PIO predictors.

Some research has been devoted to design methods to reduce PIO tendencies. However, since most of the prediction methods have close connections to feedback control theory, aircraft control system remedies are usually evident. In cases where flight control system modifications are unwise or costly, References [18], [19], and [20] describe ways in that the control stick dynamics can be altered to help alleviate or suppress PIO behavior.

3 PIO Theory

Before the specifics of the proposed analysis method are set forth, some basic concepts concerning PIO are addressed. The working definition of a PIO used in this report is given. The acceptable and unacceptable characteristics of PIO are then stated. Finally, some of the known and suspected causes of PIO are listed.

3.1 Definitions

Much discussion has been and probably will continue to be fervently pursued on the precise definition of a PIO. For the purposes of this study, a simple definition is employed,

> *A PIO results when the closed-loop pilot/vehicle system oscillates due to a loss in asymptotic stability.*

Since the current analysis methods deal primarily with mathematical models of the pilot and aircraft, this definition is easily tested. Asymptotic stability of a linear system is lost when any pole (or complex pair of poles) cross from the left half plane onto the jω axis. For a nonlinear system, in addition to examining the poles of the corresponding linearized system, the existence of a limit cycle (sustained oscillation) will be taken as a separate measure that precludes the condition of asymptotic stability of the closed-loop system.

3.2 Acceptable/Unacceptable Characteristics

The term PIO is certainly recognized by all those who work in the design and flight testing of high performance military as well as civil transportation aircraft. If we proceed from the standpoint that a PIO prone aircraft is undesirable, then any PIO is inherently unacceptable. Since it is never desirable to have an unstable closed-loop pilot/aircraft system, the above

definition dictates there can be no acceptable characteristics of a PIO. If there are oscillation tendencies due to coupling of the aircraft and pilot which have relatively benign characteristics, then these should be dealt with as separate handling qualities issues. The term PIO should be reserved for description of an unacceptable coupling between the pilot and aircraft so that it keeps its current day connotations and continues to be cause for the greatest concern.

3.3 Causes

Several dynamic factors have been documented as contributing to the occurrence of PIO. These can be separated into those that are attributed to the linear dynamics of the aircraft and pilot, and those that are nonlinear in nature. Also, it has been noted by several researchers that a trigger event is often necessary to excite the PIO. A brief list of the causes of PIO and a description of events associated as triggers is given below.

3.3.1 Linear

Aspects of the linear dynamics of an aircraft that have been associated with causing PIO include: 1) sluggish response modes, 2) lightly damped modes, 3) low stick force per g, 4) sensitive stick gradients, 5) unusual coupling responses, and 6) excessive lags in the augmented aircraft. The most common aspect of the linear pilot that is attributed to causing PIO is an increased pilot gain. In the subsequent analysis, the effect of changes in pilot gain on system stability is of primary concern.

3.3.2 Nonlinear

Nonlinearities associated with PIO include: 1)surface actuator rate and position limiting, 2) nonlinear stick characteristics, and 3) mode switching. Although saturation of the control surface actuators is common in PIOs, it is not clear whether it is the cause or effect of PIO. The

examples discussed in this report will focus on the affect of actuator rate and command limiting of the augmented aircraft on the occurrence of PIO.

3.3.3 Trigger Events

While trigger events are not causes of PIO *per se*, they are often needed to excite a response of the pilot that will "trigger" or start the oscillation event. A trigger event can be something as simple as a gust of wind or something more complicated such as control system mode switching or a control system failure. In the subsequent analysis, closed-loop stability is analyzed in the face of changes in both the aircraft and pilot models. That is, the post trigger dynamic situation is to be analyzed.

4 PIO Analysis Process

The process outlined below is intended to distinguish between aircraft that are PIO susceptible and aircraft that are PIO resistant. The analysis is based on determining the stability of the closed-loop pilot/aircraft system in the face of variations in the pilot model as well as uncertainties in key aircraft parameters. The process is able to account for many of the nonlinearities present in both the pilot and aircraft. For the purposes of this report, those analysis methods which include pilot models are considered "closed-loop methods" even if they only consider the open-loop pilot/vehicle characteristics. Methods which do not include a pilot model are considered "open-loop methods". This point of view is taken for convenience and is not meant to strictly categorize any particular method.

4.1 Process Outline

The underlying purpose of the analysis is to determine under what conditions the pilot/aircraft system is capable of producing a sustained oscillation. The unified multivariable analysis method consists of four steps. The first step is to determine an analytical model of the human pilot that is appropriate for the flying task under study. Any accepted modeling method can be used, although the results may vary. Both crossover and "optimal control" model forms are acceptable. A synchronous (constant gain) model is also appropriate for some cases although a model with at least a -20 dB/decade high-frequency roll-off characteristic (to help attenuate feedback signal superharmonics) is desirable.

The second analysis step is to identify and isolate the dynamic elements suspected of contributing to PIO behavior. Linear and nonlinear elements can be considered simultaneously.

Aerodynamic nonlinearities, control system nonlinearities, nonlinear stick gradients, various pilot model parameters, and control surface rate limits are of particular interest.

The third step is to perform a stability robustness analysis using the structured singular value method. This analysis will yield a bound on the largest allowable parameter variation before instability is possible. The structured singular value analysis leads to a sufficient condition for stability and may be conservative. If the closed-loop system operates in a fashion such that the predicted bound on the uncertainty is not exceeded, then the closed-loop system will remain stable *and will not limit cycle.* However, if the predicted bound is exceeded, the system may or may not be unstable and may or may not limit cycle.

The final analysis step is to search for limit cycle behavior of the nonlinear pilot/aircraft system. A limit cycle is a self sustained oscillation that is particular to nonlinear systems. The limit cycle search is carried out in the frequency domain. Results yield frequency and amplitude of the oscillation as well as a prediction of limit cycle stability. Stable limit cycles will return to a constant amplitude oscillation following a perturbation whereas an unstable limit cycle will not. Limit cycle predictions are generally confirmed using nonlinear time domain simulations.

4.2 Open-loop Analysis

Though the analysis methods developed in this report are considered closed-loop, some existing open-loop methods are mentioned here as they are relevant to the construction of a unified theory in Section 4.3.5. The open-loop characteristic that appears most closely related to PIO susceptibility is the behavior of the aircraft frequency response near the pilot/aircraft gain and phase crossover frequencies. The Smith-Geddes Criterion, for example, requires computation of the magnitude slope of the aircraft frequency response in the range between 1.0 and 6.0

rad/sec.[21] This slope is then used to determine a criterion frequency where the aircraft transfer function phase angle is checked. If the phase angle is less than -180 deg, a PIO is predicted and if the phase angle is less than -165 deg, a PIO is possible. Nevertheless, the criterion frequency ω_{cr} is defined as,

$$\omega_{cr} = 6.0 + 0.24S \tag{4-1}$$

where S is the computed magnitude slope in dB/octave.

Since the aircraft transfer function phase angle becomes more negative at higher frequency, a large negative amplitude slope reduces the criterion frequency and naturally leads to a larger phase angle. Therefore, the Smith-Geddes PIO criterion tends to identify aircraft configurations having the characteristic of large negative magnitude slopes in the frequency range of 1.0 to 6.0 rad/s as PIO resistant. In addition, an aircraft with a shallow phase angle slope in the same frequency range will decrease the phase angle sensitivity to criterion frequency changes and will be predicted less PIO susceptible. Since the Smith-Geddes Criterion phase angle is -180 deg, it is reasonable to suggest that configurations with shallow phase angle slopes in this region will be predicted less PIO susceptible.

The flight test data base given in Reference [8] provides experimental data which can be used to evaluate (longitudinal) PIO prediction methods. The data base has been referred to elsewhere as the HAVE PIO data base,[11] and that designation is continued in this report. The experiments were conducted using the USAF/Calspan variable stability NT-33 aircraft. The 18 aircraft/flight control system configurations were evaluated in landing approach tasks. The four baseline configurations (H2-1, H3-1, H4-1, H5-1) were chosen to have different short period dynamics that all met MIL-F-8785C Level 1 boundaries for Category C landing approach. The phugoid

and lateral/directional characteristics, which all met Level 1 requirements, were held constant. PIO ratings, Cooper-Harper pilot ratings, and pilot comments were obtained.

For Configuration H2-1, the control stick deflection to pitch attitude transfer function is,

$$g(s) = \frac{(1.4)}{s[.64 \setminus 2.4][.68 \setminus 26]} \tag{4-2}$$

where the shorthand notation is $(\tau) = (\tau s+1)$ and $[\zeta\setminus\omega_n] = (s/\omega_n)^2 + 2\zeta s/\omega_n + 1$. The aircraft transfer function for Configuration H2-5 is,

$$g(s) = \frac{(1.4)}{s(1.0)[.64 \setminus 2.4][.68 \setminus 26]} \tag{4-3}$$

Figure 4-1 shows a Bode diagram of $g(j\omega)$ for HAVE PIO Configurations H2-1 and H2-5. The average PIO rating for Configuration H2-1 was 1.0 while H2-5 was given average rating of 4.33. An aircraft receiving a rating above 2.0 is considered PIO susceptible.

In the frequency range from 1.0 to 6.0 rad/sec, Configuration H2-5 has a steeper magnitude slope than Configuration H2-1, but H2-1 exhibits a shallower phase angle slope. Although the criterion frequency for H2-5 is lower than that for H2-1 (approximately 3 rad/sec as opposed to 4 rad/sec), the phase angle for H2-5 is less than -180 deg and the phase angle for H2-1 is greater than -165 deg at the corresponding criterion frequencies. Therefore, one can see from Figure 4-1 that Configuration H2-5 will be more susceptible to PIO than Configuration H2-1.

Mitchell and Hoh advocate a PIO criterion that specifies a maximum phase angle change after the phase angle crosses negative 180 deg.[22] Their criterion is specified in terms of a phase delay parameter, τ_p, that is defined by,

$$\tau_p = \frac{\Delta\Phi}{2(57.3)\omega_{180}} \tag{4-4}$$

where $\Delta\Phi$ is the phase loss from ω_{180} to $2\omega_{180}$ and ω_{180} is the frequency where the aircraft

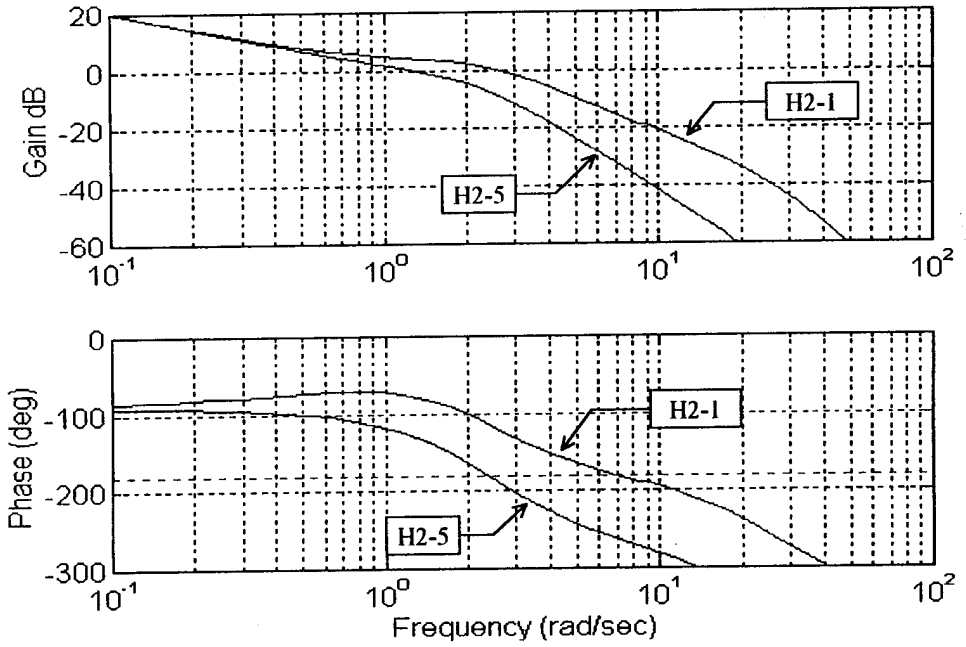

Figure 4-1. Bode Plots for HAVE PIO H2-1 and H2-5.

transfer function reaches -180 degrees. An aircraft is considered PIO susceptible if the phase delay $\tau_p \geq .12$ sec (.15 sec in landing).

One can see by (4-4) that upper limits on the phase delay parameter will tend to limit the aircraft phase angle slope near the -180 deg point. A small value of τ_p is needed to categorize the aircraft as PIO resistant, so it will therefore require a small value of $\Delta\Phi$ and/or a large value of ω_{180}. These requirements, in effect, will list aircraft that have shallow phase angle slopes in the frequency range where the phase angle crosses -180 deg as PIO resistant.

In summary, these open-loop methods deal directly with the shape of the aircraft transfer function near the point where the phase angle is -180 deg and near where the pilot/vehicle crossover frequency is likely to occur (1-6 rad/sec).

4.3 Closed-loop Analysis

The four steps in the multivariable PIO analysis process outlined in Section 4.1 are discussed in detail in the following sections. Sections 4.3.5 and 4.3.6 use stability robustness ideas to establish ties between existing methods and to set forth a new analysis procedure. A detailed example of the multivariable analysis method is then presented in Section 4.3.7.

4.3.1 Pilot Modeling

Advances in the theory of pilot modeling have led to new theories of pilot-in-the-loop oscillations. Early PIO criteria involved concepts from the crossover model of the human operator while more recent research has focused on the optimal control model. Kleinman's optimal control model (OCM) of the human operator is based upon Linear, Quadratic, Gaussian (LQG) control theory. The model includes a set of state-feedback gains that are computed using a special quadratic cost function. The state-feedback control law is then augmented with a state estimator and a predictor. The purpose of the predictor is to model the human's ability to adapt to his/her inherent time delay.

A modified version of the Kleinman model has been developed by Davidson and Schmidt.[23] The modified optimal control model (MOCM) replaces the pure time delay with a Pade' approximation of the time delay. The Pade' approximation used by Davidson and Schmidt is given by,

$$e^{-\tau_d s} \cong \frac{1-\tau_d s/2+(\tau_d s)^2/8}{1+\tau_d s/2+(\tau_d s)^2/8} \tag{4-5}$$

where τ_d is the human pilot time delay. The principal advantage of the Pade' approximation is that its use allows for direct computation of a human operator transfer function. Whereas Kleinman's

model yields only frequency response (describing function) information of the human response, the Davidson model provides detailed information of dominant response modes. Therefore, the interaction between the pilot and aircraft can be more readily identified.

Anderson has recently revised the Davidson model to use state-space solutions for both H_2 and H_∞ norm minimizing controllers.[3] This latest extension uses the "standard" optimal control solutions that have been published recently by Doyle, et. al.[24] The "standard" model form is given by the following state-space model,

$$\begin{bmatrix} \dot{x} \\ y_1 \\ y_2 \end{bmatrix} = \begin{bmatrix} A & B_1 & B_2 \\ C_1 & D_{11} & D_{12} \\ C_2 & D_{21} & D_{22} \end{bmatrix} \begin{bmatrix} x \\ u_1 \\ u_2 \end{bmatrix} \tag{4-6}$$

For application to pilot modeling, the vector u_1 represents the external noise or command, u_2 is the vector containing the pilot manipulator input, y_1 is the vector representing the pilot's task objective, and y_2 represents the pilot's observation variables.

Because the newer "standard" H_2/H_∞ model has not yet been validated for aircraft applications, Davidson and Schmidt's MOCM is used throughout this work. The specific MOCM pilot models used in the examples presented in this report share the modeling parameters shown in Table 4-1.

Table 4-1. MOCM Pilot Model Parameters.

Parameter	Value
time delay	0.2 sec
neuromuscular time constant	0.1 sec
observation signal-to-noise ratio	0.01
neuromotor signal-to-noise ratio	0.003

The optimal MOCM cost function is assumed to be given by,

$$J = \frac{1}{2\pi}\int_{-\infty}^{\infty}\left[e^2(t) + \rho\dot{\delta}_c^2(t)\right]dt \qquad (4\text{-}7)$$

where e(t) is the error signal and $\delta_c(t)$ is the pilot manipulator command input. The control rate weighting ρ is chosen to achieve the desired neuromuscular time constant as described in Reference [14]. Note that the error rate is retained in the observation vector but is not weighted in the cost function (4-7).

Smith has described a contactor pilot model for study of fully developed PIO behavior.[25] The contactor nonlinearity is essentially a relay that yields a fixed positive value for any positive value input and a fixed negative value of any negative value input. For example, if the input to the nonlinearity is +1, the relay output might be +2. For an input of +4, the output of the same relay is still +2. This model will also be used in Section 4.3.5.4.

4.3.2 Identify Dynamic Elements Suspected of Contributing to PIO

With given models of the aircraft dynamics and the human pilot, the elements suspected of contributing to PIO must be identified and isolated. The elements directly associated with the causes of PIO given in Section 3.3 can be considered here. Since the pilot model plays a key role in the current analysis, any of the pilot model parameters may need to be considered as uncertain elements that can contribute to PIO tendency.

4.3.3 Stability Robustness Analysis

A PIO is fundamentally a stability problem. Sustained oscillations only occur in linear systems when the dynamics of the system lose damping. An example is an undamped spring-mass system that will oscillate from an initial displacement with constant amplitude motion.

Stability robustness analysis is the study of how model parameter variation or "uncertainty" affects feedback loop stability. Since the mid 1980's, a resurgence in frequency-domain analysis methods for stability robustness has occurred. These methods have relied on the singular value matrix norm as a "measure" of relative stability. For example, gain and phase margins for multivariable feedback systems can be defined using the singular-value based analysis method.[26] Stability margins defined in such a manner are very useful in that they define the gain or phase variation that can occur *simultaneously in each feedback loop.* As a result, an investigation of multiple parameter variations can be carried out rather easily.

Doyle is widely regarded as the key developer of the structured singular value analysis method.[27] The structured singular value method allows the research engineer to investigate not only simultaneous model parameter variations, but also the effect of multiple parameters located arbitrarily throughout the feedback system. Thus, parameter variation is not confined to just the feedback loop signals, but can include individual system parameters.

4.3.3.1 Basic Theory

Perhaps the most important contribution of the structured singular value method is the construction of analysis block diagrams like Figure 4-2. The transfer function matrix M(s) in Figure 4-2 does not necessarily represent the aircraft, the pilot, or a series combination of feedback loop elements. The function M(s) represents the transfer function matrix as seen by each model parameter that is varying – regardless of where the parameter occurs in the feedback loop. For example, a variation due to inaccurate aerodynamic modeling can be analyzed in conjunction with a variation in the pilot's loop gain. Consequently, model variations from many different sources can be analyzed at once.

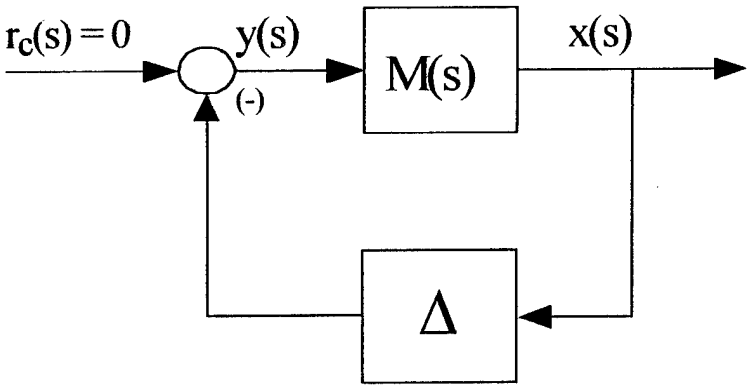

Figure 4-2. Stability Robustness Analysis Diagram.

Stability of the feedback loop can be investigated from the loop equations represented in Figure 4-2,

$$y(s) = -\Delta\, x(s) \tag{4-8}$$

$$x(s) = M(s)\, y(s) \tag{4-9}$$

Solving (4-9) in terms of x(s) yields,

$$[I + M(s)\Delta]\, x(s) = 0 \tag{4-10}$$

The matrix $[I + M(s)\Delta]$ is known as the return difference matrix. Stability robustness analysis involves finding the size of the (block) diagonal matrix Δ that satisfies $\det[I + M(j\omega)\Delta] = 0$. Doyle, therefore, defined the structured singular value $\mu(M,\omega)$ as,

$$\frac{1}{\mu(M,\omega)} = \min_{\Delta} \{\sigma_{max}(\Delta) \mid \det[I + M(j\omega)\Delta] = 0\} \tag{4-11}$$

where σ_{max} is the largest matrix singular value. The structured singular value computation attempts to find the smallest uncertainty block Δ that can destabilize the feedback system. Since

the minimization problem of Equation (4-11) can be difficult to solve, Doyle derived expressions for upper and lower bounds on the structured singular value. Namely,

$$\max_{U} \rho(UM) \leq \mu(M,\omega) \leq \min_{D} \sigma_{max}(DMD^{-1}) \tag{4-12}$$

where U is unitary and D is a real scaling matrix such that $D\Delta D^{-1} = \Delta$. The lower bound is not used as a measure of robustness but is used to determine how close the upper bound approximates the exact value. For practical systems the upper and lower bounds differ by less than 15% showing the upper bound to be a reasonable approximation.[28] The upper bound is still posed as an optimization problem, but it is one that has no non-global minima.[29] This optimization involves finding the scaling matrix that minimizes the maximum singular value of DMD^{-1}. The optimum scaling matrix D can be found through standard nonlinear optimization techniques, but is often approximated using an iterative method first developed by Osborne.[30] Osborne's technique finds that D which minimizes the Frobenius norm of DMD^{-1}. Because the Frobenius norm acts as an upper bound on the 2-norm (maximum singular value), reducing the Frobenius norm helps reduce the 2-norm.[29] Since the Frobenius norm is an upper bound on the 2-norm, use of Osborne's technique to select D yields a conservative estimate of the stability margin, but the technique is very efficient.

As given above, the elements of Δ can be complex. When the parameter variations modeled in Δ are known to be real only, a less conservative upper bound, developed by Jones [28], can be found for the structured singular value. This upper bound is given by,

$$\mu_r(M,\omega) \leq \min_{D} \{ \max_{\Phi} \sigma_{max}[(DM(j\omega)D^{-1}\Phi + (DM(j\omega)D^{-1}\Phi)^T)/2] \} \tag{4-13}$$

where D is determined as before. The set of matrices defined by Φ contains all possible combinations of ± 1 on the diagonal. These matrices represent the possible directions of variation

(positive or negative) of each of the real uncertainties. Use of the upper bound for real parameter variations yields not only the minimum size of Δ that can destabilize the system, but also the worst case directions for each of the individual variations.

The structured singular value analysis method can also be used to study the effect of isolated, single-valued nonlinear elements on system stability. If a sector can be drawn around the graph of a nonlinear element, then the structured singular value can be used to determine if the sector-bounded nonlinearity can destabilize the closed-loop system. References [31] and [32] describe analysis of nonlinear saturation using structured singular value analysis and sector-bounding methods, respectively.

Whether the matrix Δ represents linear or sector-bounded nonlinear elements, the result of the structured singular value analysis is only the minimum size of Δ. The character of the instability that may result if the size of Δ is greater than the minimum is not known. For example, it is not known whether the resulting instability is purely exponential or oscillatory.

4.3.3.2 M-Δ Construction

An essential part of the stability robustness analysis is the construction of the M matrix shown in Figure 4-2. A first step involves identification of the uncertainties to be analyzed. Three basic types of uncertainty will be considered herein. Figure 4-3 shows a multiplicative uncertainty and a additive uncertainty. The variation (δ) represents a percentage signal change for the multiplicative uncertainty and an absolute change for the additive uncertainty. Figure 4-4 illustrates the modeling of a nonlinear saturation by an equivalent, but uncertain gain. The effect of a saturation element is to reduce the effective gain, down from unity, when the input to the nonlinear element

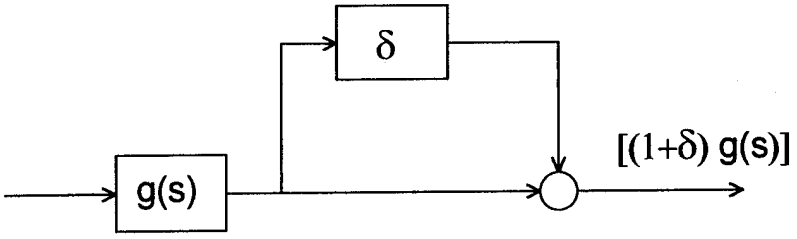

a) Multiplicative Uncertainty

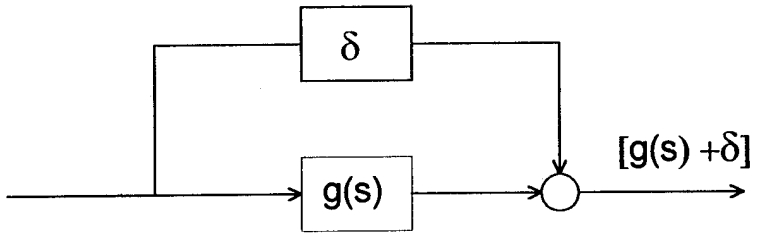

b) Additive Uncertainty

Figure 4-3. Representation of Uncertainty.

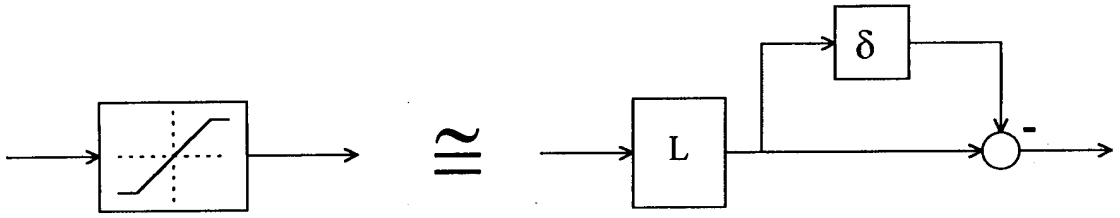

Saturation

Equivalent Gain Representation

Figure 4-4. Representation of a Nonlinear Saturation Element by an Equivalent but Uncertain Gain.

exceeds the saturation limit. Therefore, the effective gain is a function of the input to the nonlinear element.

Once the uncertainties have been identified, the system must be put in the standard M-Δ form for analysis. While some algorithms exist to aid in the construction of the necessary matrix, [33]

it is suggested that a graphical simulation program like SIMULINK™ be used to determine the state-space model for M(s). SIMULINK™ allows the user to linearize a feedback system and define the input and output from any signal in the feedback loop. To linearize a system, SIMULINK™ inport and outport elements are placed around the uncertainties as illustrated in Figure 4-5. This diagram is for multiplicative uncertainty shown in Figure 4-3(a). Note a negative sum is needed to generate the proper representation of M(s) as defined in Figure 4-2. With all the inport/outport pairs in place, a state-space model of M(s) is produced using the MATLAB™ *linmod* command. With M(s) computed, the affect of the modeled uncertainties on system stability is analyzed using the structured singular value method. Note that the system under study can be completely linear (and does not need to be linearized). However, the *linmod* feature of MATLAB™ provides a convenient and useful way to form M(s) for complicated block diagrams.

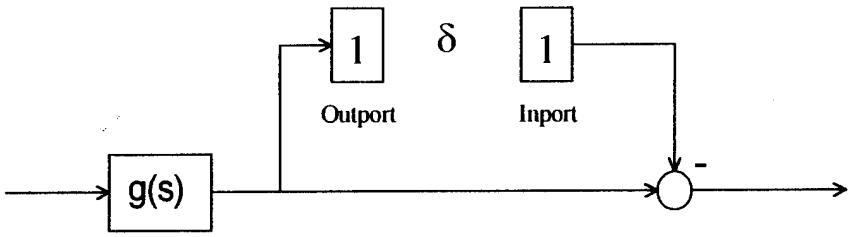

Figure 4-5. Model of Uncertainty in a SIMULINK™ Diagram.

4.3.3.3 Numerical Algorithms

MATLAB™ contains two routines (in the Robust Control Systems toolbox) to calculate the upper bound on the structured singular value (*ssvbode* and *perron*). Both of these algorithms compute the structured singular value bound of Equation (4-12) which considers complex

uncertainties. These algorithms are based on the work of Safonov.[34] These routines can yield overly conservative estimates for systems with only real parameter variations.

For the immediate purpose of analyzing pilot/aircraft systems, only real uncertainties have been considered. Therefore, an algorithm based on that outlined by Reference [29] has been written to calculate the bound of Equation (4-13). The algorithm outline is given below.

Algorithm to Compute Upper Bound on the
Structured Singular Value for Real Parameter Variations

1. Define frequency range of interest, $\omega_i \leq \omega \leq \omega_f$.

2. Set up 2^q x q matrix (Φ_T) whose rows account for the possible permutations of 1 and -1 (q = number of uncertainties).

3. Over all ω,

   a) Calculate the transfer function matrix at $s = j\omega$, i.e. $M(j\omega)$.
   b) Use Osborne's technique to find D.
   c) For each row , k , in Φ_T ,
      1) Calculate diagonal Φ matrix as Φ = diag[k^{th} row of Φ_T].
      2) Find $\sigma_{max}[(DM(j\omega)D^{-1}\Phi + (DM(j\omega)D^{-1}\Phi)^T)/2]$. Store result as SV(k).
   d) Find the maximum value in SV(k) calculated above. This represents $\mu_r(M,\omega)$ at this frequency.

4. Plot the $\log(\mu_r(M,\omega))$ versus $\log(\omega)$.

The maximum (real) structured singular value over all frequencies will be denoted μ_r and will be used to define the maximum allowable variation while guaranteed stability is maintained. Assuming $D=\text{diag}[\delta_1,\delta_2,\ldots,\delta_q]$, the closed-loop system will remain stable as long as $|\delta_i| < 1/\mu_r$.

4.3.3.4 Verification

To ensure the stability robustness algorithms work as desired, an analysis of two configurations of the HAVE PIO database was conducted. Configurations H2-1 and H2-5 were modified to include a first order actuator as shown in Figure 4-6. Table 4-2 gives the vehicle and

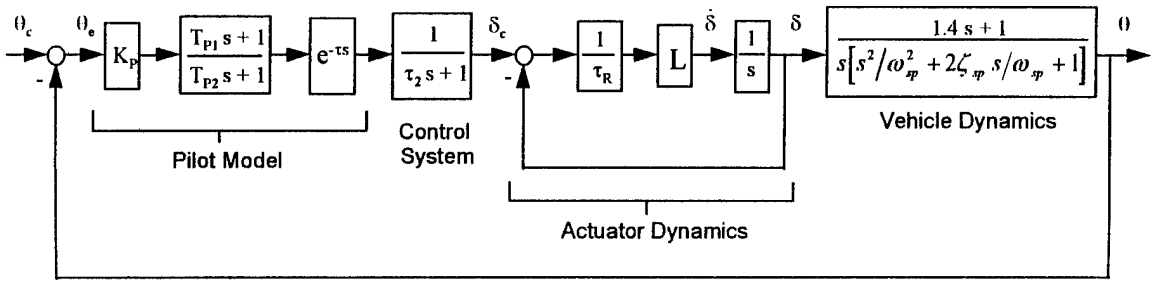

Figure 4-6. HAVE PIO Configuration Model Modified to Include Actuator Dynamics.

Table 4-2. Vehicle and Pilot Model Parameters for Modified HAVE PIO Configurations.

Configuration	ω_{sp} / ζ_{sp} (rad/s/-)	τ_2 (s)	τ_R (s)	L	K_P	T_{P1} (s)	T_{P2} (s)	τ (s)
H2-1	2.4 / 0.64	0	0.05	1.0	0.74	0.27	0	0.3
H2-5	2.4 / 0.64	1.0	0.05	1.0	0.52	2.37	0	0.3

pilot model parameters used in the analysis. The pilot model parameters were chosen using rules from the Neal-Smith criteria.[35]

The two dynamic effects to be considered here are a simultaneous change in pilot gain and control surface actuator rate limiting. The rate limit is modeled by a saturation element in the actuator model and is represented by an equivalent but uncertain gain. A representation of the SIMULINK™ diagram used to define M(s) is shown in Figure 4-7. The first variation represents a percentage change in the pilot gain while the second represents a percentage change in the unity gain model of the saturation element.

Figure 4-8 shows the inverse real structured singular value calculation for both configurations using Equation (4-13). The minimum of the inverse structured singular value plot reveals the

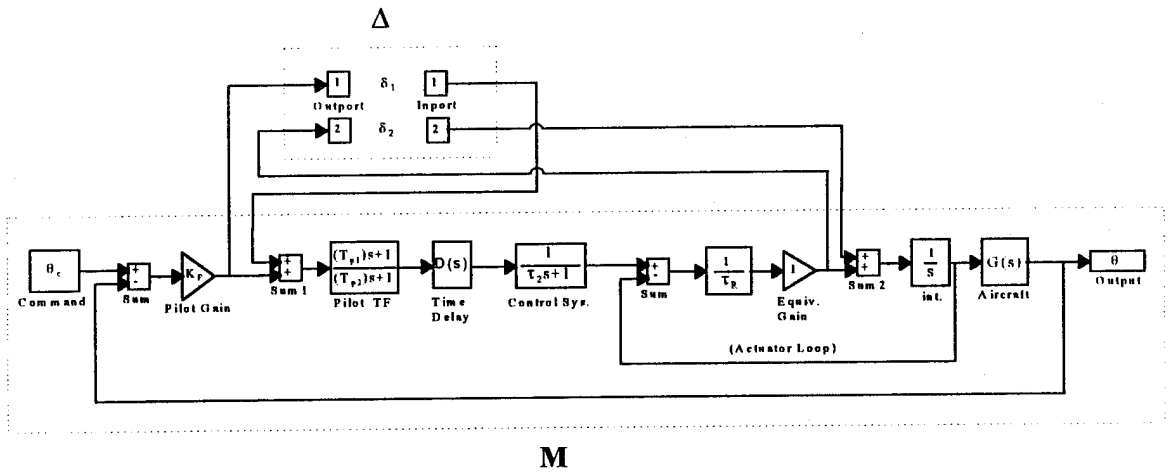

Figure 4-7. SIMULINK™ Diagram Used to Define M(s) for Structured Singular Value Analysis.

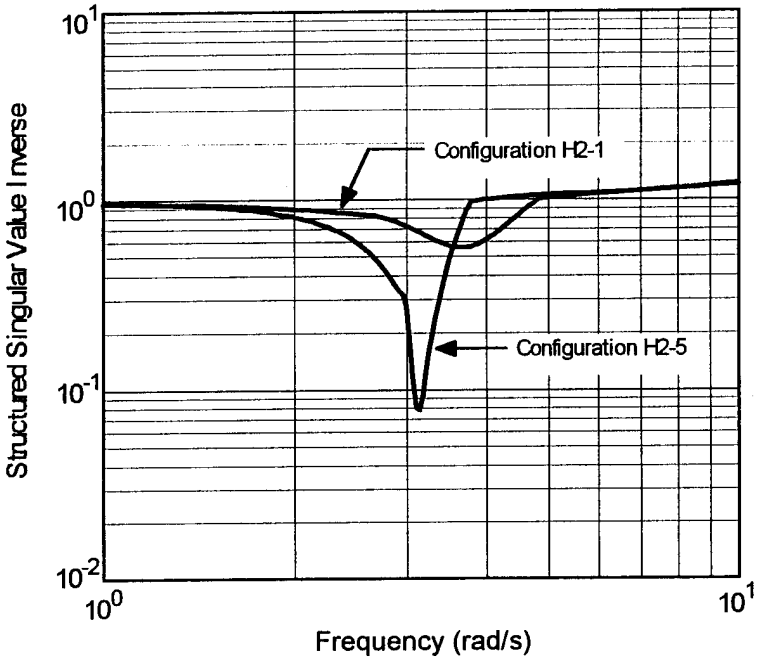

Figure 4-8. Inverse Structured Singular Value of M(s).

largest bound on δ_1 and δ_2 (from Figure 4-7) before instability is possible. The minimum value is 0.56 for configuration H2-1 and 0.08 for configuration H2-5. The structured singular value calculation of Equation (4-13) also reveals the direction of the worst case variation. At the

frequency where the minimum is found, the matrix Φ that maximized (4-13) is Φ = diag[+1, -1]. Therefore, the worst case variation in pilot gain is an increase of $(1+\delta_1)$ and the worst case gain variation due to rate limiting is $(1-\delta_2)$.

The stability boundary calculated from the real structured singular value analysis of configurations H2-1 and H2-5 are shown in Figures 4-9 and 4-10 respectively. The shaded blocks represent values for pilot gain and equivalent gain due to rate limiting for which the structured singular value analysis guarantees stability. A direct calculation of the system poles yields the stability boundaries shown by the solid curves. The dashed lines represent the nominal values of the pilot gains in each case. The nominal value for the equivalent gain due to rate limiting is L = 1. Figures 4-9 and 4-10 illustrate how well the structured singular value approximation fills the stable region in the parameter space. The corners of the structured singular value boundaries

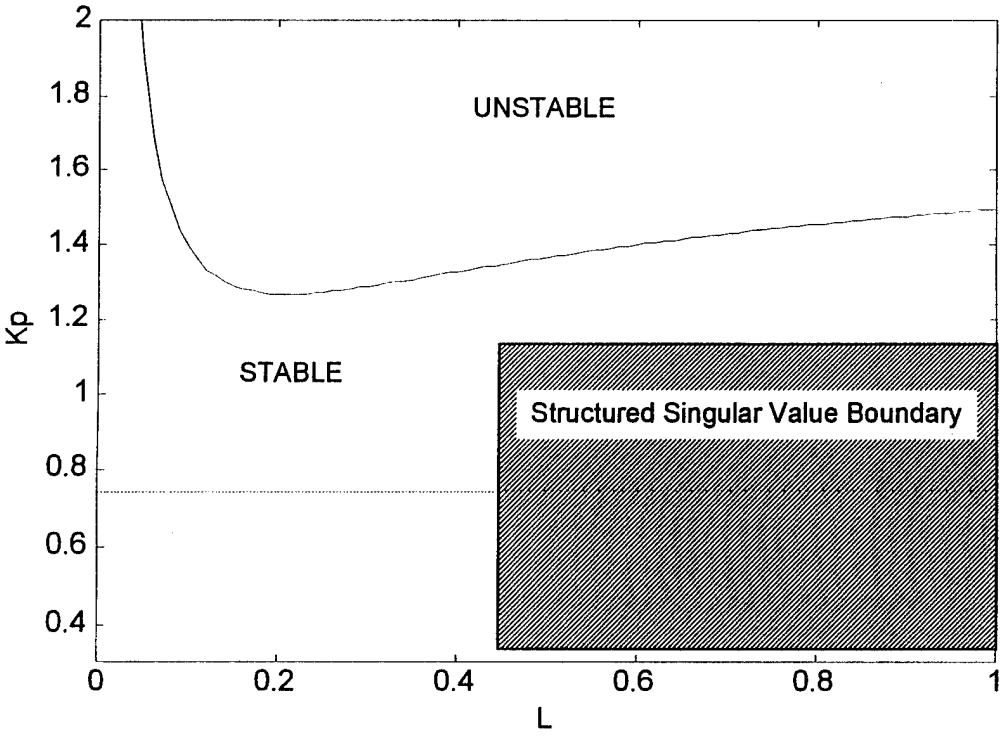

Figure 4-9. Stability Boundary For Configuration H2-1.

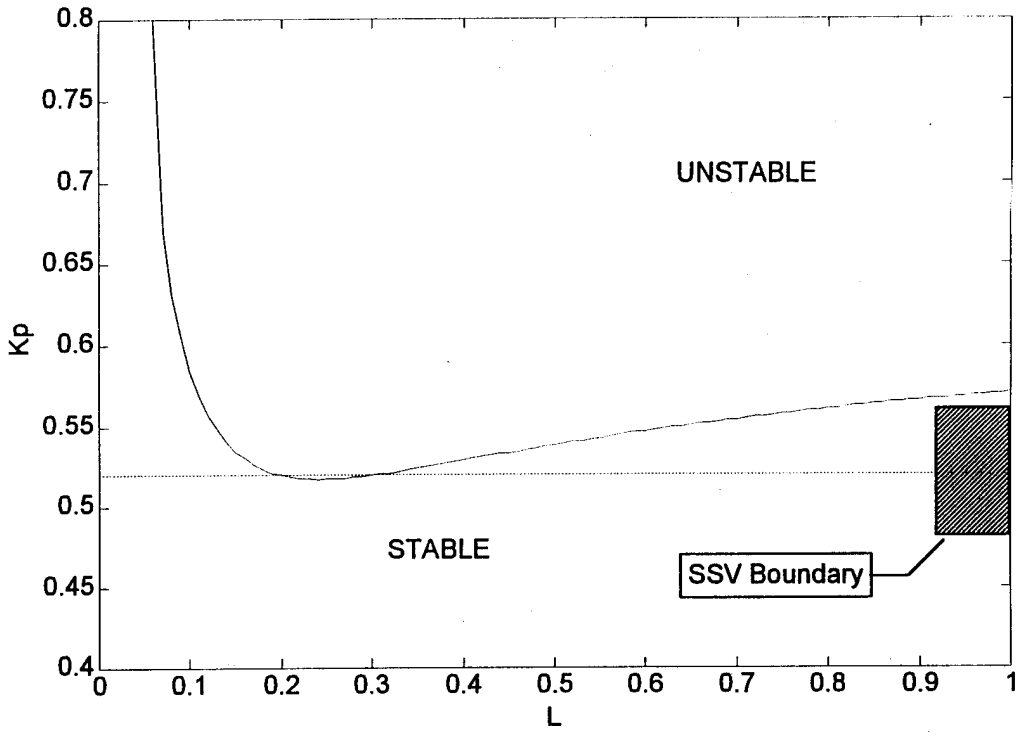

Figure 4-10. Stability Boundary for Configuration H2-5.

closely approach the curves separating the stable and unstable regions in the parameter space indicating the structured singular value to be a good approximation to the actual stability boundary.

4.3.3.5 Summary

When $\Delta=0$, M(s) represents the nominal system. When the uncertain parameters are known to vary over a given range, they are usually scaled such that $-1 \leq \delta \leq 1$ encompasses the given variation. With a scaled system and $1/\mu_r \geq 1$, the system can handle the given variation and remain stable. If $1/\mu_r \leq 1$, then the system can tolerate variations up to at least $1/\mu_r$ while maintaining system stability. For the case of a variation in a unity gain representing a saturation element, the value of $1/\mu_r$ represents the percent saturation of the element. That is, the system can

tolerate an input to a nonlinear element up to $\mu_r/(1-\mu_r)$ percent greater than the saturation limit while guaranteed stability is maintained.

4.3.4 Multivariable Describing Functions

Some researchers have noted that PIOs are analogous to limit cycles.[36,25] A limit cycle is an unforced, sustained oscillation of a nonlinear system. The dynamics associated with pilot/aircraft interaction are fundamentally nonlinear. In fact, both the pilot and aircraft are very complicated nonlinear systems. Graham and McRuer also note that friction and hysteresis characteristics of early jet fighter flight control systems led to serious PIOs.[36] Thus, methods for predicting limit cycles for nonlinear systems should also be considered in the development of new, unified PIO analysis methods.

A useful class of nonlinear systems includes nonlinearities isolated as separate entities while the remaining linear elements are represented in lumped-parameter form. For this particular class of systems, an analysis based upon quasi-linear harmonic approximations is readily completed. The quasi-linear approximations are usually known as describing functions.[37,38] For PIO analysis, a describing function approach is particularly attractive as it has close ties with linear frequency-domain analysis. Most existing PIO analysis methods are also based on control-theoretic, frequency-domain methods.

4.3.4.1 Basic Theory

Assume the input to a single-input, single-output nonlinear element is sinusoidal with a given amplitude and frequency. The output of the nonlinear element will generally not be sinusoidal, but will be periodic with the same period as the input sinusoid. If the output wave is then analyzed in terms of its Fourier components, the fundamental component can be related to the

input in familiar terms of an amplitude ratio and a phase angle. The complex ratio of the fundamental component of the output to the input is defined as the sinusoidal input describing function (SIDF).[37]

For a sinusoidal input to the nonlinear element, $x(t) = \alpha \sin(\omega t)$, the output y(t) is expressed in terms of its Fourier series. Namely,

$$y(t) = a_0 + \sum_{n=1}^{\infty} (a_n \cos n\omega t + b_n \sin n\omega t) \tag{4-14}$$

where,

$$a_n = \frac{1}{\pi} \int_0^{2\pi} y(t) \cos n\omega t \, d(\omega t)$$
$$b_n = \frac{1}{\pi} \int_0^{2\pi} y(t) \sin n\omega t \, d(\omega t)$$

For a skew symmetric nonlinearity, $a_0 = 0$, the fundamental component of the output becomes,

$$y_1(t) = a_1 \cos \omega t + b_1 \sin \omega t \tag{4-15}$$

The describing function is then given by,

$$N(\alpha, \omega) = \frac{\sqrt{a_1 + b_1}}{\alpha} \angle \phi_1 \quad , \phi_1 = \tan^{-1}\left(\frac{a_1}{b_1}\right) \tag{4-16}$$

and a_1 and b_1 are obtained using the integral expressions in (4-14). In general the describing function can depend on both the amplitude and frequency of the input signal. However, when the nonlinearity contains no energy storage element, N is a function of amplitude only.[39] All simple (single valued) nonlinearities and many complex nonlinearities have describing functions which are frequency invariant. Table 4-3 lists 4 nonlinearities and their frequency invariant describing functions.

Table 4-3. Four Nonlinearities and the Corresponding Sinusoidal Input Describing Functions.

Nonlinear Element	Sinusoidal Input Describing Function
Saturation 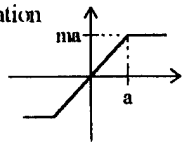	m (for $\alpha/a \le 1$) $\frac{2m}{\pi}\left[\sin^{-1}(a/\alpha)+(a/\alpha)\sqrt{1-(a/\alpha)^2}\right]$ (for $\alpha/a \ge 1$)
Dead-zone 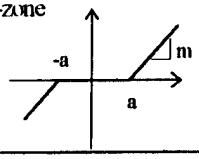	0 (for $\alpha/a \le 1$) $m-\frac{2m}{\pi}\left[\sin^{-1}(a/\alpha)+(a/\alpha)\sqrt{1-(a/\alpha)^2}\right]$ (for $\alpha/a \ge 1$)
Contactor 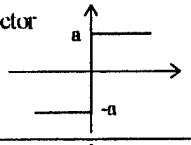	$\frac{4a}{\pi\alpha}$
Preload 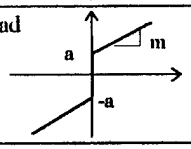	$m+\frac{4a}{\pi\alpha}$

Figure 4-11 shows an example of replacing a nonlinear element by its SIDF resulting in a quasi-linear feedback system. The remnant consists of the higher harmonics of the Fourier series of the output (terms with $n > 1$ in Equation (4-14)). The output of the actual nonlinearity is equal to the sum of the input times the SIDF plus the remnant. In considering only the fundamental harmonic when developing the describing function, it is automatically assumed that the remnant has little affect on the system output. This assumption holds if the linear part of the system is sufficiently low-pass as to attenuate the higher harmonics present in the remnant. Also, the maximum amplitude present in the remnant is normally much less than the magnitude of the fundamental harmonic. For the case of a saturation nonlinearity and a K/s type plant, Reference [37] states the largest term in the remnant (which is the third harmonic) is never more than 28% of the amplitude of the fundamental component of the output of the nonlinearity. When attenuated by the integrator, the amount of the third harmonic present in the error signal , x(t), as

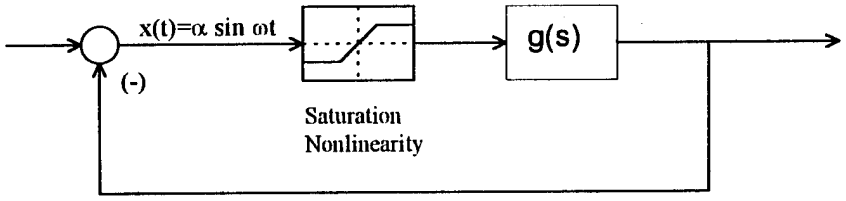

a) Nonlinear System

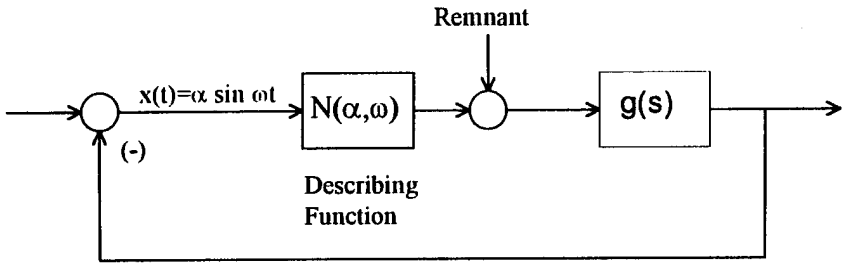

b) Quasi-Linear System

Figure 4-11. Replacement of a Nonlinear Element by a Sinusoidal Input Describing Function.

compared to the fundamental is not more than 9%. This value is a measure of the error introduced by ignoring the contribution of the remnant.

Although the above discussion considers a single-loop system with a single nonlinearity, extension to a multi-loop multiple-nonlinearity system is straightforward. Let Δ from Figure 4-2 represent a diagonal matrix of nonlinear elements and M(s) now represents the linear part of the system as seen by the nonlinear elements in Δ. Assume that the input signal to each nonlinear element in Δ is sinusoidal and oscillating at the same frequency ω, so that,

$$x_i = \alpha_i \sin(\omega t + \theta_i) \tag{4-17}$$

Again, to use describing function approximations, the linear part of the system represented by M(s) is assumed to act like a low-pass filter so that superharmonic signal components can be

neglected in the analysis. Under these assumptions, the nonlinear elements can be replaced by their sinusoidal-input describing functions (SIDF), i.e.,

$$\Delta \rightarrow N(A,\omega) \tag{4-18}$$

where 'A' is a vector containing the amplitudes of the sinusoids entering each nonlinear element and $N(A,\omega)$ is a diagonal matrix of describing functions made up of individual elements like those in Table 4-3.

In order to investigate the stability of the multivariable nonlinear feedback system, solution of the system characteristic equation is considered. Since it is assumed that each feedback loop is oscillating at the same frequency, the Laplace operator in (4-10) can be replaced with $s=j\omega$. Equation (4-10) then becomes,

$$[I + M(j\omega)N(A,\omega)]\, x(j\omega) = 0 \tag{4-19}$$

Equation (4-19) represents the harmonic-balance equations for the system. Solutions to (4-19) predict the existence of a limit cycle.

4.3.4.2 M-Δ Construction

Within the current framework, it is convenient to cast the multivariable describing function problem in a form similar to the stability robustness analysis. Using a standard M-Δ configuration to define the structure of the nonlinear system brings a needed organization to the general problem of predicting the occurrence of limit cycle behavior. In this case, M(s) represents the transfer function matrix as seen by each nonlinear element and as such can contain parts of the vehicle, control system, and pilot. It is suggested that a state-space representation of M(s) be found in a manner analogous to that of Section 4.3.3.2. Figure 4-12 shows how the SIMULINK™ inport and outport blocks are used to separate out a typical nonlinear element.

Note a gain of -1 must be added at either the inport or outport if the form of Equation (4-19) is to be used. If no such gain is added, then the negative of the transfer function matrix (-M(s)) is returned from the *linmod* command.

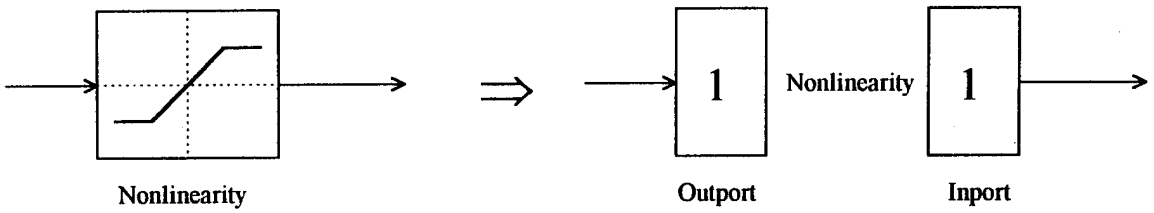

Figure 4-12. Model of Nonlinear Element in SIMULINK™ Diagram for M-Δ Construction.

4.3.4.3 Numerical Algorithms

Since $x(j\omega) = 0$ represents a trivial solution to (4-19), many researchers have used the following determinant to predict limit cycles,

$$\det [I + M(j\omega)N(A,\omega)] = 0 \qquad (4\text{-}20)$$

Alternatively, one could search for values of ω and A that yield one or more zero eigenvalues of $[I + M(j\omega)N(A,\omega)]$ or eigenvalues of $[M(j\omega)N(A,\omega)]$ equal to $-1+j0$.[40]

There are several computational methods available to aid in the search for limit cycle behavior. Besides searching (4-19) or (4-20) directly, Gray and Nakhla use Gershgorin bands as an eigenvalue check.[41] Gray and Taylor have developed a search method that considers each feedback loop in a sequential order, while systematically eliminating solution possibilities throughout the search.[42] Chang, et. al. have recently extended the sequential loop method of Gray and Taylor to include a homotopy algorithm with claims of global convergence.[43] At

about the same time, Pillai and Nelson reported search method results based upon Newton-Raphson optimization methods.[44]

The method of Chang, et. al. warrants further explanation as it is easily implemented under the current M-Δ formulation. Also, the use of a linear homotopy to improve the convergence of the search algorithm is desirable. When cast in the standard M-Δ form above, the set of nonlinear equations that Chang refers to as "auxiliary characteristic equations" reduce exactly to equation (4-19). This equation can be rewritten as a set of n complex nonlinear equations (one for each nonlinear element) of the form,

$$f_i = x_i(j\omega) + \sum_{k=1}^{n} M_{ik}(j\omega)\, N_k(A_k, \omega)\, x_k(j\omega) = 0 \tag{4-21}$$

where $x_i(j\omega)$ is the result of replacing $s=j\omega$ in the Laplace transform of $x_i(t)$ of Equation (4-17). With some straightforward substitutions and cancellations, it can be shown that for numerical solution, $x_i(j\omega)$ in the above equation can be replaced by,

$$x_i(j\omega) \rightarrow x(A_i, \theta_i) = A_i e^{j\theta_i} \tag{4-22}$$

The existence of a limit cycle is then found by solving the system of n complex equations given in (4-21), with the substitution of (4-22), for the 2n unknowns $(A_1,\omega,A_2,\theta_2,\ldots,A_n,\theta_n)$. The phase angle of the sinusoid entering the first nonlinear element is taken to be zero ($\theta_1=0$) without loss of generality.

When a good initial guess of the solution is available, the system of nonlinear equations can likely be solved by any method normally used for nonlinear systems (e.g. Newton-Raphson). However, since an adequately good guess is not always available, a homotopy method of solution is recommended. Define the linear homotopy H as,

$$\vec{H}(\vec{z}, t) = (1 - t)(\vec{z} - \vec{z}_0) + t\vec{f}(\vec{z}) \tag{4-23}$$

The solution of $\vec{H} = \vec{0}$ for all $t \in [0,1]$ forms a space trajectory. For t = 0, the solution is simply $\vec{z} = \vec{z}_0$. At t = 1, the solution is that desired $\vec{H} = \vec{f} = \vec{0}$. Therefore if one can trace the solution $\vec{H} = \vec{0}$ from t = 0 to t =1, the desired solution will have been reached. One way to trace the solution is to integrate the differential equation obtained by taking the total derivative of $\vec{H}$ with respect to t. Namely,

$$\frac{d\vec{z}}{dt} = -\left[\frac{\partial \vec{H}(\vec{z}, t)}{\partial \vec{z}}\right]^{-1} \frac{\partial \vec{H}(\vec{z}, t)}{\partial t} \tag{4-24}$$

where,

$$\frac{\partial \vec{H}(\vec{z}, t)}{\partial \vec{z}} = (1 - t)I + t\frac{\partial \vec{f}(\vec{z})}{\partial \vec{z}} \qquad \frac{\partial \vec{f}(\vec{z})}{\partial \vec{z}} = \begin{bmatrix} \frac{\partial f_1}{\partial z_1} & \cdots & \frac{\partial f_1}{\partial z_n} \\ \vdots & \ddots & \vdots \\ \frac{\partial f_n}{\partial z_1} & \cdots & \frac{\partial f_n}{\partial z_n} \end{bmatrix}$$

$$\frac{\partial \vec{H}(\vec{z}, t)}{\partial t} = -(\vec{z} - \vec{z}_0) + \vec{f}(\vec{z})$$

The necessary partial derivatives can be computed numerically if desired.

When a solution is obtained, it indicates the frequency of the resulting oscillation along with the input amplitudes and phase angles to each isolated nonlinear element. Since the solution of a limit cycle governs the behavior of a dynamic system, it is reasonable to speak of the stability of the limit cycle. When a system that has fallen into a stable limit cycle is perturbed slightly from the limit cycle condition, the system will return to the limit cycle. If a system were able to operate at an unstable limit cycle condition and was perturbed slightly from that condition, it would not return. The resulting behavior could be divergent, asymptotically stable, or could converge to a different (stable) limit cycle. For this reason, an unstable limit cycle cannot be observed experimentally. According to Chang[43], the stability of the limit cycle is determined by

considering a real perturbation in the limit cycle frequency, $s = \sigma + j\omega$. The limit cycle will be stable as long as $d\sigma/dA_1 < 0$.

Graham[37] further distinguishes between soft and hard self excitation of a stable limit cycle. Soft self excitation exists when any nonzero initial condition will result in the sustained oscillation of the stable limit cycle. Soft self excitation is common in systems where the linear transfer function matrix describes an unstable system. On the other hand, hard self excitation exists when the input and subsequent removal of a certain amplitude or wave form signal is required to excite the oscillation.

4.3.4.4 Verification

To ensure the multivariable describing function analysis methods work as desired, an analysis based on that of Reference [4] is given. Reference [4] considers three alternative longitudinal and lateral/directional limited authority back-up control systems for the F-4C. The research of Reference [4] was undertaken to develop analytical techniques for determining the minimum levels for the back-up control system parameters. A companion project utilized piloted, fixed-base simulation to empirically determine the minimum levels for the back-up control system parameters. A PIO analysis is conducted in the reference by applying sinusoidal input describing function theory. Susceptibility to initiating an oscillation is investigated by assuming the pilot controls in a normal way except the amount of lead equilization is reduced. The ability to sustain the oscillation is investigated assuming the pilot behaves in a synchronous manner. The dynamic model contains two types of nonlinear elements: actuator rate and displacement limits for a fully powered manual control system, and direct manual control authority limits determined by pilot strength or by control surface travel stops.

Figure 4-13 shows the block diagram for the longitudinal back-up control system A. The shorthand notation used in Figure 4-13 is $(\omega) = (s+\omega)$. The parameters for the pilot loop closures for the configuration in Figure 4-13 are given in Table 4-4. The pilot model is used as given in Reference [4] and was developed using techniques based on the crossover pilot model.

Table 4-4. Model Parameters for the F-4C.

K_u = 30.0 unit thrust/(ft/sec)	K_θ = -0.393	$K_{\dot{\theta}}$ = -0.244 sec
K_d = -0.03 deg/ft	$K_{\dot{d}}$ = -0.0015 deg/(ft/sec)	τ_T = 0.33 sec
τ_s = 0.2 sec	ω_n = 10 rad/sec	ω_2 = 0.5 rad/sec
ω_3 = 10 rad/sec	ω_4 = 2.25 rad/sec	

Figure 4-14 shows the deflection and rate limited actuator model used in the describing function analysis. Reference [4] develops a single SIDF for the combination of the two nonlinear elements represented in Figure 4-14 and uses graphical means to predict the existence of limit cycles. However, the methods of this section can be employed to treat the two nonlinear elements as separate entities. The SIMULINK™ diagram needed to define M(s) is given in Figure 4-15. The first inport/outport pair corresponds to the actuator rate limit while the second inport/outport pair corresponds to the actuator deflection limit.

The results of applying the limit cycle search algorithms given in Section 4.3.4.3 are presented in Tables 4-5 and 4-6. Also shown in the tables are the results from the given reference. A dash in a column indicates that no limit cycle is predicted for the corresponding configuration. The tables show results for all configurations studied in Reference [4] though only longitudinal back-up control system A has been presented in any detail here. The results found with the current method agree extremely well with those given in the reference. The newly calculated amplitudes

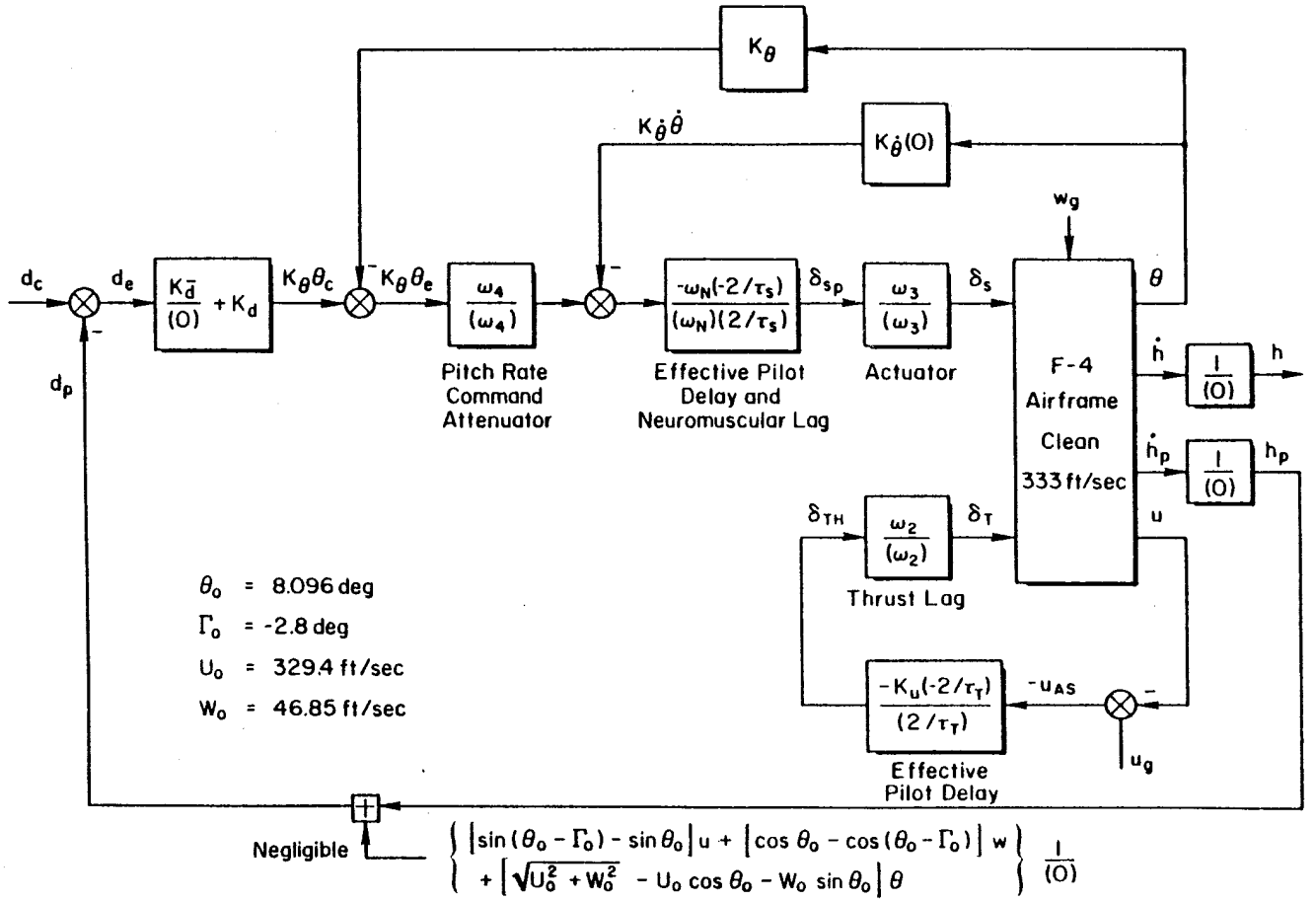

Figure 4-13. Longitudinal Block Diagram for F-4C Back-up Control System A.

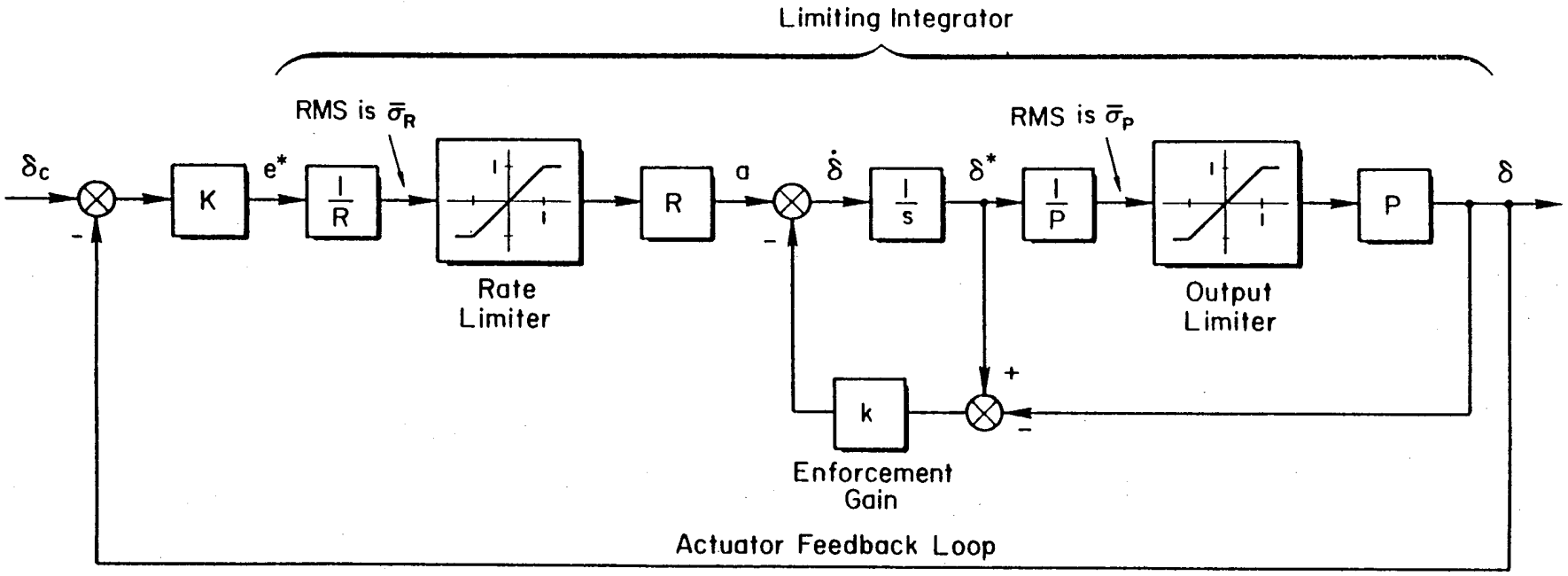

K = Small Signal Open Loop Gain of Actuator

R = Rate Limit

P = Output Limit

Figure 4-14. Rate and Position Limited Actuator.

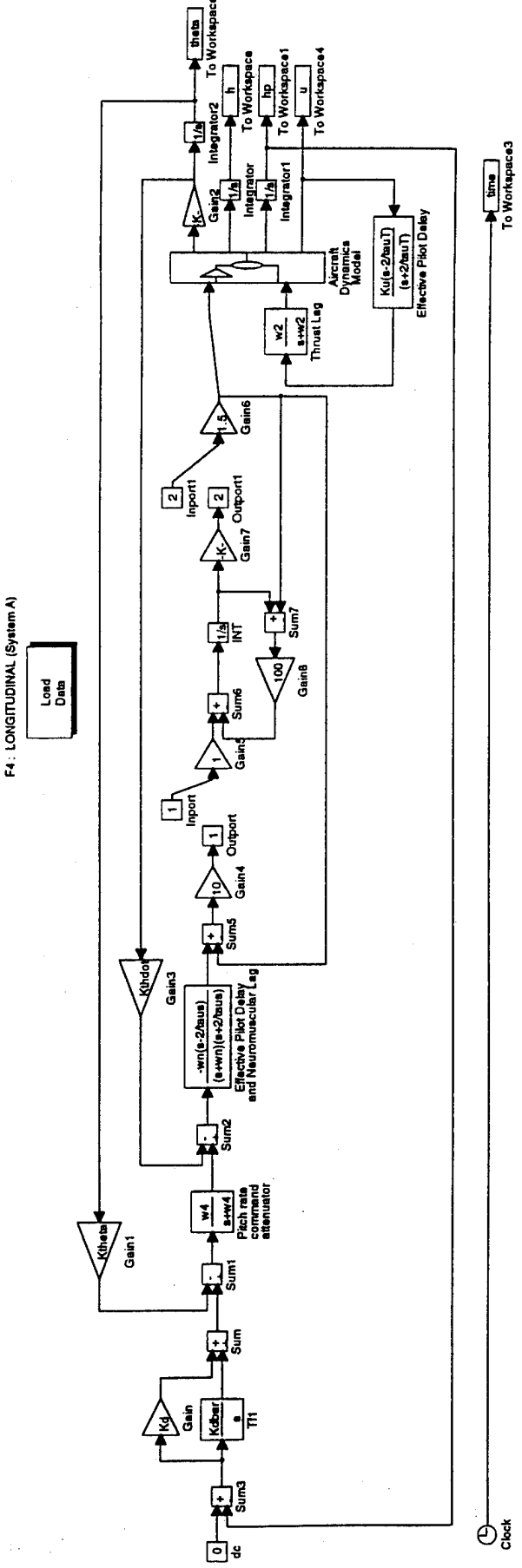

Figure 4-15. SIMULINK™ Diagram for Describing Function Analysis.

vary by less than 5% from those given except for lateral/direction system C which varied by 10%. The predicted frequencies vary by less than 3% from those given in the reference. Since the amplitudes have been scaled such that values greater than unity indicate limiting of the saturation elements, it is seen that only lateral/directional system A is simultaneously rate and position limited.

Table 4-5. Comparison of Limit Cycle Results for the Longitudinal Systems.

			Reference [4]			Multivariable Analysis			
Back-up System	τ_s (sec)	$K_{\dot{\theta}}$ (sec)	Rate Amp.	Deflection Amp.	ω (rad/s)	Rate Amp.	Deflection Amp.	ω (rad/s)	Phase Difference (deg)
A	0.2	0	12.3	-	1.1	12.2	0.79	1.07	-90
A	0	0	10.0	-	1.2	10.4	0.71	1.19	-90
B	0.2	0	-	1.3	1.4	-	1.30	1.43	-
B	0	0	-	-	-	-	-	-	-

Table 4-6. Comparison of Limit Cycle Results for the Lateral/Directional Systems.

			Reference [4]			Multivariable Analysis			
Back-up System	τ_a (sec)	$K_{\dot{\phi}}$ (sec)	Rate Amp.	Deflection Amp.	ω (rad/s)	Rate Amp.	Deflection Amp.	ω (rad/s)	Phase Difference (deg)
A	0.2	0	15.0	1.0	0.14	14.3	1.01	0.14	-4
B	0.2	0	-	4.3	0.13	-	4.4	0.13	-
C	0.2	0	-	5.0	0.23	-	4.5	0.23	-

Figure 4-16 shows the simulation results for longitudinal system A with $\tau_s = 0.2$. The resulting amplitudes, frequency, and phase are seen to be as predicted by the multivariable analysis techniques. Figures 4-17 and 4-18 show the altitude-altitude rate phase plane for the same configuration as Figure 4-16 for small and large initial conditions respectively. The resulting closed curves on the phase plane are characteristic of limit cycles and it is noted that the same closed curve is obtained for both initial conditions.

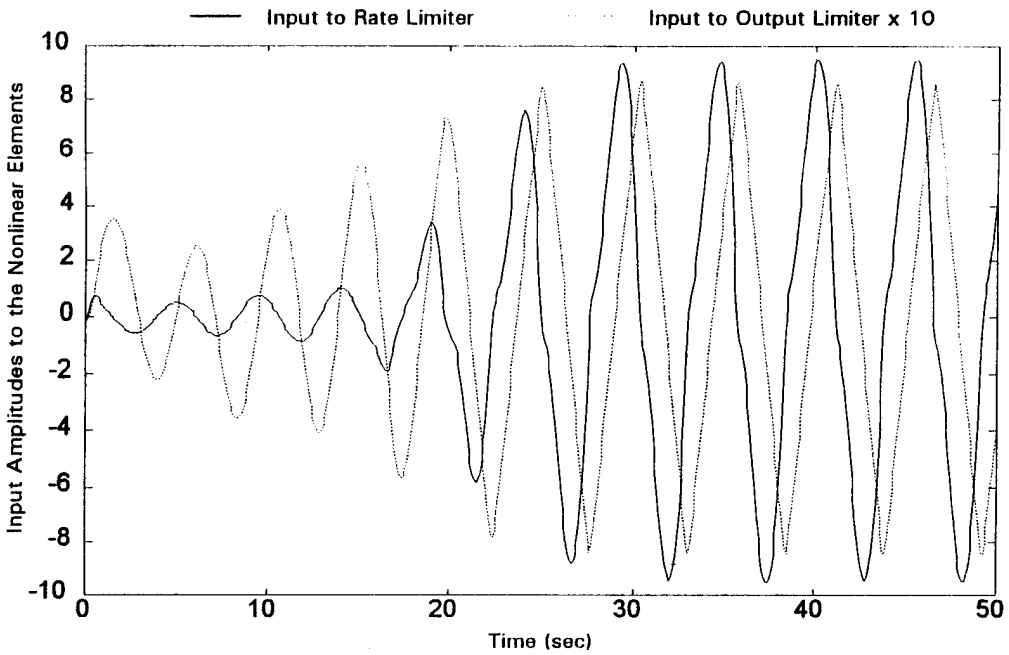

Figure 4-16. Simulation Results for F-4C.

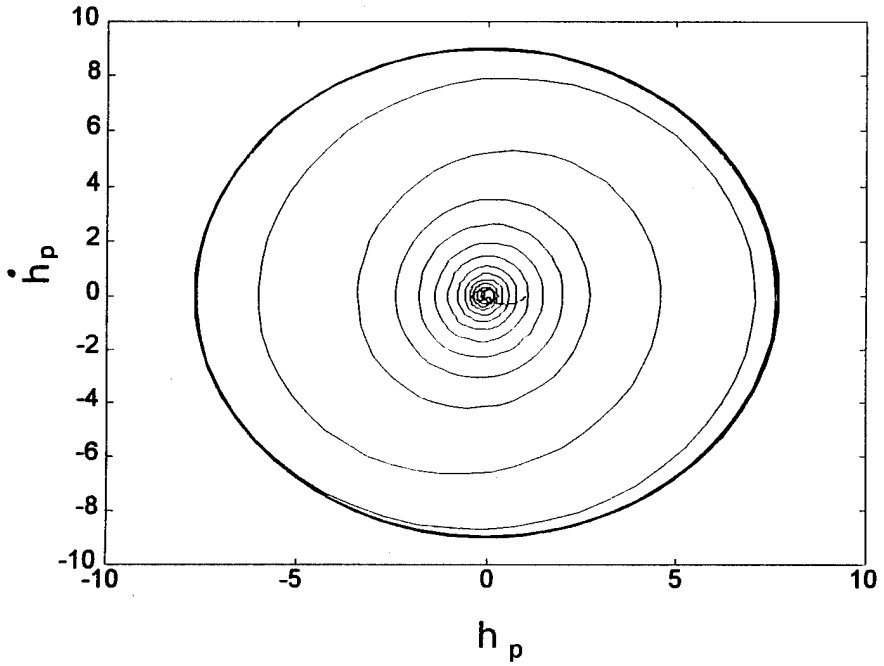

Figure 4-17. Altitude-Altitude Rate Phase Plane (Small Initial Condition).

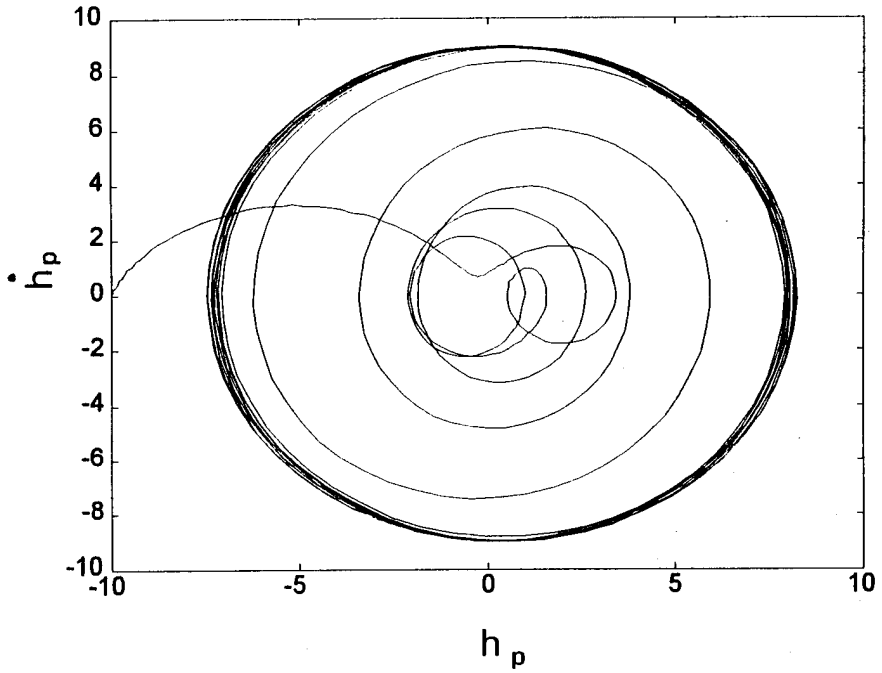

Figure 4-18. Altitude-Altitude Rate Phase Plane (Large Initial Condition).

While Equation (4-21) can be searched directly using a nonlinear equation solver, often times a good initial guess is necessary to ensure convergence. For this reason, the homotopy method as described above is used as the first solution technique. Since the homotopy algorithm can be slow to converge when using numerical partial derivatives, and since nonlinear equation solvers can be quite rapid when in the neighborhood of a solution, a combination of the two methods can be useful in obtaining the solution in the following manner. An initial guess is obtained from examining the stability robustness results. The homotopy equations are integrated using a low tolerance to yield a new initial guess. The nonlinear equation solver can then be employed to yield a more accurate solution.

4.3.4.5 Summary

Describing function analysis provides more information about instability than structured singular value analysis because more information is known about how the model parameters vary. The structured singular value calculation yields a bound on the largest parameter variation or the largest sector bound of a nonlinearity. The describing function analysis, on the other hand, yields the magnitude and phase of resulting oscillations. However, the describing function analysis requires a fairly sophisticated search for solutions whereas computationally efficient approximations to the structured singular value are well-known. As a result, these two analysis methods are very complementary to the study of pilot-in-the-loop oscillations. Also, the existence of hard self excitations may help explain why certain aircraft exhibit acceptable flying qualities for some pilots and yield severe PIOs for others. Recall, hard self excitation describes the condition where a certain amplitude or waveform of an input signal is necessary to excite the limit cycle.

4.3.5 Unified Single-Loop Analysis

This report section will establish ties between existing single, closed-loop PIO analysis methods and multivariable stability robustness methods. The purpose of this discussion is not to refute any existing methods but to show how these PIO analysis methods are closely related to concepts in stability robustness theory. In fact, the existing methods will form a foundation to establish a specific new single-loop criteria.

4.3.5.1 Develop Pilot Model

For the examples of this section, three different types of pilot models are considered. Both synchronous and MOCM pilot models are used in the stability robustness analysis of Section 4.3.5.3. For the synchronous (pure gain) pilot model, the pilot gains were chosen such that the

pilot/vehicle transfer functions have at least 6dB of gain margin and 45 degrees of phase margin. The values for the MOCM model are as given in Table 4-1 and were chosen as in Reference [11] with the disturbance filter taken as $1/(s+1)^2$. Smith's nonlinear contactor pilot model is used for the describing function analysis of Section 4.3.5.4.

4.3.5.2 Identification of the Dynamic Elements Suspected of Contributing to PIO

PIO susceptibility will be examined in the face of variations in the pilot model. For this section, the variation will be taken as a multiplicative uncertainty in pilot equalization.

4.3.5.3 Stability Robustness Analysis

The standard form M-Δ diagram is shown in Figure 4-2. A feedback loop uncertainty or variation is represented by the matrix Δ while M(s) represents the linear, lumped parameter part of the feedback system. The harmonic balance equations are found by substituting $s=j\omega$ in (4-10) to yield,

$$[I + M(j\omega)\Delta]\, x(j\omega) = 0 \tag{4-25}$$

Note that Δ may also be a function of frequency, i.e. $\Delta(\omega)$. Since we are interested in non-trivial solutions ($x(j\omega) \neq 0$), one can search for solutions of (4-25) above from,[41,42]

$$\det[I + M(j\omega)\Delta] = 0 \tag{4-26}$$

For this section only, we will consider only a single variation parameter. Thus, the matrix Δ is actually a scalar variable that will be called δ_m and M(s) is a single-input, single-output transfer function that will be represented by m(s). Under these conditions, Equation (4-26) becomes,

$$1 + m(j\omega)\delta_m = 0 \tag{4-27}$$

or,

$$m(j\omega) = -1/\delta_m \tag{4-28}$$

Now consider the block diagram shown in Figure 4-19. This block diagram represents a pilot/aircraft closed-loop system. The transfer function g(s) models the aircraft while $p_o(s)$ models the (nominal) pilot. The parameter δ will represent in-line multiplicative variations in the pilot equalization. These variations might come from inappropriate pilot action, for example. One might think of the actual pilot p(s) as a multiplicative combination of a nominal model $p_o(s)$ and a variation δ, i.e. $p(s) = \delta p_o(s)$.

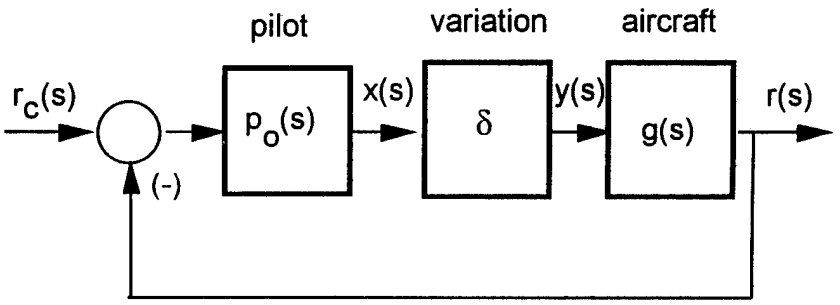

Figure 4-19. Single Loop Pilot/Aircraft System.

The governing equations for the block diagram of Figure 4-19 are,

$$y(s) = \delta x(s) \tag{4-29}$$

$$x(s) = -p_o(s)g(s)y(s) \tag{4-30}$$

Substituting (4-29) into (4-30) yields,

$$[1 + p_o(s)g(s)\delta]x(s) = 0 \tag{4-31}$$

so that the harmonic balance equations for this case are,

$$[1 + p_o(j\omega)g(j\omega)\delta]x(j\omega) = 0 \tag{4-32}$$

Ignoring the trivial solution of (4-32), we are therefore interested in solutions to,

$$1 + p_o(j\omega)g(j\omega)\delta = 0 \tag{4-33}$$

or,

$$p_o(j\omega)g(j\omega) = -1/\delta \tag{4-34}$$

Comparing (4-34) and (4-28), one should quickly see that m(s) is simply the open-loop transfer function $p_o(s)g(s)$. The pilot model variation parameter δ is identical to δ_m. Equation (4-34) can be used to describe several existing PIO analysis methods.

Let the variation parameter in Figure 4-19 be an arbitrary change in pilot gain. Let δ be written as $\delta = K_\delta$, where K_δ represents the change in pilot gain. Assuming a synchronous nominal pilot model K_p, the harmonic balance equation (4-34) is then,

$$K_p g(j\omega) = -1/K_\delta \tag{4-35}$$

Unfortunately, we do not have a specific value of K_δ to test (4-35) for a given airplane. It is expected that the actual pilot gain variation would occur when the pilot becomes excited or agitated during a PIO event. One might expect that an aircraft that resists changes in pilot gain might be less susceptible to PIO than an airplane that is very sensitive to pilot gain changes.

The stability test implied by (4-35) is simply a test for adequate gain margin of the pilot/aircraft system. This test can be performed using a Nyquist plot or a Bode diagram as shown in Figure 4-20 for Configurations H2-1 and H2-5 of the HAVE PIO database. Using the synchronous pilot model, the nominal pilot gains for Configurations H2-1 and H2-5 were chosen as $K_p = 1.24$ and $K_p = 1.09$ respectively.

The first thing to notice in Figure 4-20 is that the gain margin of Configuration H2-1 is much larger than H2-5. The average PIO rating for Configuration H2-1 was 1.0 while the average rating for H2-5 was 4.33 (a rating above 2.0 is considered PIO susceptible). Consequently, one might claim that the gain margin is a good indicator of PIO susceptibility. Figure 4-21 shows the gain margin for each of the eighteen HAVE PIO configurations plotted with the average PIO

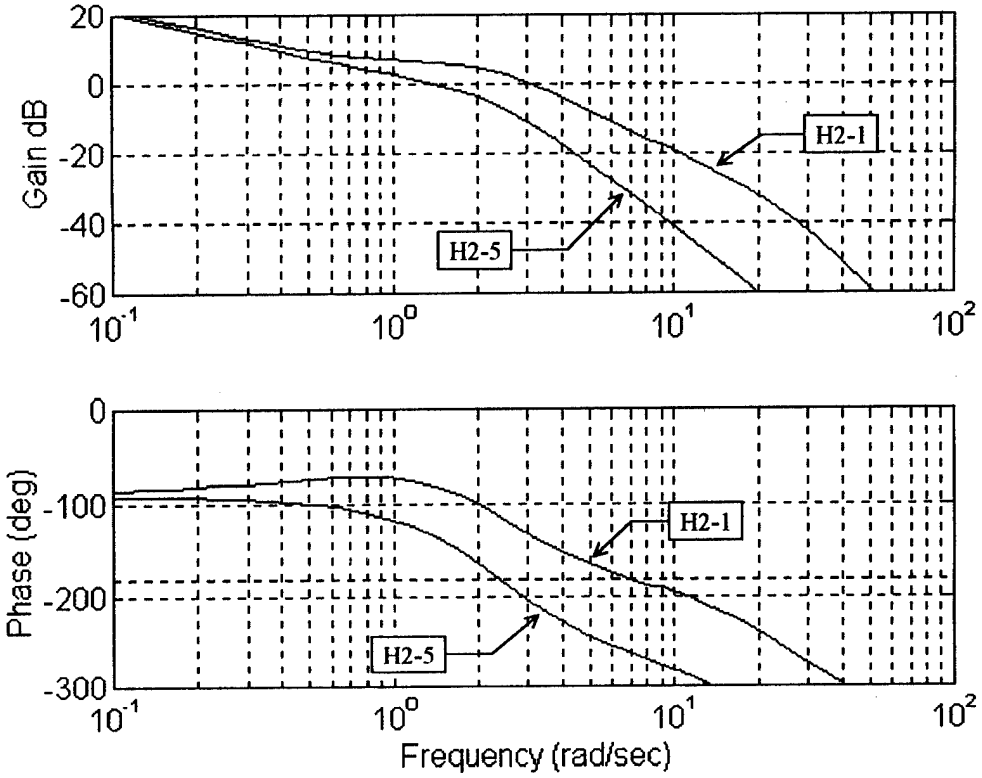

Figure 4-20. Bode Plots for HAVE PIO Configurations H2-1 and H2-5.

rating given during flight. As expected, Figure 4-21 shows that the PIO rating has a definite correlation with gain margin. The configurations with large relative gain margins tend to have lower PIO ratings. However, one can also see from Figure 4-21 that some configurations with small relative gain margins (on the order of 2-3 absolute) still yield low PIO ratings.

Figure 4-20 also shows that the phase margins for Configuration H2-1 and H2-5 are nearly identical. The identical phase margins stem from the criteria used to choose the nominal synchronous model pilot gain K_p (to insure at least 45 deg phase margin and 6 dB gain margin). Thus, using this method for choosing pilot gain leads to the conclusion that phase margin does not seem to correlate with PIO rating.

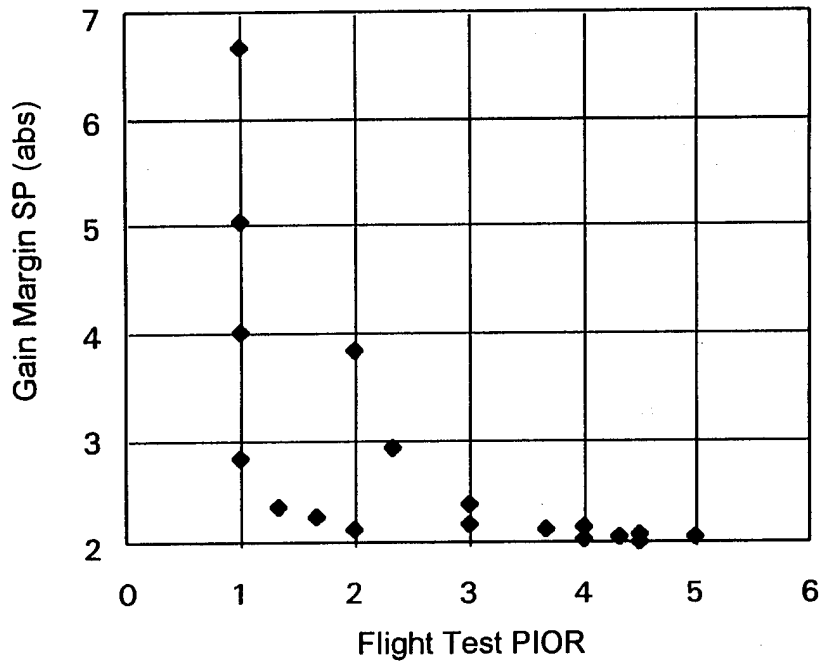

Figure 4-21. HAVE PIO Configuration Gain Margins.

Hess and Kalteis have developed a PIO criterion that explicitly defines the required magnitude slope of the pilot/aircraft open-loop system.[11] The recommended pilot model is an Optimal Control Model (OCM). The Hess-Kalteis Criterion is shown graphically in Figure 4-22. Note that the boundary limits the minimum gain crossover frequency to 2.0 rad/s. For a pilot/aircraft open-loop response with a crossover of exactly 2.0 rad/s, the criterion also limits the magnitude slope to at least -20 dB/decade in the crossover frequency range. Thus, like the open-loop criteria of Smith-Geddes and Hoh, the Hess-Kalteis criterion tends to identify configurations with steeper magnitude slopes in the crossover frequency range as PIO resistant.

The military flying qualities specification includes the Neal-Smith closed-loop criteria for analysis of longitudinal short-period dynamics.[35] A complete lead/lag (crossover) pilot model is

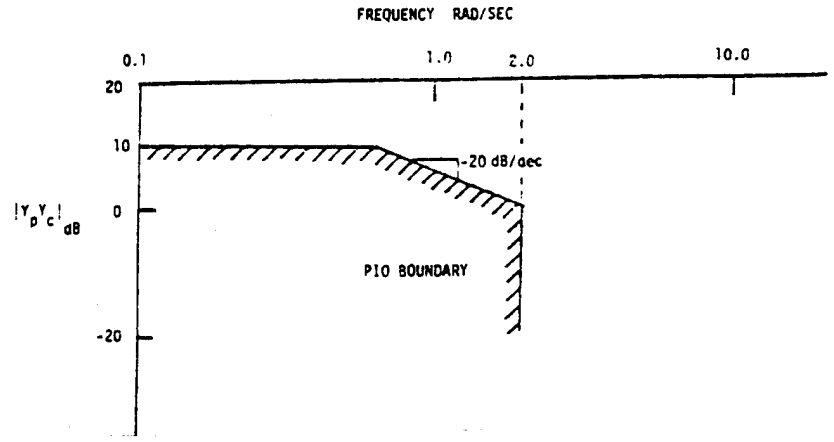

Figure 4-22. Hess-Kalteis PIO Criterion.

specified, and measures such as bandwidth and closed-loop resonant peak are used to determine the aircraft's flying qualities rating.

A variation of the Neal-Smith criteria can also be developed using the M-Δ standard form. Using the harmonic equations from (4-33), add and subtract $p_o(j\omega)g(j\omega)$ to yield,

$$1 + p_o(j\omega)g(j\omega)\delta + p_o(j\omega)g(j\omega) - p_o(j\omega)g(j\omega) = 0 \tag{4-36}$$

Now combine terms in (4-36) so that,

$$[1 + p_o(j\omega)g(j\omega)] + (\delta - 1)p_o(j\omega)g(j\omega) = 0 \tag{4-37}$$

and dividing by $[1 + p_o(j\omega)g(j\omega)]$ reveals,

$$1 + \frac{(\delta-1)p_o(j\omega)g(j\omega)}{[1+p_o(j\omega)g(j\omega)]} = 0 \tag{4-38}$$

or,

$$\frac{p_o(j\omega)g(j\omega)}{[1+p_o(j\omega)g(j\omega)]} = \frac{-1}{\delta-1} \tag{4-39}$$

From (4-39), one should see that now $\delta_m = 1/\delta - 1$. The transfer function m(s) is equal to $p_o(s)g(s)/(1+p_o(s)g(s))$, which is the same as the closed-loop transfer function from $r_c(s)$ to r(s) in Figure 4-19.

The Neal-Smith flying qualities criteria specifies the maximum allowable resonant peak of the closed-loop frequency response. For Level 1 airplanes, the resonant peak must be less than 3 dB and for Level 2, the resonant peak must be less than 9 dB. Let this resonant peak be denoted by P, therefore,

$$P = \max_{\omega} \left| \frac{p_o(j\omega)g(j\omega)}{[1+p_o(j\omega)g(j\omega)]} \right| \tag{4-40}$$

If δ is not a function of frequency, (4-39) is satisfied whenever,

$$P = \left| \frac{-1}{\delta-1} \right| \tag{4-41}$$

Now suppose δ represents only a change in pilot gain, i.e. $\delta = K_\delta$ as before. When $\delta = K_\delta$, (4-41) can be solved for K_δ in terms of P to yield,

$$K_\delta = 1 + 1/P \tag{4-42}$$

Using (4-42), the Neal-Smith criteria can be interpreted as a limitation on the maximum tolerable increase in pilot gain. For Level 1 aircraft, (4-42) reveals that when P = 3 dB, then K_δ = 1.71 (4.65 dB). This result means that the Level 1 Neal-Smith criteria allows up to a 1.71 factor increase in pilot gain. Not surprisingly, the Level 2 criteria of P = 9 dB translates to a maximum pilot gain increase of K_δ = 1.35 (2.64 dB). Thus, a Level 2 airplane can therefore tolerate less pilot gain change than a Level 1 airplane.

In summary, each of the existing single, open-loop and closed-loop criterion appear to focus upon various measures of frequency response shape. It is also important to note that each of these existing criteria can be motivated by how arbitrary pilot gain changes can affect closed-loop stability. The Smith-Geddes and Hess-Kalteis methods deal mainly with the pilot/aircraft magnitude slope near the actual (Hess-Kalteis) or implied (Smith-Geddes) gain crossover frequency. Changes in pilot gain will affect the pilot/aircraft gain crossover frequency directly.

The Neal-Smith closed-loop criterion can also be interpreted as limiting the maximum pilot gain variation. Therefore, each of these methods would appear to relate directly to stability robustness with respect to changes or variations in pilot gain.

Pilot gain also affects phase margin. Since phase margin is defined relative to the -180 degree point, it is reasonable to develop criteria governing the shape of the aircraft phase response near the phase angle of -180 deg. Hoh's bandwidth criteria directly specifies a minimum phase slope near ω_{180} while the Smith-Geddes criteria indirectly favors shallow phase slopes.

It has already been shown that gain margin correlates fairly well with PIO rating for the HAVE PIO configurations. Since most of the existing criteria studied herein have direct ties to gain margin and, to a lesser extent, phase margin concepts, it seems worthwhile to consider methods which can measure simultaneous gain and phase variations. The idea of a vector stability margin is therefore offered as a unified measure of PIO susceptibility. The vector margin was originally developed as a stability robustness measure for linear systems.[45]

Figure 4-23 shows the graphical definition of a vector stability margin for the pilot/vehicle representation shown in Figure 4-19. The vector margin β is defined as the minimum distance from the graph of $p_o(j\omega)g(j\omega)$ to the critical -1+j0 point. One can see that β is related to traditional gain and phase margins. Note from Figure 4-23 that the vector β is smaller then β_1, which is the vector which defines the traditional gain margin. It is also smaller than β_2, which is the vector which defines the traditional phase margin. Therefore, when $\beta = \beta_1$, the length of the vector β can be used to give an exact representation for traditional gain margin. Conversely, when $\beta = \beta_2$, the length of β can be used to find the exact value of the traditional phase margin (e.g. $PM = 2\sin^{-1}(\beta_2/2)$).

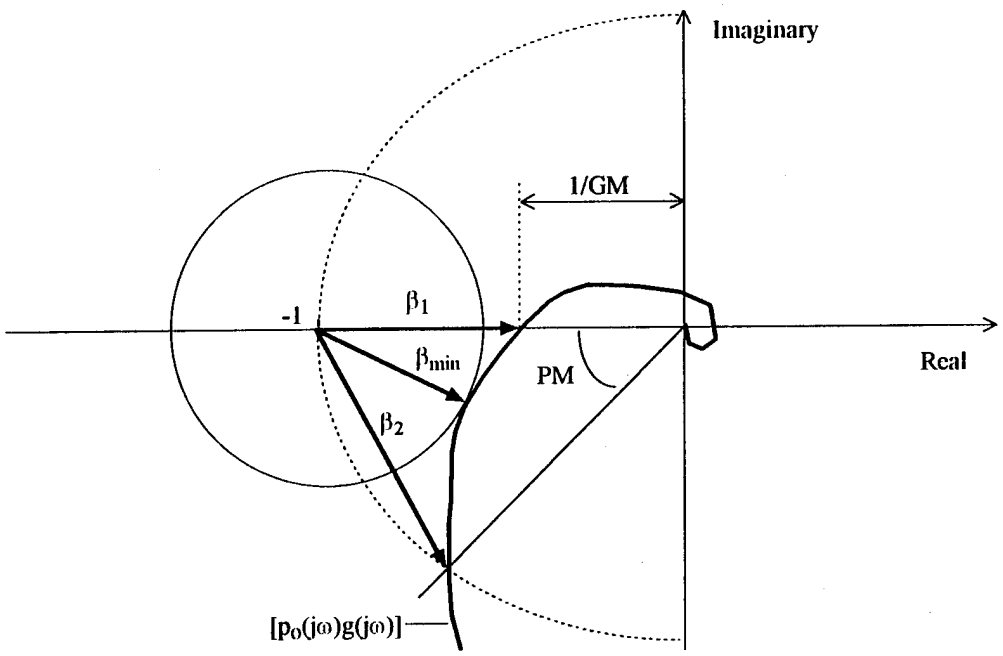

Figure 4-23. Vector Margin Definition.

The vector stability margin has many appealing characteristics when considered for PIO analysis. The vector margin deals with the shape of the pilot/aircraft frequency response near the critical point in a manner very similar to the various existing PIO criteria. In addition, the vector margin automatically establishes a critical frequency as the frequency ω where $p_o(j\omega)g(j\omega)$ is nearest the -1+j0 point. Note that this frequency point is not necessarily the open-loop gain crossover frequency or the frequency point associated with -180 phase angle. It is hypothesized that this frequency point will be closely related to the frequency of PIO.

The vector margin can be readily developed from the M-Δ concepts described previously. Consider (4-33) again, add and subtract δ to yield,

$$1 + p_o(j\omega)g(j\omega)\delta + \delta - \delta = 0 \tag{4-43}$$

Combine terms in (4-43),

$$(1 - \delta) + [1 + p_o(j\omega)g(j\omega)]\delta = 0 \tag{4-44}$$

and divide by δ,

$$[1 + p_o(j\omega)g(j\omega)] = \frac{\delta\text{-}1}{\delta} = 1\text{-}1/\delta \tag{4-45}$$

Comparing (4-45) to (4-28), we note that $m(s) = 1 + p_o(s)g(s)$ and $\delta_m = \delta\text{-}1/\delta$.

The vector margin is a vector pointing from $p_o(j\omega)g(j\omega)$ to the -1+j0 point. Since we are interested in the smallest distance, let β be the smallest magnitude of $[1 + p_o(j\omega)g(j\omega)]$ or,

$$\beta = \min_{\omega} |1 + p_o(j\omega)g(j\omega)| \tag{4-46}$$

We will also define the critical frequency as the frequency where the minimum is obtained in (4-46).

The value of β is shown graphically in Figure 4-23. The aircraft depicted in Figure 4-23 is the B-2 pitch attitude response during air-to-air refueling.[46] Using a synchronous pilot model gain of $K_p = 20$, the length of the vector margin in this case is $\beta = 0.457$ at a frequency of 8.13 rad/s. For reference, this aircraft was known to experience PIOs in the configuration under study.

Figure 4-24 shows a magnitude plot of $1 + p_o(j\omega)g(j\omega)$ for HAVE PIO Configurations H2-1 and H2-5. The nominal pilot model is again chosen to be a simple gain $p_o(s) = K_p$. The value of β will be the minimum point on this frequency response. From Figure 4-24, we can see that β = 0.54 for Configuration H2-1 and $\beta = 0.43$ for Configuration H2-5. The critical frequencies are 4.1 and 2.0 rad/s for Configurations H2-1 and H2-5, respectively.

As expected, the value of β is smaller for H2-5 than H2-1. This characteristic means the Nyquist plot of $p_o(j\omega)g(j\omega)$ comes closer to the -1+j0 point for Configuration H2-5 than for H2-1.

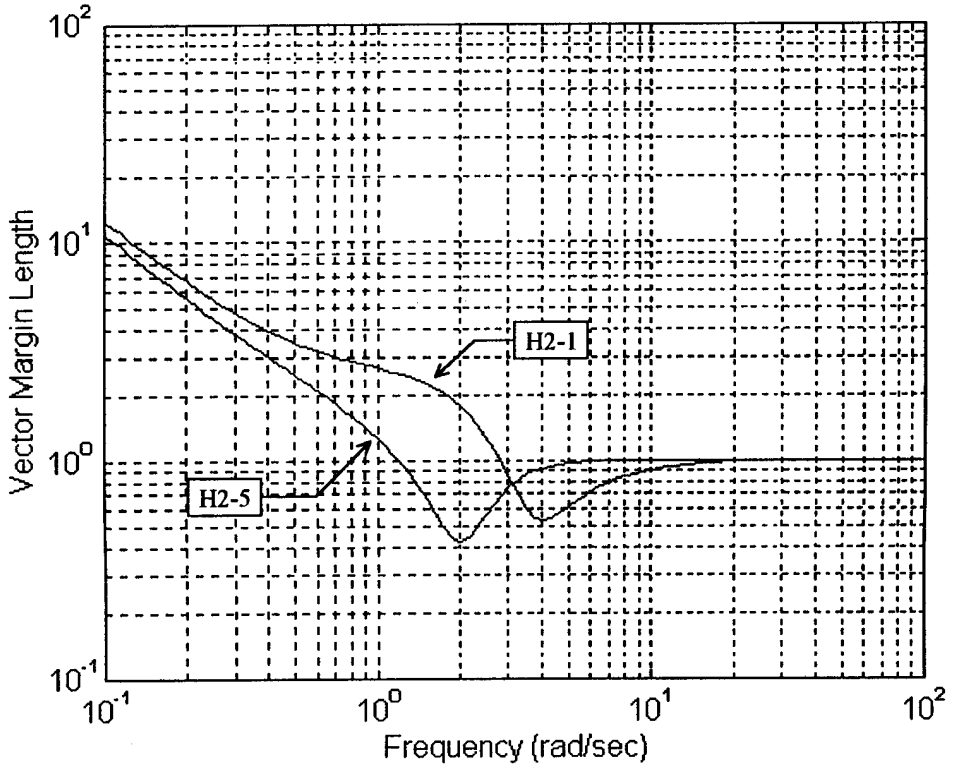

Figure 4-24. Vector Margins for H2-1 and H2-5 (Synchronous Pilot).

It also means that Configuration H2-1 can sustain larger *simultaneous* pilot gain and phase changes than can H2-5.

Table 4-7 summarizes the results of computing the vector margin for each of the HAVE PIO Configurations. A nominal synchronous gain pilot model was used for these results. Again, the pilot model gain K_p was chosen as the minimum value which leads to at least 6 dB gain margin and at least 45 deg phase margin. Also shown in Table 4-7 is the critical frequency where β is found.

Figure 4-25 shows the vector margin plotted with the average PIO rating given in flight for each HAVE PIO configuration. The trend of increasing PIOR with decreasing vector margin is clearly evident in Figure 4-25.

Table 4-7. Vector Margin using Synchronous Pilot.

Configuration	PIOR	K_p	β	ω_{crit} (rad/s)
H2-B	2.0	1.88	0.57	7.15
H2-1	1.0	1.24	0.54	4.10
H2-5	4.33	1.09	0.43	2.05
H2-7	3.0	0.93	0.43	3.33
H2-8	4.0	0.78	0.45	3.11
H3-D	1.0	1.83	0.49	6.67
H3-1	2.33	2.20	0.51	8.50
H3-3	1.67	1.38	0.45	4.25
H3-6	2.0	1.27	0.47	5.81
H3-8	3.67	0.95	0.48	4.71
H3-12	4.5	0.67	0.46	1.98
H3-13	4.5	0.70	0.46	2.61
H4-1	1.0	1.54	0.53	5.41
H4-2	1.33	1.16	0.45	4.25
H5-1	1.0	1.27	0.55	2.90
H5-9	4.0	0.81	0.42	2.12
H5-10	5.0	0.62	0.45	1.91
H5-11	3.0	0.91	0.45	2.35

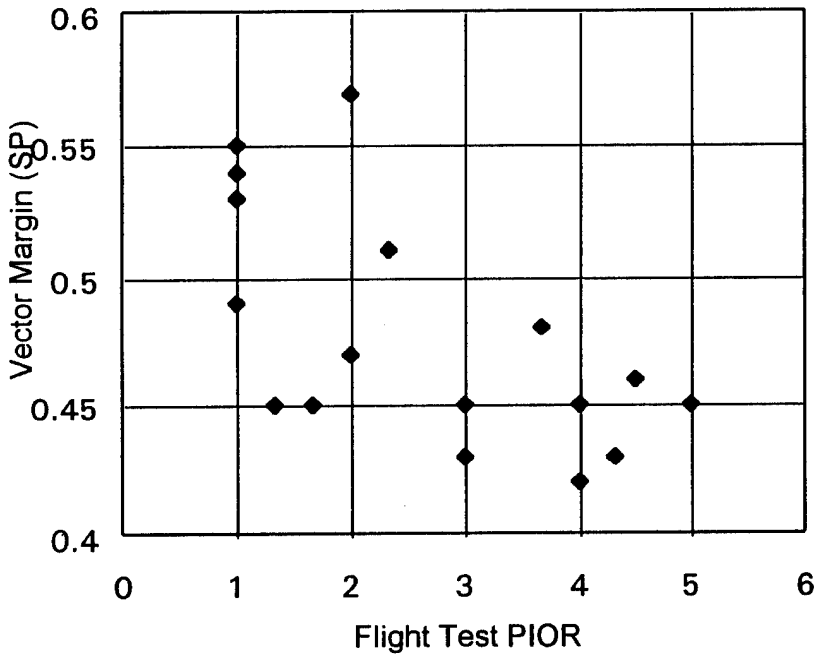

Figure 4-25. Vector Margin and PIO Rating (Synchronous Pilot).

Figure 4-26 shows the critical frequency and the actual PIO frequency for the thirteen HAVE PIO configurations that actually resulted in a PIO event. The correlation of the vector margin critical frequency and the actual PIO frequency is good. These results show that the actual PIO frequency is slightly higher than the critical frequency predicted by the vector margin.

Figure 4-27 shows the critical frequency plotted against the vector margin using the synchronous pilot model. Note that with only two exceptions (H3-1 and H3-8) the PIO-prone configurations (PIOR > 2.0) are grouped together with small vector margins and low critical frequencies. The PIO-free configurations tend to have larger vector margins and critical frequencies.

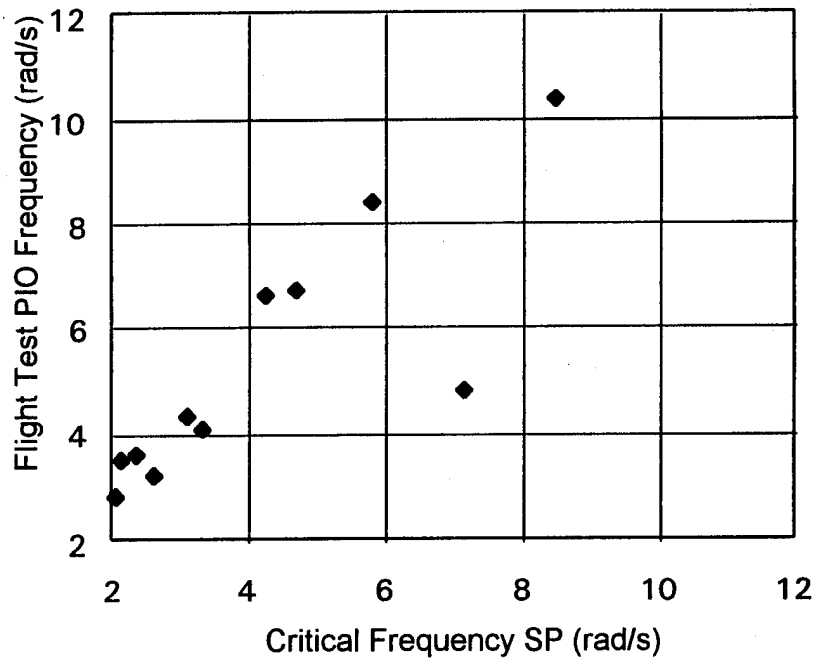

Figure 4-26. Predicted PIO Frequencies (Synchronous Pilot).

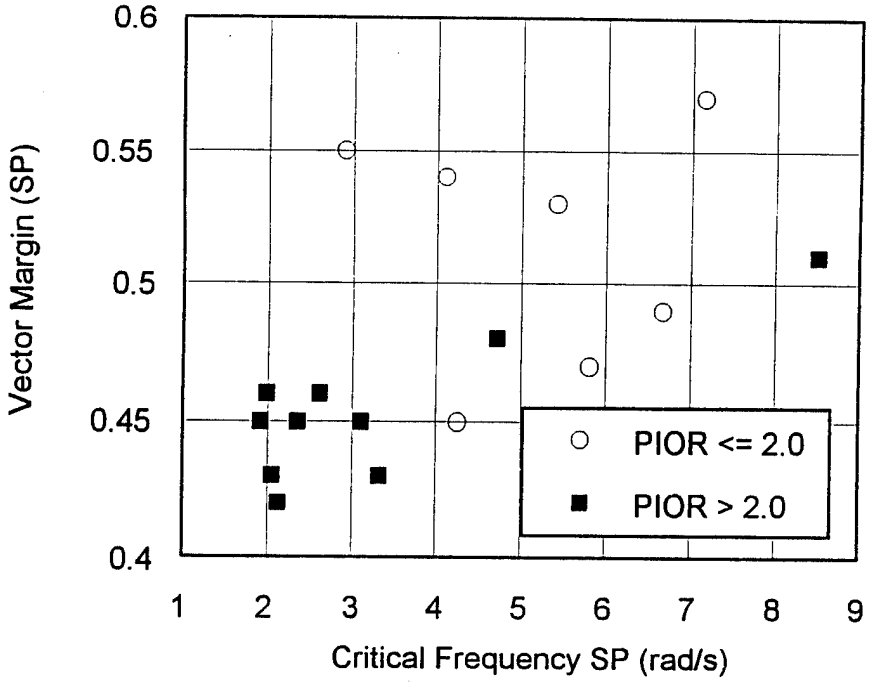

Figure 4-27. Vector Margin and Critical Frequency (Synchronous Pilot).

The two exceptions to the trends in Figure 4-27 are configurations H3-1 and H3-8. Configuration H3-1 has a short-period natural frequency of 4.1 rad/s and damping ratio of 1.0. No other dynamics are included in H3-1, yet the configuration was flown three times with ratings of 3, 2, and 2. The PIO frequency experienced during flight test was 10.4 rad/s. As a result, it would appear that this configuration may have encountered a higher-frequency phenomenon than is considered herein. Other PIO criteria have also had difficulty predicting the behavior of H3-1.[11]

A nominal synchronous pilot model was used in the preceding results. The vector margin can also be computed using more sophisticated pilot models. Table 4-8 shows the results of using the more sophisticated MOCM operator model described in Section 4.3.1

Table 4-8. Vector Margin using MOCM Pilot.

Configuration	PIOR	β	ω_{crit} (rad/s)
H2-B	2.0	0.433	6.44
H2-1	1.0	0.429	5.81
H2-5	4.33	0.408	4.40
H2-7	3.0	0.412	5.23
H2-8	4.0	0.410	5.05
H3-D	1.0	0.423	6.44
H3-1	2.33	0.429	6.67
H3-3	1.67	0.414	5.61
H3-6	2.0	0.415	6.01
H3-8	3.67	0.410	5.61
H3-12	4.5	0.405	4.25
H3-13	4.5	0.408	4.55
H4-1	1.0	0.425	6.22
H4-2	1.33	0.413	5.61
H5-1	1.0	0.436	5.42
H5-9	4.0	0.408	4.55
H5-10	5.0	0.405	4.25
H5-11	3.0	0.413	4.71

Notice that the values for β are much smaller using the MOCM operator model as opposed to the synchronous model. This result occurs because the MOCM model includes neuromuscular dynamics as well as time delay. These pilot limitations have the effect of reducing the vector stability margins. In a sense, the synchronous pilot model leads to a somewhat optimistic prediction of pilot/aircraft stability robustness.

Figure 4-28 shows the MOCM vector margins plotted with their associated critical frequencies for the HAVE PIO configurations. Figure 4-28 now shows that the PIO-prone configurations are all grouped together with only the exception of H3-1. These configurations are grouped in an area where the vector margin is less than $\beta \cong 0.415$ and the critical frequency is less than approximately 5.5 rad/s.

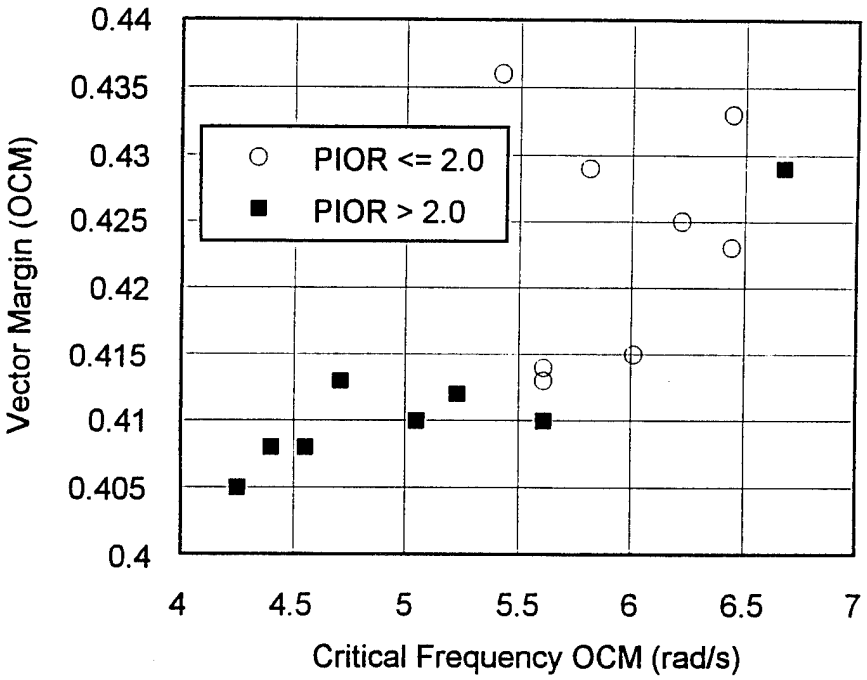

Figure 4-28. Vector Margin and Critical Frequency (MOCM Pilot).

To help establish the value of β that defines PIO-resistant and PIO-prone aircraft, one can consider the relationship of the vector margin to the Neal-Smith criteria. If only pilot gain variations are considered so $\delta = K_\delta$, then (4-45) and (4-46) become,

$$\beta = 1 - 1/K_\delta \tag{4-47}$$

It was previously found that the Neal-Smith criteria would allow a pilot gain variation of up to $K_\delta = 1.71$ for Level 1 flying qualities. Using equation (4-47), we find that the Neal-Smith Level 1 criteria yields the value of $\beta = 0.415$.

Figure 4-29 shows the critical frequency predicted by the vector margin and the MOCM plotted along with the actual PIO frequencies. The correlation in frequency is fairly good;

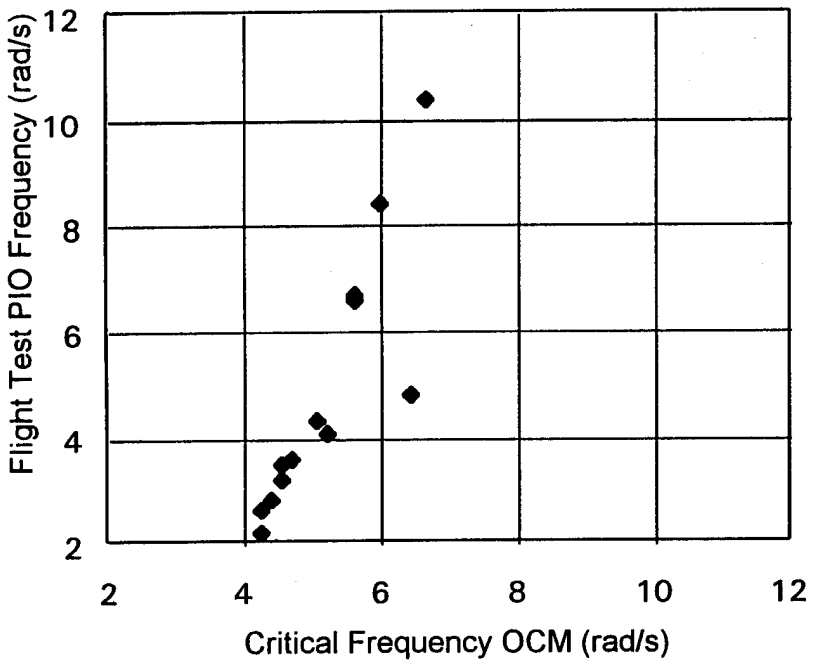

Figure 4-29. Predicted PIO Frequencies (MOCM Pilot Model).

however, the critical frequencies are predicted too large when the actual value is small and vice versa. Nevertheless, the trend of predicted critical frequency and actual PIO frequency is clearly evident.

4.3.5.4 Multivariable Describing Function Analysis

The preceding analysis has studied the effect of pilot gain and phase variations on closed-loop stability. One particular pilot gain variation occurs when the pilot response is limited. Now, consider the case where the pilot is to be modeled by Smith's contactor pilot model.[25] Since we are searching for instances of sinusoidal behavior, the contactor can be modeled using its sinusoidal describing function in Table 4-3,

$$N(\alpha,\omega) = \frac{4}{\pi}\frac{a}{\alpha} \tag{4-48}$$

where it has been assumed that the input to the contactor is $x(t) = \alpha\sin(\omega t)$ and the contactor output level is 'a'. Note that whenever the input amplitude is smaller than the output level, i.e. $a/\alpha > 1$, the describing function magnitude is greater than unity. In this case, the contactor output level might represent the maximum control stick deflection or force level available to the pilot.

Returning to Figure 4-19, we will assume that the nominal pilot is modeled by a simple gain K_p (a synchronous pilot model). The contactor will represent the variable element δ. As a result, the stability condition (4-34) becomes,

$$p_o(j\omega)g(j\omega) = -1/\delta \Rightarrow K_p g(j\omega) = -1/N(\alpha,\omega) = -\frac{\pi}{4}\frac{\alpha}{a} \qquad (4\text{-}49)$$

The existence of solutions to (4-49) can be found using a Nyquist diagram. Figure 4-30 shows a Nyquist diagram of $K_p g(j\omega)$ where $g(j\omega)$ models Configuration H2-5 of the HAVE PIO database.[8] The nominal pilot gain is as previously chosen, $K_p = 1.09$.

The Nyquist plot in Figure 4-30 shows the two sides of (4-49), i.e. $K_p g(j\omega)$ and $-1/N(\alpha,\omega)$. The plot of $-1/N(\alpha,\omega)$ assumes that the ratio α/a varies from 0.2 to 2.0. When the two lines in Figure 4-30 cross, a solution to (4-49) is obtained. Figure 4-30 shows that (4-49) has a solution when $\omega = 2.4$ rad/s and $\alpha/a = 0.56$. This solution corresponds to a stable limit cycle of the pilot/aircraft closed-loop system. Figure 4-31 shows the phase plane trajectory for this limit cycle when the contactor output level is $a = 1$. Note that the response starts with a very small initial condition and builds to a constant magnitude oscillation which can be likened to a fully developed PIO. The contactor describing function in (4-49) amounts to a change in pilot gain with respect to its nominal value. The gain change has a specific relationship to input magnitude and can lead to possible oscillatory behavior.

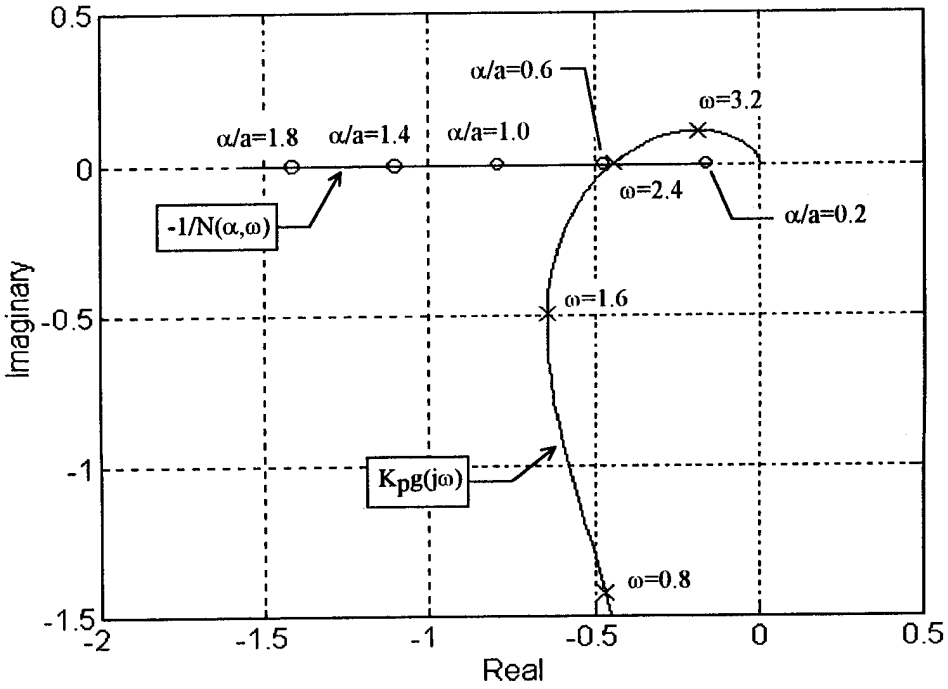

Figure 4-30. Nyquist Plot for Contactor Pilot Model.

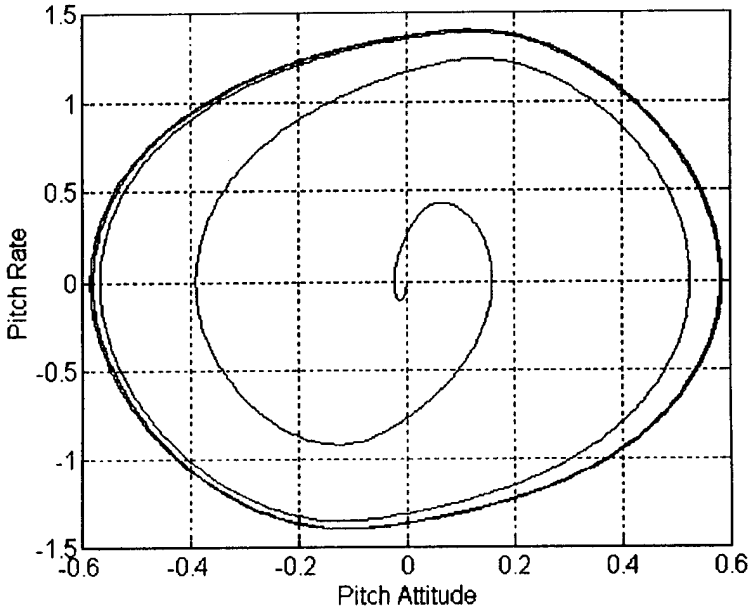

Figure 4-31. Stable Limit Cycle from Contactor Pilot Model.

4.3.5.5 Summary

Existing PIO criterion seem to focus on various measures of the frequency response shape. Furthermore, each of these existing criteria can be motivated by how arbitrary pilot dynamic changes can affect closed-loop stability. Therefore, each of these methods would appear to relate directly to stability robustness with respect to changes or variations in pilot gain. The vector stability margin is offered as one unifying measure of the shape of the pilot/aircraft frequency response near the critical point and as an indication of PIO susceptibility.

4.3.6 Unified Multi-Loop Analysis

The vector margin concept is readily extended to multi-loop systems because the single-loop margin previously discussed is actually a special case of a more general theory.

4.3.6.1 Develop Pilot Model

The methods of pilot modeling given in the previous section can be extended for use in the multi-loop case. However, for this section, only a generic transfer function representation of the pilot is considered without reference to how the model is to be derived.

4.3.6.2 Identification of the Dynamic Elements Suspected of Contributing to PIO

The impact of simultaneous gain and phase variations in each loop of the pilot model will be considered as the primary uncertainties in this section. No specific nonlinearities are considered.

4.3.6.3 Stability Robustness Analysis

Consider the block diagram in Figure 4-32. The transfer function matrix G(s) in Figure 4-32 represents the aircraft transfer functions. $P_0(s)$ is a matrix of transfer functions representing the pilot. The matrix Δ represents changes in pilot equalization and is assumed to be diagonal. This block diagram assumes single, individual pilot variations in each pilot manipulator channel. For

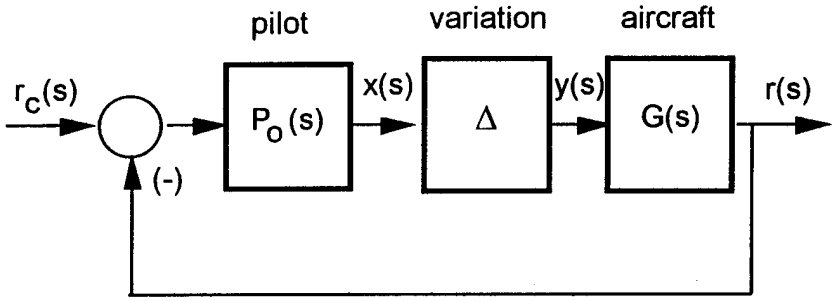

Figure 4-32. Multi-Loop Pilot/Aircraft System.

example, a lateral-directional model might include pilot gain and phase variations in the lateral control stick and rudder pedal channels.

From Figure 4-32, the loop equations are ($r_c(s) = 0$),

$$y(s) = \Delta x(s) \tag{4-50}$$

$$x(s) = -P_o(s)G(s)y(s) \tag{4-51}$$

Combining the loop equations and substituting $s=j\omega$ leads to the expression,

$$[I + P_o(j\omega)G(j\omega)\Delta]\, x(j\omega) = 0 \tag{4-52}$$

Comparing (4-52) to (4-25) shows that M(s) is equal to the open-loop return ratio matrix $P_o(s)G(s)$ for this case. Since we are interested in non-trivial solutions to (4-52), we seek to find solutions of,

$$I + P_o(j\omega)G(j\omega)\Delta = 0 \tag{4-53}$$

As before, add and subtract Δ,

$$(I - \Delta) + [I + P_o(j\omega)G(j\omega)]\Delta = 0 \tag{4-54}$$

and multiply by Δ^{-1} to yield,

$$[I + P_o(j\omega)G(j\omega)] = (\Delta - I)\Delta^{-1} \tag{4-55}$$

Equation (4-55) is essentially the multi-loop equivalent to (4-45). However, since (4-55) is a matrix expression, some measure of matrix norm is required to define the distance to the critical -1+j0 point. Most often the matrix singular value is used as the measure, in which case the multi-loop vector margin is defined as,

$$\beta = \min_{\omega} \sigma_{min}[I + P_O(j\omega)G(j\omega)] \tag{4-56}$$

where σ_{min} is the minimum matrix singular value.

Equation (4-56) would be utilized in the same manner as the single-loop equivalent in (4-46). A value of β is computed from (4-56) and checked against a minimum acceptable value (yet to be determined). The frequency at which the minimum in (4-56) is found will determine the predicted PIO frequency.

The vector margin defined by (4-56) has been used for several years to define the gain and phase stability margins for multi-loop feedback systems.[47] For example, let $\Delta = diag(K_i e^{j\phi_i})$ where i is the loop index. The right hand side of (4-55) can then be written as,

$$(\Delta - I)\Delta^{-1} = I - \Delta^{-1} = diag(1 - 1/K_i e^{j\phi_i}) = diag(1 - e^{-j\phi_i}/K_i) \tag{4-57}$$

Now substitute $e^{-j\phi} = \cos\phi - j\sin\phi$ into (4-57) and find the largest magnitude,

$$\max_{i} |(1 - \cos\phi_i/K_i) + j\sin\phi_i/K_i| \tag{4-58}$$

After further manipulation, one finds that (4-55) will not have a solution as long as,

$$\beta > \max_{i} \sqrt{(1 - 1/K_i)^2 + 2(1 - \cos\phi_i)/K_i} \tag{4-59}$$

Equation (4-59) establishes a relation between pilot gain variations K_δ, phase variations ϕ, and the vector margin β. Any combinations of K_δ and ϕ that satisfy (4-59) will insure that the harmonic conditions in (4-55) are not met. Therefore, (4-59) has been used to define the largest

gain and phase margins that a multi-loop feedback system can tolerate before a stability condition is violated.[26] For application to PIO analysis, the multi-loop vector margin measures the largest simultaneous gain and phase variations that the pilot can introduce in each loop channel before oscillatory behavior of the closed-loop system is possible.

A minimum acceptable value of β for the multi-loop case is not yet known. It is likely that PIO resistant aircraft will have smaller values of β in the multi-loop case than in the single-loop case simply because several pilot loops are involved at once. However, the minimum singular value measure is also known to be conservative with respect to unit scaling. Therefore, a scaling matrix like that used in structured singular value analysis will be required. These subjects will be considered in future research.

4.3.6.4 Multivariable Describing Function Analysis

Once the nonlinear elements of the multi-loop system are isolated, a describing function analysis can be carried out exactly as described in Section 4.3.4.

4.3.6.5 Summary

The vector stability margin is given for the multi-loop case. It is suggested that the vector margin could be used as an indication of PIO susceptibility in a manner similar to that of Section 4.3.5. However, a minimum acceptable value for this margin is not yet known.

4.3.7 Unified Multivariable Analysis

This section describes a unified method for multivariable PIO analysis. The term multivariable is used here to imply that the variable dynamics might appear anywhere in the pilot/vehicle feedback system. In order to exercise the stated multivariable analysis method, it was desired to use the techniques to analyze an aircraft that had experienced in flight PIOs. For the analysis to be meaningful, sufficient modeling data needed to be available for the vehicle along with flight time histories of the oscillation events. The M2-F2 lifting body vehicle was chosen as an example case study. All information for the M2-F2 was taken from Reference [48].

The M2-F2 was a half cone lifting body designed as part of the manned lifting body flight test program conducted in the 1960s. Basic research was being conducted on manned reentry vehicles designed to maneuver and land unpowered at a specified location. The M2-F2 had a conventional fighter aircraft type cockpit with aerodynamic control being provided by upper elevon flaps, a lower flap, and twin rudders. A three view representation of the M2-F2 taken from Reference [48] is given in Figure 4-33. The upper elevon flaps provided coarse longitudinal trim and were deflected differentially (aileron deflection) to provide roll control. Because of adverse yaw due to aileron deflection, a mechanical aileron-to-rudder interconnect was provided. The interconnect ratio was adjustable by the pilot. A stability augmentation system was used to improve damping in the pitch, roll, and yaw axes.

The M2-F2 was dropped from a B-52 at an altitude of 45,000 feet and a Mach number of about 0.6. Flight test maneuvers were performed during the unpowered descent to assess the handling characteristics of the vehicle. The pilots were thoroughly familiar with the flight plan and predicted handling qualities of the research vehicle as a result of training on a six-degree-of-freedom fixed base simulator. The M2-F2 exhibited good handling qualities longitudinally, but

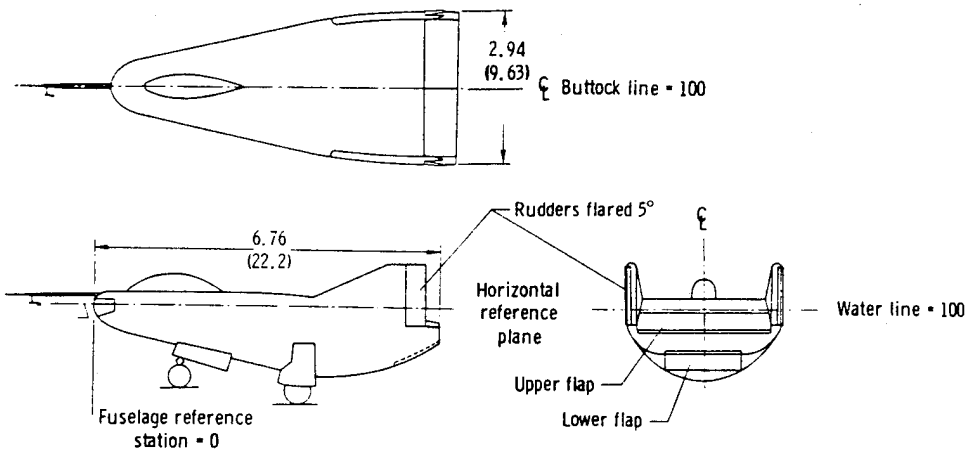

Figure 4-33. Three-View Drawing of the M2-F2. Dimensions in meters (feet).

the lateral/directional characteristics were rated consistently lower than the longitudinal; due partly to the appearance of a coupled roll spiral mode at low angles of attack. The vehicle experienced severe lateral/directional oscillations during three of its sixteen flights. Each of the oscillations occurred when the pilot was attempting to closely control the bank angle at negative angles of attack. The PIO of the final flight contributed to a gear-up landing in which the vehicle was extensively damaged.[48] As the result of the accident, a center fin was added to the vehicle to improve the lateral/directional dynamics and the slightly redesigned vehicle was designated the M2-F3.

4.3.7.1 Develop Pilot Model

The task under consideration is the tight control of the bank angle and will be modeled as a compensatory tracking task. A modified optimal control model of the human pilot will be considered for this example. The pilot model is designed based on the linear transfer function of the controlled system. For simplification and comparison to Reference [48], only the pilots aileron input is considered. This restriction should not pose a problem as simulation analysis in

Reference [48] indicated PIO for the situation of aileron only input as well as for coordinated aileron/rudder input during turn to final approach. A simplified block diagram of the situation under consideration is given in Figure 4-34. The MOCM code of Reference [23] was used to compute the pilot model. The parameters used in the MOCM model are identical to those given in Table 4-1 with the disturbance filter given by $13.31/(s^2+2(0.7)(0.5)s+(0.5^2))$. The values are based on those given in Reference [49] for the roll axis.

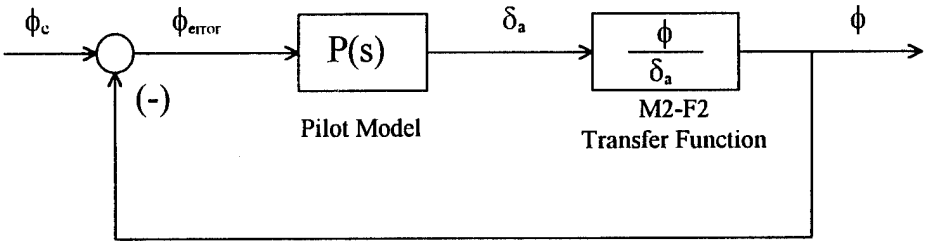

Figure 4-34. Block Diagram for Single Axis Tracking Task.

4.3.7.2 Identification of the Dynamic Elements Suspected of Contributing to PIO

A first step in the closed-loop analysis is to identify those elements of the aircraft and stability augmentation system that are suspected to be contributing factors in the PIO occurrence. A block diagram of the M2-F2 lateral/directional flight control system is given in Figure 4-35. Since actuator rate limiting is known to contribute to PIO, the rate limits of both the aileron and rudder actuators will be considered in the analysis. Furthermore, since a mechanical aileron-to-rudder interconnect is needed to provide acceptable lateral/directional characteristics, it also poses a potential threat in terms of oscillation tendencies. This threat was recognized during the fixed based simulations as depicted in Figure 4-36 which is taken from Reference [48]. Command

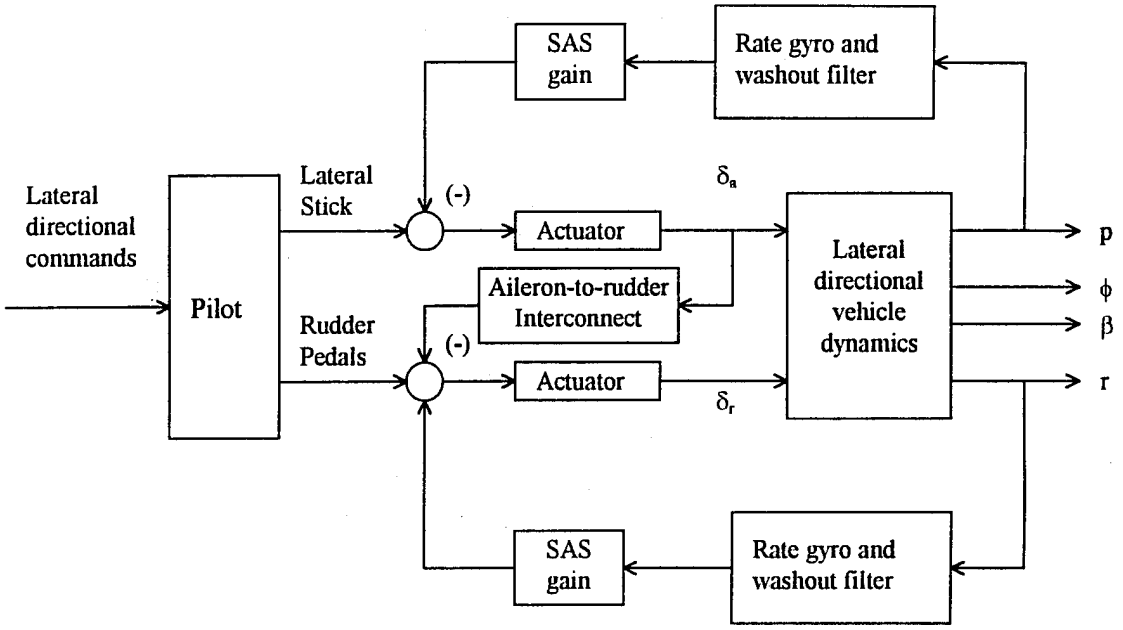

Figure 4-35. Block Diagram of M2-F2 Lateral/Directional Control System.

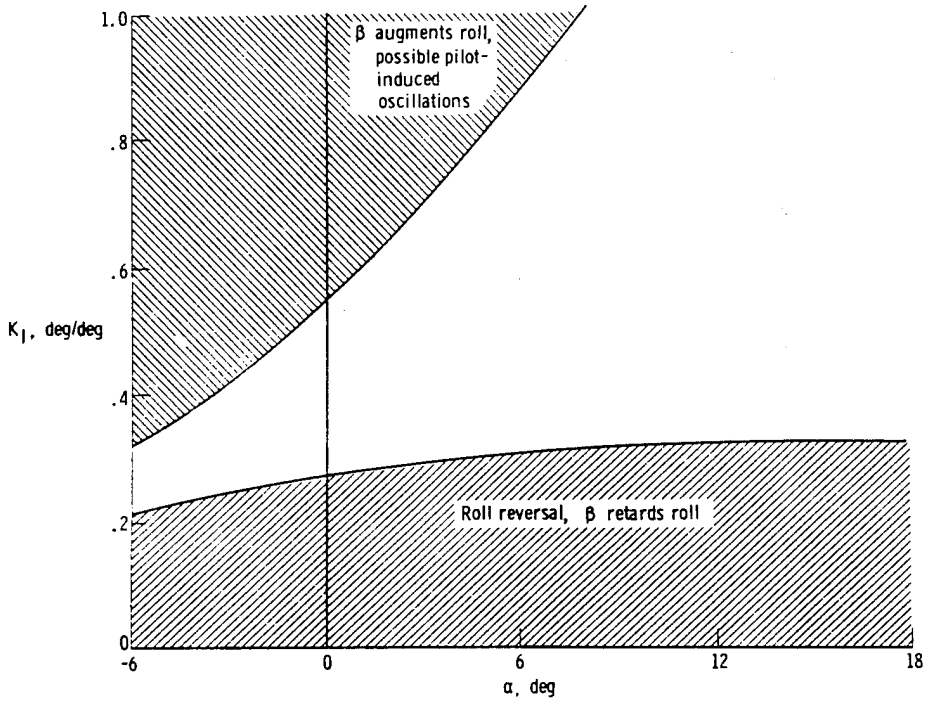

Figure 4-36. Simulator Predicted Regions of Lateral Control Problems as a Function of Angle of Attack and Aileron-to-Rudder Interconnect Ratio.

authority limits were placed on the pilot input as well as both the roll and yaw SAS commands. These command limits, together with the actuator rate limits, comprise a total of five nonlinear elements that will be considered as possible contributors to PIO. The rate and command limits are given in Table 4-9. Along with the aileron-to-rudder interconnect ratio, variations in the roll and yaw SAS gains will be considered as linear elements of the vehicle suspected of contributing to undesirable oscillations.

Table 4-9. M2-F2 Actuator Rate and Command Authority Limits.

Upper Flap Rate (Aileron)	Rudder Rate	Pilot Aileron Command Authority	Roll SAS Authority	Yaw SAS Authority
30 deg/sec	22 deg/sec	±10 deg	±5 deg	±4.2 deg

In addition to elements of the aircraft and SAS, various aspects of the pilot are also considered. The underlying concept of the closed-loop analysis is that a PIO resistant aircraft will remain stable in the face of variations in the pilot model. At this point, certain aspects of the model seem reasonable to consider. The most obvious suspect is the pilot gain. Increased pilot gain is often associated with tight tracking tasks such as approach and landing.

4.3.7.3 Stability Robustness Analysis

Those elements identified as possible contributors to PIO in Section 4.3.7.2 will now be considered in a stability robustness analysis. The linear elements will all be considered to have a multiplicative uncertainty as shown in Figure 4-3. The linear elements are the pilot gain (K_{pilot}), the roll SAS gain (K_p), the yaw SAS gain (K_r), and the interconnect ratio (K_I). The nonlinear elements (the three command limits and the two actuator rate limits) will be modeled with the

equivalent gain representation of Figure 4-4. The SIMULINK™ diagram used to define M(s) for the stability robustness analysis is given in Figure 4-37. Associated with each uncertainty to be considered is an inport outport pair. The inport/outport pairs and the corresponding dynamic elements are listed in Table 4-10. When the *linmod* command is issued, a state-space representation of M(s) is returned having q inputs and q outputs (q equals the total number of uncertainties so q = 6 in this case). If it is desired to consider only a subset of the defined uncertainties, the one need only to extract the relevant portions of the state-space model. If, for example, only the combined effect of an uncertain pilot gain in conjuncture with rate limiting of the aileron actuator is to be considered, then only the first and third inputs and outputs of the system M(s) are needed.

Table 4-10. Inport/Outport Pairs for Stability Robustness Analysis.

Inport/Outport Pair	Description of Dynamic Element
1	Aileron Rate Limit
2	Rudder Rate Limit
3	Pilot Gain
4	Roll SAS Gain
5	Yaw SAS Gain
6	Interconnect Ratio

With the M-Δ construction complete, the structured singular value can be used to calculate the pertinent stability margins. As stated previously, when bounds are known to exist on a given variation, the corresponding uncertainty should be scaled to reflect this variation. If, for example, the roll SAS gain is known to vary by no more than 10% from the nominal value, then the scaling

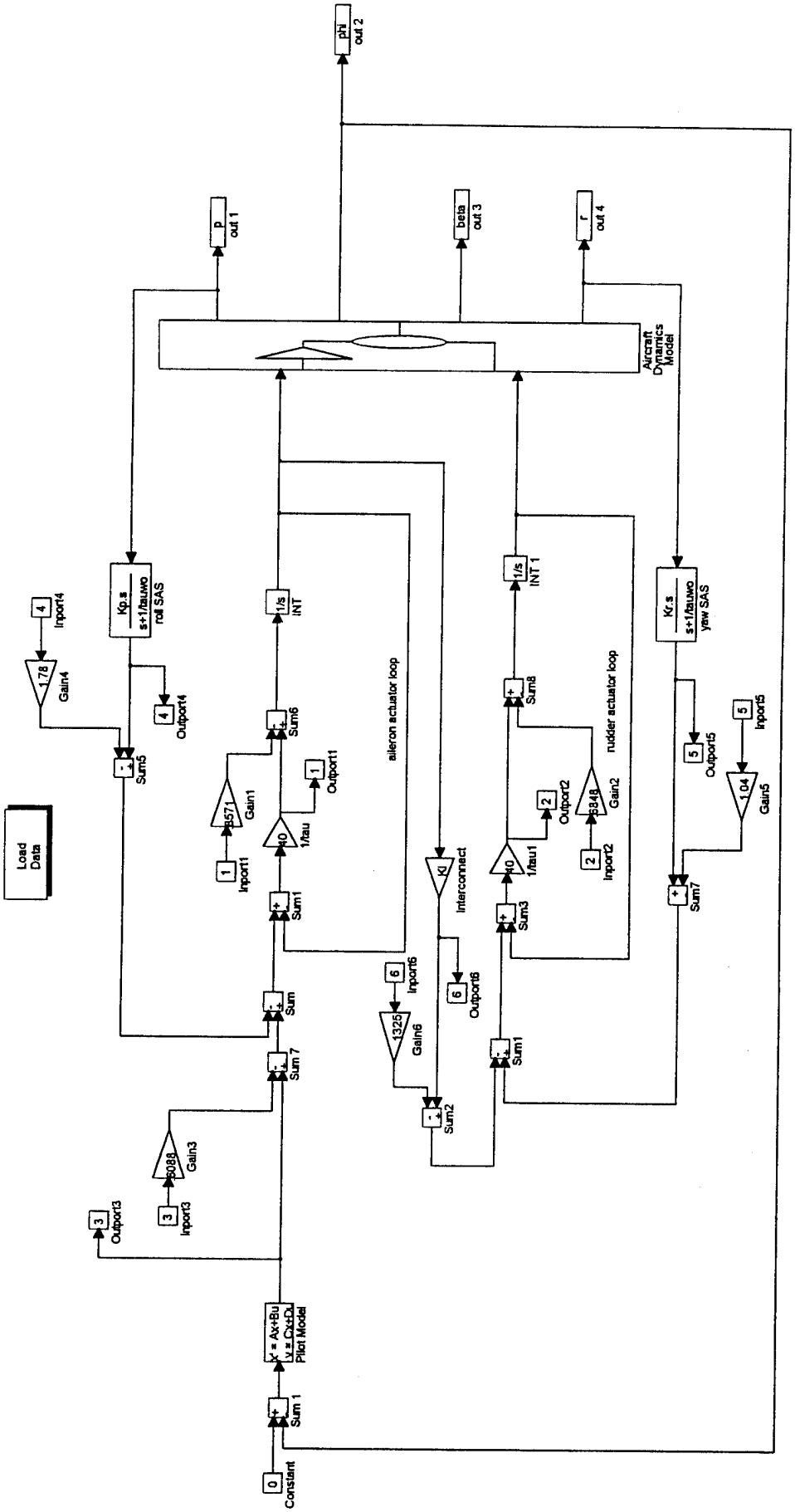

Figure 4-37. SIMULINK™ Diagram for Stability Robustness Analysis of M2-F2.

gain of 0.1 should be applied to the corresponding inport/outport. This scaling ensures that as δ varies from -1 to 1, the corresponding SAS gain varies from Kp(1- .1) to Kp(1 +.1), or a variation of $\pm 10\%$ from the nominal gain. However since no such information is given for the M2-F2, an alternate approach is used. With all the scaling gains set to unity, the structured singular value for real parameter variations is used to estimate the single uncertainty stability margins for each of the uncertainties. The results of this analysis are presented in Table 4-11. A 1 or -1 in a column represents the corresponding "worst case" variation is either positive or negative. The value indicated by $\min(1/\mu_r)$ represents the size of the real parameter variation necessary before instability is possible. The frequency at which the minimum of the structured singular value inverse occurs is denoted ω_{min}. Also given in the table are the exact uncertainties necessary to cause instability and the corresponding frequencies. The estimated stability margins are between 93% and 98% of the exact values.

Table 4-11. Single Uncertainty Stability Margins for the M2-F2.

Pilot Gain	Aileron Rate	Rudder Rate	Roll SAS	Yaw SAS	Interconnec Ratio	Minimum $(1/\mu_r)$	δ_{exact}	ω_{min} (rad/sec)	ω_{exact} (rad/sec)
1	0	0	0	0	0	.6088	.6315	5.55	5.92
0	-1	0	0	0	0	.8571	.9032	4.11	2.93
0	0	-1	0	0	0	.6848	.7285	2.65	2.28
0	0	0	-1	0	0	1.7883	1.9050	4.78	4.31
0	0	0	0	-1	0	1.0485	1.0516	2.75	2.70
0	0	0	0	0	-1	.1325	.1357	3.30	3.44

For those uncertainties with $\min(1/\mu_r) < 1$, the scaling gains are now set equal to the single uncertainty stability margin estimates. For example, the scaling gain on the pilot gain uncertainty inport is set to 0.6088. This results in scaling the uncertainties to their single loop equivalent

stability margins with the exception of the uncertainties in the roll and yaw SAS gains which are left at unity. Now, the effect of varying the parameters simultaneously can be considered without undue scaling bias. The results of the scaled simultaneous variations are given in Table 4-12. The stability margins given in this table now represent margins that are subordinate to the single loop margins. Consider the case of varying pilot gain and the interconnect ratio simultaneously. The margin is given as 0.6586. This means that the closed-loop system is guaranteed to remain stable as long as both parameters remain below 66% of the their corresponding single loop instability values. This means, assuming all other uncertainties are zero, as long as the pilot gain does not increase by more than 0.6586*0.6088=40% and the interconnect ratio does not decrease by more than 0.6586*0.1325=9%, the closed-loop system will remain stable.

Table 4-12. Multiple Uncertainty Stability Margins for the M2-F2.

Pilot Gain	Aileron Rate	Rudder Rate	Roll SAS	Yaw SAS	Interconnect Ratio	Minimum $(1/\mu_r)$	ω_{min} (rad/sec)
1	-1	0	0	0	0	.6894	5.12
1	0	-1	0	0	0	.8196	6.30
1	0	0	-1	0	0	.6298	5.24
1	0	0	0	-1	0	.6736	5.81
1	0	0	0	0	-1	.6586	3.01
1	-1	-1	0	0	0	.6566	5.62
1	-1	0	-1	0	0	.5235	5.06
1	0	-1	0	-1	0	.5506	2.88
1	0	0	-1	-1	0	.4893	5.55
1	-1	0	0	1	0	.5559	4.51
1	0	-1	-1	0	0	.5879	5.62
1	-1	0	0	0	1	.5539	3.79
1	0	-1	0	0	1	.5076	3.30
1	0	0	-1	0	-1	.4961	5.36
1	0	0	0	-1	1	.4525	3.12
1	-1	0	-1	0	-1	.4351	5.24
1	-1	-1	0	0	1	.4662	3.34
1	0	-1	0	-1	1	.3696	3.05
1	-1	-1	-1	-1	1	.3277	3.08

It is obvious that stability margins calculated for multiple uncertainties are greatly affected by the scaling gains. Therefore, when bounds on the model parameter variations are *not* known, this analysis can only be used to determine relative stability due to various combinations of uncertainties. With this reasoning, the results of Table 4-12 can be viewed as a sort of sensitivity analysis.

Based upon a percentage from nominal, from the single uncertainty margins of Table 4-11, the interconnect ratio distinguishes itself as the parameter to which stability of the closed-loop system is by far the most sensitive. The pilot gain is a distant second. Since we are primarily interested in examining the stability of the system with respect to variation in the pilot, all of the multiple uncertainty margins given in Table 4-12 include a variation in the pilot gain. The first 5 rows of Table 4-12 show the results for varying only two parameters. Again, stability of the system is strongly affected by variations in the pilot gain and the interconnect ratio. The next six rows show the results for varying three parameters simultaneously while keeping the interconnect ratio at its nominal value. The remaining rows show the results for varying pilot gain, interconnect ratio and some combinations of the other parameters.

Of interest to note are the results for varying pilot gain, aileron rate limit, and roll SAS gain (row #7) as compared with varying pilot gain, rudder rate limit, and yaw SAS gain (row #8) for the cases of constant (row #7 and #8) and varying (row #16 and #18) interconnect ratios. When the interconnect ratio is held constant, system stability is more sensitive to variations in the aileron rate limit and roll SAS gain ($\min(1/\mu_r) = 0.52$ as opposed to 0.55). System stability is more sensitive to variations in the rudder rate limit and the yaw SAS gain when the interconnect ratio is allowed to vary ($\min(1/\mu_r) = 0.37$ compared to 0.44). Since the pilot command affects the rudder

only through the interconnect ratio, this switch in sensitivity is understandable. Note also, the "worst case" direction of variation of the interconnect ratio is different for the two cases.

Another trend that can be found in Table 4-12 is that an increase in the interconnect ratio causes a decrease in the corresponding frequency. This trend is easily seen in comparing the first four rows to rows 12 through 15. A last trend to note is perhaps the most obvious. Namely, the stability margins decrease as any single parameter is added to an already existing combination. The stability margin for varying pilot gain, aileron rate limit ,and roll SAS gain (0.5235) is less than the stability margin for varying only pilot gain and aileron rate limit (0.6894),or only pilot gain and roll SAS gain (0.6298).

4.3.7.4 Multivariable Describing Function Analysis

The stability robustness analysis of the previous section produced guaranteed stability bounds. That is to say, as long as the given parameters stay within the bounds, the closed-loop system will remain stable and *will not limit cycle*. However, the structured singular value analysis yields little information about the behavior of the instability when the bounds are breached. Also, since the variations of the equivalent gains representing the nonlinearities are input amplitude dependent, it is more difficult to ascertain if these bounds will be breached by the operating pilot/aircraft system. To provide further insight into the system behavior, a describing function analysis is performed to identify the existence of any limit cycles.

A limit cycle can only exist when either the pilot, aircraft, or both are modeled as nonlinear systems. For the M2-F2 example, the pilot is assumed to be the linear pilot given by the MOCM while the aircraft is assumed to contain the 5 isolated saturation nonlinearities stated in Section 4.3.7.3. Figure 4-38 shows the SIMULINK™ diagram used to determine M(s) for the limit cycle search. When the *linmod* command is used, a state space representation of M(s) is returned

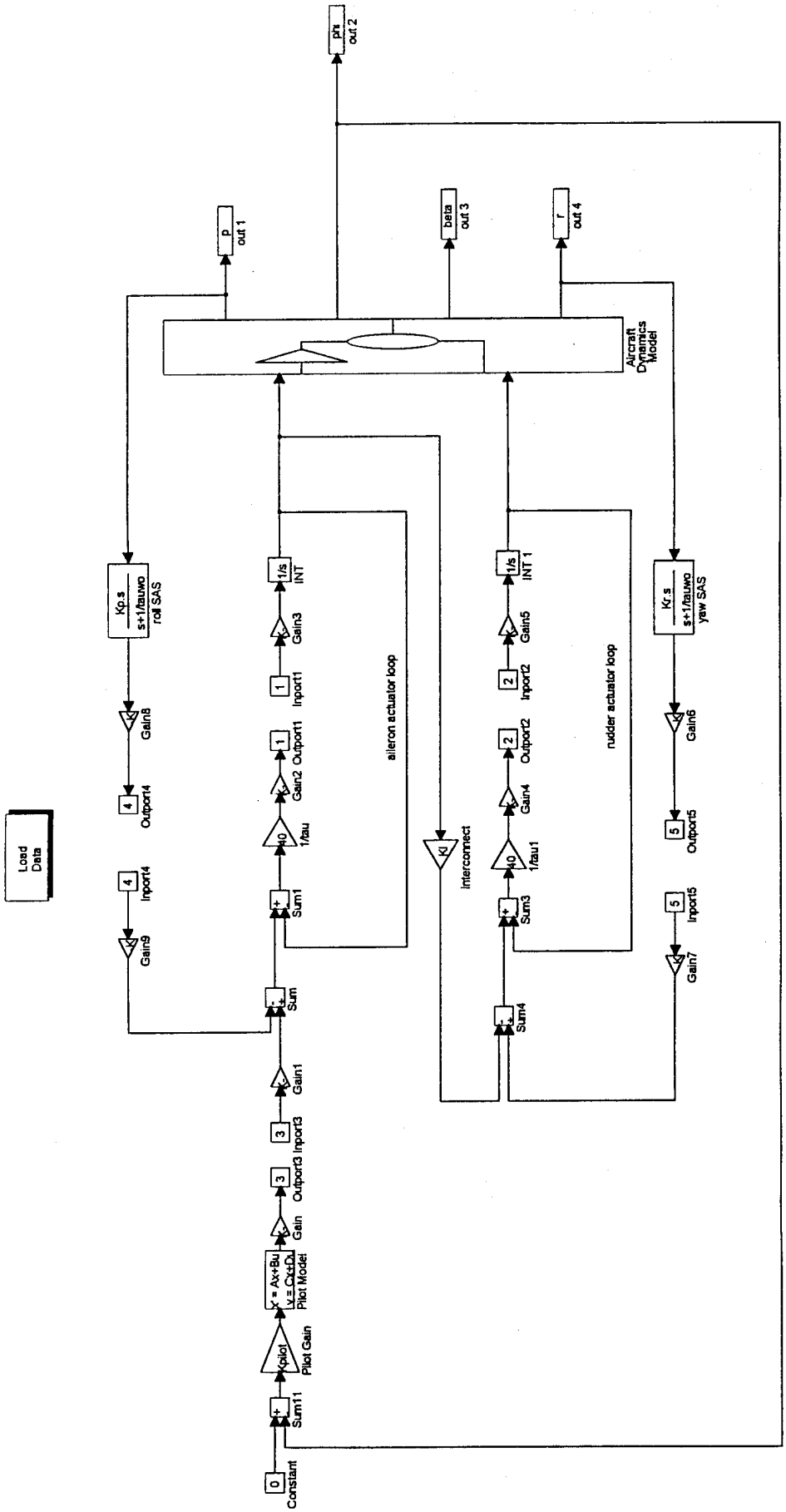

Figure 4-38. SIMULINK™ Diagram for Describing Function Analysis of M2-F2.

having 5 inputs and 5 outputs, one input/output pair for each of the nonlinear elements modeled. Table 4-13 lists the SIMULINK™ inport/outport pairs and the corresponding dynamic elements. If it is desired to analyze only a subset of the nonlinearities as modeled, the new system cannot be obtained by simply examining certain elements of the original system as was done for the stability robustness analysis. Separate SIMULINK™ diagrams containing only the particular subset of the nonlinearities should be used to extract the desired state space representation of M(s). An entirely new M(s) needs to be generated because the nominal system is not obtained by setting $\Delta=0$ in the describing function analysis. Instead, the loop is opened at each nonlinear element when $\Delta=0$.

Table 4-13. Inport/Outport Pairs for Describing Function Analysis.

Inport/Outport Pair	Description of Dynamic Element
1	Aileron Rate Limit
2	Rudder Rate Limit
3	Pilot Command Limit
4	Roll SAS Command Limit
5	Yaw SAS Command Limit

With the system recast in the standard M-Δ form, the numerical methods of Section 4.3.4.3 can be used to search for the existence of limit cycles. The limit cycle search is a search for the inputs to the nonlinear elements of the form of equation (4-17) that solve the harmonic balance equation (4-19). This search can include many of the same variations as the stability robustness analysis. Presented here will be the results of considering all five nonlinearities in conjunction with a variation in pilot gain and a variation in the interconnect ratio. The pilot gain and interconnect are suspected of contributing to the oscillation tendencies as is indicated by the results of the stability robustness analysis of the previous section. The results of the limit cycle

search are given in a set of three tables. Each table contains limit cycle solutions over a range of pilot gains for a single value of the interconnect ratio.

In addition to the inputs to the nonlinear elements, the magnitudes and phases of other signals in the loop may be of interest. In the present case, the bank angle response (ϕ) is of primary concern as an indication of the severity of the oscillation. When other such signals are desired, they may be approximated by standard block diagram manipulation. Figure 4-39 shows the relationship between the bank angle and the inputs to the actuator rate limiting nonlinearities. With the input signals,

$$x_a(t) = \alpha_a \sin(\omega t + \theta_a) \tag{4-60}$$

$$x_r(t) = \alpha_r \sin(\omega t + \theta_r) \tag{4-61}$$

The steady state bank angle output is given by,

$$\begin{aligned}\phi(t) &= \alpha_a |G_a(j\omega)| \sin(\omega t + \theta_a + \angle G_a(j\omega)) + \alpha_r |G_r(j\omega)| \sin(\omega t + \theta_r + \angle G_r(j\omega)) \\ &= \alpha_\phi \sin(\omega t + \theta_\phi)\end{aligned} \tag{4-62}$$

where G_a and G_r are as indicated in Figure 4-39 and the magnitudes and phases are to be calculated at the limit cycle solution. N_a and N_r are SIDF representations of the saturation nonlinearity. The bank angle output phase and amplitude can then be given as,

$$\theta_\phi = \tan^{-1}\left(\frac{\alpha_a |G_a| \sin(\theta_a + \angle G_a) + \alpha_r |G_r| \sin(\theta_r + \angle G_r)}{\alpha_a |G_a| \cos(\theta_a + \angle G_a) + \alpha_r |G_r| \cos(\theta_r + \angle G_r)}\right) \tag{4-63}$$

$$\begin{aligned}\alpha_\phi &= \frac{\alpha_a |G_a| \sin(\theta_a + \angle G_a) + \alpha_r |G_r| \sin(\theta_r + \angle G_r)}{\sin\theta_\phi} \\ &= \frac{\alpha_a |G_a| \cos(\theta_a + \angle G_a) + \alpha_r |G_r| \cos(\theta_r + \angle G_r)}{\cos\theta_\phi}\end{aligned} \tag{4-64}$$

The bank angle results as calculated above are also included in the tables.

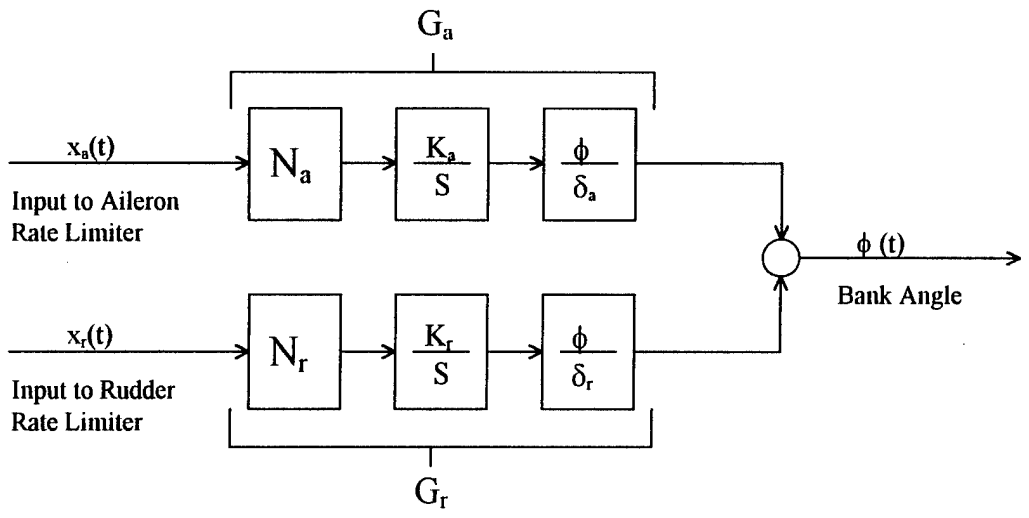

Figure 4-39. Steady State Bank Angle Output Due to Sinusoidal Inputs.

Table 4-14 gives the results for the nominal interconnect ratio of 0.45. The table shows limit cycle solutions exist for the given range of pilot gains. These solutions are characterized by a high degree of aileron saturation. The input to the aileron rate limiter has an amplitude between five and nine times the limit value. The only other saturation element that is limited is the pilot's aileron command. The commanded input is between one to two times the command limit. The remaining elements are not saturated. The solutions all oscillate at a frequency of approximately 4 rad/sec. The limit cycle solutions are predicted to be stable for pilot gains greater than or equal to 1.5 times the nominal gain and unstable at lower gains. For the nominal value of the interconnect ratio, the bank angle amplitude of the predicted limit cycles is seen to be on the order of two degrees.

From the stability robustness analysis, the gain margin for varying only pilot gain was found to be 1.6. It was found that the stable limit cycles predicted in Table 4-14 exhibit soft self excitation for pilot gains greater than this margin and hard self excitation for pilot gains below the margin.

In fact, all stable limit cycles found for the M2-F2 with MOCM pilot models seem to follow this trend. Namely, soft self excitation is observed when the parameters are set such that the stability margins of the linear system representation are violated.

The effect of varying interconnect ratio on the predicted limit cycle can be seen in Tables 4-14 through 4-16. As shown in Table 4-15, lowering the interconnect ratio to 0.375 causes the bank angle amplitude and the frequency of the oscillation to increase slightly. Also noted is that stable limit cycle solutions are predicted for lower pilot gains than for the nominal interconnect ratio. As the ratio is increased to 0.525 (Table 4-16), the predicted bank angle amplitude increases to approximately 10 degrees and the frequency decreases to under 3 rad/sec. For the increased interconnect ratio, stable limit cycles are predicted for the entire range of pilot gains given.

Table 4-14. Limit Cycle Solution for Nominal Interconnect Ratio (KI=0.45).

Kp	A1	ω (rad/s)	A2	θ2 (rad)	A3	θ3 (rad)	A4	θ4 (rad)	A5	θ5 (rad)	bank Amp.	bank phase	stable dσ/dA1
2.00	8.435	3.985	0.839	3.141	1.794	-1.172	0.450	-2.394	0.134	2.518	2.850	2.176	-0.535
1.90	8.295	4.016	0.840	3.140	1.681	-1.176	0.448	-2.389	0.134	2.505	2.815	2.182	-0.477
1.80	8.115	4.056	0.842	3.138	1.565	-1.182	0.445	-2.383	0.134	2.488	2.772	2.189	-0.414
1.70	7.870	4.111	0.844	3.136	1.444	-1.191	0.442	-2.377	0.134	2.465	2.714	2.198	-0.343
1.60	7.510	4.194	0.848	3.132	1.313	-1.205	0.437	-2.368	0.133	2.431	2.631	2.209	-0.257
1.50	6.845	4.353	0.853	3.124	1.153	-1.232	0.428	-2.357	0.131	2.367	2.481	2.225	-0.136
1.40	5.866	4.533	0.856	3.120	1.033	-1.289	0.427	-2.380	0.130	2.341	2.385	2.212	0.006
1.30	5.707	4.442	0.852	3.135	1.044	-1.318	0.447	-2.435	0.137	2.437	2.571	2.165	0.014
1.20	5.517	4.328	0.850	3.151	1.058	-1.353	0.469	-2.504	0.148	2.518	2.790	2.105	0.022
1.10	5.282	4.183	0.850	3.168	1.077	-1.393	0.492	-2.593	0.164	2.571	3.058	2.027	0.029
1.00	4.980	3.999	0.853	3.181	1.103	-1.442	0.520	-2.711	0.181	2.586	3.395	1.921	0.033

Table 4-15. Limit Cycle Solutions for Decreased Interconnect Ratio (KI=0.375).

Kp	A1	ω (rad/s)	A2	θ2 (rad)	A3	θ3 (rad)	A4	θ4 (rad)	A5	θ5 (rad)	bank Amp.	bank phase	stable dσ/dA1
2.00	9.732	4.560	0.798	3.099	1.954	-1.083	0.574	-2.166	0.186	1.931	3.170	2.422	-0.363
1.90	9.615	4.575	0.798	3.098	1.844	-1.088	0.572	-2.168	0.185	1.926	3.150	2.420	-0.345
1.80	9.470	4.593	0.799	3.096	1.733	-1.095	0.570	-2.171	0.185	1.920	3.126	2.418	-0.324
1.70	9.288	4.617	0.799	3.094	1.620	-1.103	0.567	-2.174	0.184	1.912	3.095	2.415	-0.299
1.60	9.052	4.648	0.800	3.091	1.504	-1.113	0.564	-2.179	0.183	1.902	3.055	2.411	-0.268
1.50	8.730	4.692	0.800	3.088	1.384	-1.128	0.559	-2.186	0.181	1.887	2.998	2.405	-0.230
1.40	8.251	4.761	0.801	3.082	1.254	-1.150	0.551	-2.197	0.179	1.865	2.912	2.396	-0.178
1.30	7.329	4.905	0.802	3.069	1.096	-1.196	0.534	-2.219	0.174	1.820	2.738	2.377	-0.090
1.20	6.342	5.022	0.794	3.069	1.008	-1.264	0.532	-2.273	0.163	1.842	2.690	2.334	0.004
1.10	6.196	4.961	0.783	3.091	1.009	-1.294	0.555	-2.320	0.158	1.956	2.887	2.301	0.011
1.00	6.046	4.889	0.774	3.116	1.010	-1.326	0.580	-2.373	0.159	2.088	3.108	2.263	0.017

Table 4-16. Limit Cycle Solutions for Increased Interconnect Ratio (KI=0.525).

Kp	A1	ω (rad/s)	A2	θ2 (rad)	A3	θ3 (rad)	A4	θ4 (rad)	A5	θ5 (rad)	bank Amp.	bank phase	stable dσ/dA1
2.00	5.905	2.691	0.848	3.100	5.231	-1.612	1.043	-3.433	0.120	4.350	9.907	1.070	-0.545
1.90	5.879	2.694	0.848	3.100	4.956	-1.613	1.040	-3.432	0.120	4.347	9.867	1.071	-0.485
1.80	5.849	2.697	0.848	3.101	4.679	-1.614	1.036	-3.432	0.120	4.343	9.820	1.072	-0.425
1.70	5.811	2.701	0.848	3.101	4.402	-1.615	1.032	-3.431	0.120	4.338	9.763	1.073	-0.367
1.60	5.764	2.706	0.848	3.101	4.122	-1.616	1.026	-3.430	0.120	4.332	9.692	1.074	-0.309
1.50	5.703	2.712	0.848	3.102	3.840	-1.618	1.019	-3.429	0.120	4.325	9.604	1.076	-0.250
1.40	5.620	2.720	0.848	3.102	3.554	-1.621	1.010	-3.428	0.120	4.315	9.491	1.078	-0.190
1.30	5.498	2.731	0.848	3.103	3.262	-1.624	0.998	-3.426	0.120	4.302	9.336	1.080	-0.108
1.20	5.313	2.746	0.848	3.104	2.962	-1.629	0.981	-3.423	0.119	4.283	9.118	1.084	-0.107
1.10	5.052	2.769	0.848	3.105	2.650	-1.636	0.956	-3.418	0.119	4.256	8.816	1.090	-0.105
1.00	4.660	2.804	0.847	3.107	2.321	-1.647	0.920	-3.412	0.118	4.216	8.373	1.100	-0.099

A graphical representation of the limit cycle solutions for varying interconnect ratio for a fixed pilot gain of two times the nominal gain is given in Figures 4-40 and 4-41. Figure 4-40 shows the frequency of the oscillation decreases slightly as the interconnect ratio is increased. Recall, this trend was also the case in the stability robustness analysis. The bank angle amplitude is seen to be a minimum at the nominal interconnect ratio of 0.45. The bank angle amplitude increases slightly as the interconnect ratio is decreased from its nominal value. As the interconnect ratio is increased from the nominal value, the bank angle amplitude grows rapidly.

The corresponding input amplitudes to the nonlinear elements are shown in Figure 4-41. The input amplitudes have been scaled such that values greater than unity indicate saturation of the limiters. The input amplitude to the yaw SAS command limiter and the input amplitude to the rudder rate limiter are always less than unity indicating these elements are not saturated during the limit cycles. The input amplitude to the aileron command limiter and the input amplitude to the aileron rate limiter are always greater than unity indicating these elements are saturated during the limit cycles. The input amplitude to the aileron rate limiter generally decreases with increasing interconnect ratio. The input amplitude to the aileron command limiter is a minimum at the nominal interconnect ratio and follows the same trend as the bank angle amplitude. The bank

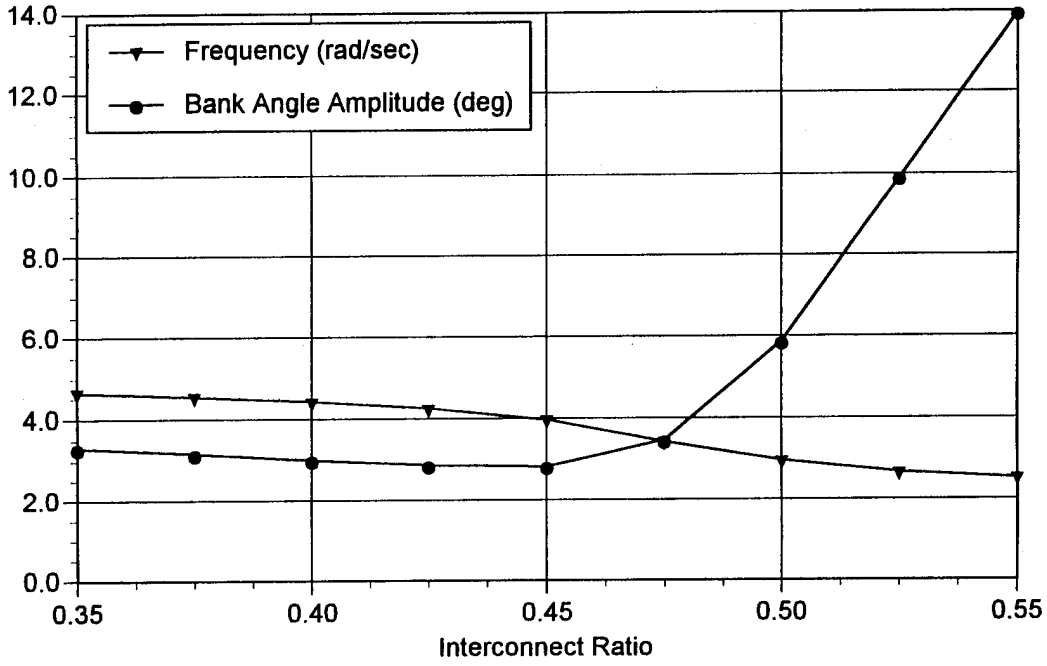

Figure 4-40. Predicted Bank Angle Amplitude and Frequency.

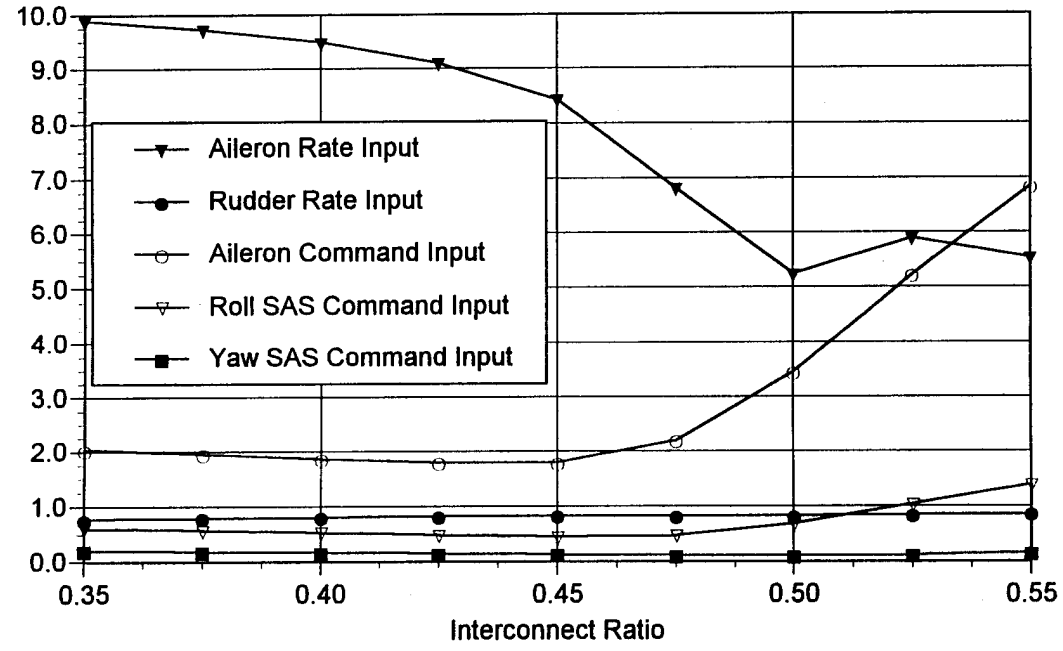

Figure 4-41. Predicted Input Amplitudes to the Saturation Elements.

angle amplitude is approximately twice the scaled value of the amplitude of the input to the aileron command limiter.

All of the predicted limit cycles indicated rate limiting of the aileron actuator as well as limiting of the pilots command input. The only other limiting observed was that of the roll SAS command when the interconnect ratio was increased above 0.52. This analysis shows the importance of the aileron rate limit and the pilots command authority limit on predicted oscillation events. From this analysis it would seem reasonable the nonlinearities associated with the rudder rate limit and the yaw SAS could have been neglected in the analysis.

The preceding analysis predicts the existence of limit cycles as the solutions to the harmonic balance equation. Computer simulation of the closed-loop pilot/vehicle system can then be used to verify the results. Figure 4-42 shows the bank angle response for the three interconnect ratios given in Tables 4-14 through 4-16 with the pilot gain in each case set to twice the nominal value for that case. The plot generally verifies the frequency and amplitude data given in the tables. However, at the larger interconnect ratio the simulation results in a bank angle amplitude that is twice that predicted. Keeping in mind that the describing function analysis is an approximation, and remembering the bank angle amplitude begins to increase sharply at large interconnect ratios, the discrepancy is understandable. Figure 4-43 shows the closed curve on the bank angle-bank angle rate phase plane that is characteristic of a limit cycle.

For a given set of parameter values, there may be more than one limit cycle solution. Table 4-17 shows another set of solutions for varying pilot gain while maintaining the nominal interconnect ratio. These solutions are characterized by large bank angle amplitudes (80 degrees) and low frequencies (1.2 rad/sec). These values agree much better with the flight data which

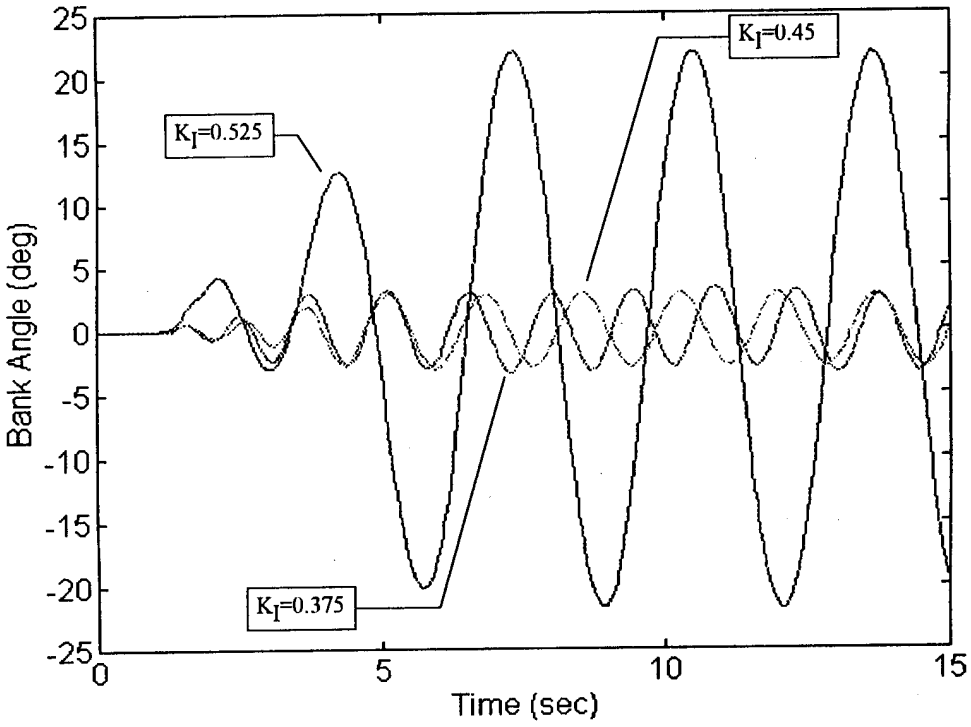

Figure 4-42. Simulated Bank Angle Response.

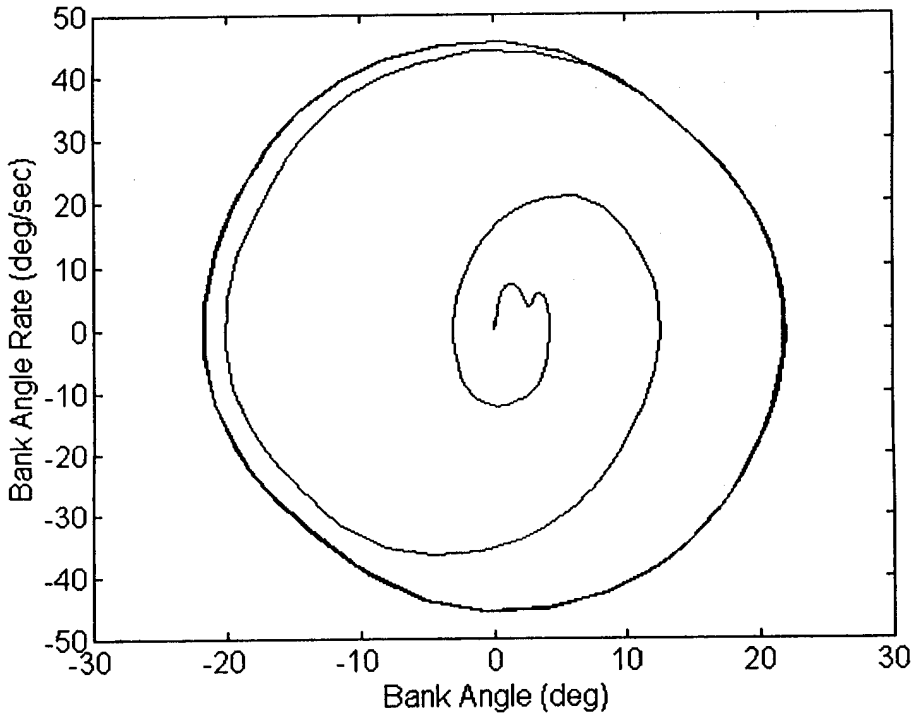

Figure 4-43. Bank Angle-Bank Angle Rate Phase Plane.

indicated bank angle amplitudes greater than 50 degrees at a frequency of approximately 1.6 rad/sec. The six-degree-of-freedom simulation data of Reference [48] for aileron only pilot control indicated bank angle amplitudes near 80 degrees at a frequency of 1.3 rad/sec. While these values agree well with those in Table 4-17, a computer simulation of this predicted limit cycle has yet to be obtained. Again it appears that the phenomena of hard self-excitation is the culprit.

Table 4-17. Additional Limit Cycle Solutions for Nominal Interconnect Ratio (KI=0.45).

Kp	A1	ω (rad/s)	A2	θ2 (rad)	A3	θ3 (rad)	A4	θ4 (rad)	A5	θ5 (rad)	bank Amp.	bank phase	stable dσ/dA1
2.00	0.627	1.203	0.391	2.884	12.513	-1.938	3.584	2.500	0.384	-0.045	82.427	0.486	-2.373
1.80	0.627	1.203	0.391	2.884	11.260	-1.938	3.583	2.500	0.384	-0.045	82.419	0.486	-2.379
1.60	0.627	1.203	0.391	2.884	10.007	-1.938	3.583	2.500	0.384	-0.045	82.407	0.485	-2.386
1.40	0.626	1.203	0.390	2.884	8.753	-1.938	3.582	2.500	0.384	-0.045	82.389	0.485	-2.396
1.20	0.626	1.203	0.390	2.884	7.499	-1.938	3.580	2.499	0.384	-0.045	82.362	0.485	-2.413
1.00	0.625	1.203	0.390	2.884	6.244	-1.939	3.577	2.499	0.384	-0.045	82.317	0.485	-2.441
0.80	0.624	1.202	0.389	2.883	4.988	-1.940	3.573	2.499	0.384	-0.045	82.234	0.484	-2.495
0.60	0.621	1.202	0.387	2.883	3.729	-1.942	3.562	2.497	0.383	-0.046	82.051	0.483	-2.626
0.40	0.612	1.199	0.381	2.881	2.461	-1.947	3.530	2.494	0.381	-0.047	81.504	0.478	-3.144
0.20	0.542	1.181	0.338	2.867	1.138	-1.997	3.290	2.463	0.364	-0.060	77.394	0.442	2.266
0.00	0.181	0.887	0.088	2.581	0.000	-1.997	2.086	1.593	0.339	-0.668	69.958	-0.550	12.056

4.3.7.5 Summary

The stability robustness analysis of the M2-F2 confirmed that the interconnect ratio, aileron rate limit, and pilot gain had a considerable affect on the closed-loop system stability. (The analysis also indicates rudder rate limiting has an impact, but the analysis considers no pilot rudder input, so it is unlikely that the rudder rate limit will be reached.) In particular, closed-loop stability is very sensitive to the value of the interconnect ratio.

The describing function analysis shows that self sustaining oscillations of the pilot/aircraft system are possible for parameter variations in the range of interest. Furthermore, the dependency of the character of these oscillations on the parameter variations emerges through the limit cycle analysis. Though the predicted characteristics of the oscillations that can currently be

simulated do not agree well with that experienced in flight, this result is not cause for alarm. First, the linear characteristics of the M2-F2 are so poor that nonlinear analysis is not necessary to predict handling qualities problems, including PIO. Further, the information available for the M2-F2 did not include actuator models for aileron and rudder. Also, the analysis was carried out at a constant angle of attack since no longitudinal dynamics were given.

One very important point needs to be stated. The current analysis is heavily dependent on the pilot model used. More precisely, the analysis is dependent on the pilot model and parameter variations of that model. At this point it seems logical that variations in pilot gain and time delay will figure prominently in future analysis. Though some idea exists about what to vary, more research needs to be performed to determine how much of a variation to consider. Since acceptable ranges of the parameter variations have not yet been established, it would be premature at this point to make any concrete assertion as to PIO proneness of any single vehicle based on the current analysis.

5 Conclusions and Recommendations

The new unified PIO analysis theory shows significant promise and warrants continued development. It can handle many simultaneous dynamic effects in a systematic way. It has ties to existing criteria and it can be used to isolate combinations of individual dynamic effects that are causing the PIO.

The analysis of HAVE PIO configurations revealed that the PIO tendencies of these configurations can be predicted using simple pilot gain/phase variation arguments. The vector margin concept, drawn from multivariable stability theory, correctly identified all but one of the HAVE PIO configurations. These configurations were also used to draw connections between several existing PIO criteria and the new unified method.

The M2-F2 example demonstrated how many individual dynamic effects can be analyzed simultaneously. In this case, the combined effect of five separate nonlinearities and two linear parameter variations were studied. While the PIO tendency in this case was most likely caused by poor flying qualities, a unified PIO analysis shows exactly which dynamic characteristics couple with the pilot to cause oscillations. For example, the analysis results showed that the PIO amplitude and frequency that occurred during flight testing and manned simulation of the M2-F2 could be accurately predicted by assuming an increased pilot gain and simultaneous limiting in the pilot command and roll SAS feedback channels.

5.1 Plan for Follow on Work

There are several activities that should be carried out before the new unified PIO analysis method will be completely accepted in industry. Some of these activities are intended to make the

analysis methods easier to use and more reliable. There are a few remaining research questions to address as well.

One remaining research question relates to the study of which pilot model parameters should be varied and to what degree they should be varied. Several variations in pilot gain, time delay, and lead/lag time constants were studied during this research. While pilot gain variations seemed to provide the best PIO predictions, there is sufficient evidence to warrant further investigation of other parameters. For example, the single-loop analysis of the HAVE PIO configurations showed that the critical frequency did not exactly predict the flight test PIO frequency. It is likely that a better correlation in frequency could be obtained if a specific variation in pilot time delay were used.

The other remaining research question focuses on the existence of hard and soft self-excitations. Recall that a soft self-excitation results when a sustained limit cycle can be obtained by simulating an initial condition response only. A hard self-excitation requires application and removal of an external input to yield a sustained oscillation. During this research, none of the predicted hard self-excitations were confirmed using the SIMULINK simulation program. Both random and deterministic input signals were tried. Continued investigation of the hard self-excitation phenomenon is important because it might shed light on the fact that some PIOs occur even after the aircraft has been in the fleet for several years.

Successful application to additional case studies will also aid in industry acceptance of the new unified method. This report demonstrated application to the HAVE PIO configurations, the F-4 (with back-up control systems), the M2-F2, and one flight condition of the B-2. Analysis of other known PIO-free and PIO-prone aircraft is needed to establish more definite design guidelines.

Finally, the software developed for this work is of research quality only. There are many improvements that could be made in order to make the software easier to use and perhaps more general in application. There are also several recently published algorithms that will improve the accuracy of the structured singular value calculations used in the unified PIO theory.[50] Reliable and efficient software developed specifically for unified PIO analysis will undoubtedly improve industry acceptance.

References

1. Dornheim, M.A., "Report Pinpoints Factors Leading to YF-22 Crash," *Aviation Week & Space Technology*, Nov. 9, 1992, pp. 53-54.

2. Young, L.R. and Meiry, J.L., "Bang-Bang Aspects of Manual Control in High-Order Systems," IEEE Transactions on Automatic Control, July 1965, pp. 336-341.

3. Anderson, M.R., "Standard Optimal Pilot Models," Paper No. 94-3627, AIAA Guidance, Navigation, and Control Conference, Scottsdale, AZ, Aug. 1994.

4. Hofmann, L.G., Shah, K.V., Graham, D., "Analysis of Limited Authority Manual Control Systems," AFFDL-TR-71-6, July 1971.

5. Hirsch, D.L. and McCormick, R.L., "Experimental Investigation of Pilot Dynamics in a Pilot-Induced Oscillation Situation," *Journal of Aircraft*, Vol. 3, No. 6, Nov.-Dec. 1966, pp. 567-573.

6. Smith, R.H., "A Theory for Longitudinal Short Period Pilot Induced Oscillations," AFFDL-TR-77-57, June 1977.

7. Twisdale, T.R. and Kirsten, P.W., "Prediction and Occurrence of Pilot-Induced Oscillations in a Flight Test Aircraft," *Journal of Guidance, Control, and Dynamics*, Vol. 7, No. 4, July-Aug. 1984, pp. 410-415.

8. Bjorkman, E.A., Silverthorn, J.T., and Calico, R.A., "Flight Test Evaluation of Techniques to Predict Longitudinal Pilot Induced Oscillations," Paper 86-2253, AIAA Guidance, Navigation, and Control Conference, Williamsburg, VA, Aug. 1986, pp. 967-975.

9. Moorhouse, D.J., "Experience with the R. Smith PIO Criterion on the F-15 STOL & Maneuver Technology Demonstrator," Paper No. 94-3671, AIAA Guidance, Navigation and Control Conference, Scottsdale, AZ, Aug. 1994, pp. 1178-1184.

10. McRuer, D.T. and Jex, H.R., "A Review of Quasi-Linear Pilot Models," *IEEE Transactions on Human Factors in Electronics*, Vol. HFE-8, No. 3, Sept. 1967, pp. 231-249.

11. Hess, R.A. and Kalteis, R.M., "Technique for Predicting Longitudinal Pilot-Induced Oscillations," *Journal of Guidance, Control, and Dynamics*, Vol. 14, No. 1, Jan.-Feb. 1991, pp. 198-204.

12. Hess, R.A., "A Model-Based Investigation of Manipulator Characteristics and Pilot/Vehicle Performance," *Journal of Guidance, Control, and Dynamics*, Vol. 6, No. 5, Sept.-Oct. 1983, pp. 348-354.

13. Hess, R.A., "Analysis of Aircraft Attitude Control Systems Prone to Pilot-Induced Oscillations," *Journal of Guidance, Control, and Dynamics*, Vol. 7, No. 1, Jan.-Feb. 1984, pp. 106-112.

14. Kleinman, D.L., Baron, S., and Levison, W.H., "An Optimal Control Model of Human Response, Part I: Theory and Validation," *Automatica*, Vol. 6, Pergamon Press, Ltd., 1970, pp. 357-369.

15. Bacon, B.J. and Schmidt, D.K., "An Optimal Control Approach to Pilot/Vehicle Analysis and the Neal-Smith Criteria," NASA CR-170416, April 1984.

16. Waszak, M.R. and Schmidt, D.K., "Analysis of Flexible Aircraft Longitudinal Dynamics and Handling Qualities," NASA CR-177943, June 1985.

17. Anderson, M.R. and Schmidt, D.K., "Closed-Loop, Pilot/Vehicle Analysis of the Approach and Landing Task," *Journal of Guidance, Control, and Dynamics*, Vol. 10, No. 2, March-April 1987, pp.187-194.

18. Powers, B.G., "An Adaptive Stick-Gain to Reduce Pilot-Induced Oscillation Tendencies," *Journal of Guidance, Control, and Dynamics*, Vol. 5, No. 2, March-April 1982, pp. 138-.

19. Velger, M. Grunwald, A., and Merhav, S., "Suppression of Biodynamic Disturbances and Pilot-Induced Oscillations by Adaptive Filtering," *Journal of Guidance, Control, and Dynamics*, Vol. 7, No. 4, July-Aug. 1984, pp. 401-409.

20. A'Harrah, R.C., "An Alternate Control Scheme for Alleviating Aircraft-Pilot Coupling," Paper No. 94-3673, AIAA Guidance, Navigation and Control Conference, Scottsdale, AZ, Aug. 1994, pp. 1194-1201.

21. Smith, R. H. and Geddes, N. D., 'Handling Quality Requirements for Advanced Aircraft Design: Longitudinal Mode," AFFDL-TR-78-154, Aug. 1979.

22. Mitchell, D.G., Hoh, R.H., Aponso, B.L., and Klyde, D.H., "The Measurement and Prediction of Pilot-in-the-Loop Oscillations," Paper No. 94-3670, AIAA Guidance, Navigation and Control Conference, Scottsdale, AZ, Aug. 1994, pp. 1167-1177.

23. Davidson, J.B. and Schmidt, D.K., "Modified Optimal Control Pilot Model for Computer-Aided Design and Analysis," NASA TM-4384, Oct. 1992.

24. Doyle, J.C., Glover, K., Khargonekar, P.P., Francis, B.A., "State-Space Solutions to Standard H_2 and H_∞ Control Problems," *IEEE Transactions on Automatic Control*, Vol. 34, No. 8, Aug. 1989, pp. 831-847.

25. Smith, R., "Predicting and Validating Fully-Developed PIO," Paper No. 94-3669, AIAA Guidance, Navigation and Control Conference, Scottsdale, AZ, Aug. 1994, pp. 1162-1166.

26. Yeh, H.H., Ridgely, D.B., and Banda, S.S., "Nonconservative Evaluation of Uniform Stability Margins of Multivariable Feedback Systems," *Journal of Guidance, Control, and Dynamics*, Vol. 8, No. 2, March-April 1985, pp. 167-174.

27. Doyle, J.C., "Analysis of Feedback Systems with Structured Uncertainties," IEE Proc., Vol. 129, Pt. D, No. 6, Nov. 1982, pp. 242-250.

28. Jones, R.D., 'Structured Singular Value Analysis for Real Parameter Variations," Paper No. 87-2589, AIAA Guidance, Navigation and Control Conference, Monterey, CA, Aug. 1987, pp. 1424-1432.

29. Manning, M.K. and Banda, S.S., "Approximate Structured Singular Value Computation via Frobenius Norms," International Conference on Systems Engineering, Dayton, OH, Aug 24-26, 1989.

30. Osborne, E.E., 'On Pre-Conditioning of Matrices," *Journal of the Association for Computing Machinery*, Vol. 7, 1960, pp. 338-345.

31. Anderson, M.R. and Schmidt, D.K., "An Uncertainty Model for Saturated Actuators," American Control Conference, Pittsburgh, PA, June 1989.

32. Kapasouris, P. and Athans, M., "Multivariable Control Systems with Saturating Actuators Antireset Windup Strategies," American Control Conference, Boston, MA, June 1985, pp. 1579-1584.

33. Manning, M.K. and Banda, S.S., 'Algorithm to Obtain M-Δ Form for Robust Control," International Conference on Systems Engineering, Dayton, OH, Aug 24-26, 1989.

34. Safanov, M. G., 'Stability Margins of Diagonally Perturbed Multivariable Feedback Systems," IEE Proc., Vol. 129, Pt. D, No. 6, Nov. 1982. pg. 251-256.

35. Military Standard, Flying Qualities of Piloted Aircraft, MIL-STD-1797A, 30 Jan. 1990.

36. Graham, D. and McRuer, D., "Retrospective Essay on Nonlinearities in Aircraft Flight Control," *Journal of Guidance, Control, and Dynamics*, Vol. 14, No. 6, Nov.-Dec. 1991, pp. 1089-1099.

37. Graham, D. and McRuer, D., *Analysis of Nonlinear Control Systems*, John Wiley & Sons, Inc., 1961.

38. Gelb, A. and VanderVelde, W.E., *Multiple Input Describing Functions and Nonlinear System Design*, McGraw Hill Book Co., 1968.

39. Ogata, K., *Modern Control Engineering, Second Edition*, Prentice Hall, Inc., 1990.

40. Mees, A., "Describing Functions, Circle Criteria, and Multiple-Loop Feedback Systems," Proc. IEE, Vol. 120, No. 1, Jan. 1973, pp. 126-130.

41. Gray, J.O. and Nakhla, N.B., "Prediction of Limit Cycles in Multivariable Nonlinear Systems," IEE Proc., Vol. 128, Pt. D, No. 5, Sept. 1981, pp. 233-241.

42. Gray, J.O. and Taylor, P.M., "Computer Aided Design of Multivariable Nonlinear Control Systems using Frequency Domain Techniques," *Automatica*, Vol. 15, 1979, pp. 281-297.

43. Chang, H.C., Pan, C.T., Huang, C.L., and Wei, C.C., "A General Approach for Constructing the Limit Cycle Loci of Multiple-Nonlinearity Systems," *IEEE Transactions on Automatic Control*, Vol. AC-32, No. 9, Sept. 1987, pp. 845-848.

44. Pillai, V.K. and Nelson, H.D., "On an Extension of the Describing Function Method," American Control Conference, Atlanta, GA, June 1988, pp. 2168-2173.

45. Smith, O.J.M., *Feedback Control Systems*, McGraw-Hill, New York, 1958.

46. Givens, M.L., "Evaluation of B-2 Susceptibility to Pilot-Induced Oscillations," Northrop-Grumman, B-2 Division, White Paper No. 120-4, March 1994.

47. Mukhopadhyay, V. and Newsom, J.R., "Application of Matrix Singular Value Properties for Evaluating Gain and Phase Margins of Multiloop Systems," AIAA Guidance, Navigation, and Control Conference, San Diego, CA, Aug. 1982, pp. 420-428.

48. Kempel, R. W., "Analysis of a Coupled Roll-Spiral-Mode, Pilot-Induced Oscillation Experienced With the M2-F2 Lifting Body," NASA TN D-6496, September 1971.

49. McRuer, D.T. and Schmidt, D.K., 'Pilot-Vehicle Analysis of Mulit-Axis Tasks," Paper No. 87-2538-CP, AIAA Guidance, Navigation and Control Conference, Monterey, CA, Aug. 1987.

50. Dailey, R.L., "A New Algorithm for the Real Structured Singular Value," American Control Conference, June 1990, pp 3036.